Design, Synthesis and Characterization of Multiresponsive Microgels

A Thesis
Presented to
The Academic Faculty

by

Satish P. Nayak

In Partial Fulfillment
of the Requirements for the Degree
Doctor of Philosophy in the
School of Chemistry and Biochemistry

Georgia Institute of Technology
November 2004

Design, Synthesis and Characterization of Multiresponsive Microgels

Approved by:

Dr. L. Andrew Lyon, Advisor
School of Chemistry and Biochemistry
Georgia Institute of Technology

Dr. Nicholas V. Hud
School of Chemistry and Biochemistry
Georgia Institute of Technology

Dr. Jiri Janata
School of Chemistry and Biochemistry
Georgia Institute of Technology

Dr. Christopher W. Jones
School of Chemical & Biomolecular Engineering
Georgia Institute of Technology

Dr. Marcus Weck
School of Chemistry and Biochemistry
Georgia Institute of Technology

November 18, 2004

ACKNOWLEDGEMENTS

First of all I would like to thank my advisor Dr. L. Andrew Lyon for allowing me to work in his lab. He has always given me the freedom to work on the projects which I thought were interesting. It is the result of this freedom that I was able to broaden my knowledge of science. The discussions that I have had with him have helped me in achieving a better perspective towards science and life in general. He has always been there to talk about the problems and come up with fitting solutions to them, but has also encouraged independent thinking. I would also like to thank all the members of the Lyon group, especially Michael Serpe, Clint Jones and Jongseong Kim who have helped me at various stages and as a result of the time spent together have become very good friends of mine. I am also thankful to the friendship that I have forged with Ameya, Sawant, Sandeep, Ashish, Pranav, Ramesh, Pratik and Katrin who have provided me with a great outside-work atmosphere. Finally, I would like to thank my parents and my siblings, Nandu and Harish, for everything they have done for me.

TABLE OF CONTENTS

LIST OF TABLES

LIST OF FIGURES

LIST OF ABBREVIATIONS

NIPAm	*N*-isopropylacrylamide
BIS	*N,N'*-Methylene(bisacrylamide)
AAc	Acrylic Acid
pNIPAm	Poly(*N*-isopropylacrylamide)
VPT	Volume Phase Transition
LCST	Lower Critical Solution Temperature
pNIPAm-co-AAc	Poly(*N*-isopropylacrylamide-*co*-acrylic acid)
VPTT	Volume Phase Transition Temperature
SDS	Sodium Dodecyl Sulfate
APS	Ammonium Persulfate
RI	Refractive Index
PCS	Photon Correlation Spectroscopy
APTMS	3-Aminopropyltrimethoxysilane
AFA	4-Aminofluorescein
DIC	Differential Image Contrast
DNA	Deoxyribose Nucleic Acid
PEG	Poly(ethylene glycol)
CMC	Critical Micelle Concentration
DHEA	*N,N'*-(1,2-Dihydroxyethylene)-bisacrylamide
APMA	*N*-(3-Aminopropyl)methacrylamide hydrochloride
DLS	Dynamic Light Scattering

MWCO	Molecular Weight Cut Off
MALG	Malachite green isothiocyanate
PheMMA	(9-Phenanthryl)methyl methacrylate
THF	Tetrahydrofuran
DMF	Dimethyl formamide
$NaIO_4$	Sodium Periodate
NaAMPS	2-acrylamido-2-methylpropanesulfonate
MADQUAT	{2-(methacryloyloxy)ethyl}trimethylammonium chloride
FR	Folate receptor
EDC	1-ethyl-3-(3-dimethylaminopropyl)carbodiimide
PBS	Phosphate Buffered Saline
MTT	Methylthiazolyldiphenyl-tetrazolium bromide
FCSHI	Heat-inactivated fetal bovine serum
avidin-HRP	Avidin-horse radish peroxidase conjugate
HABA	2-(4'-hydroxyazobenzene) benzoic acid

SUMMARY

This dissertation is aimed towards using thermoresponsive pNIPAM microgels in various constructs. Chapter 1 gives a detailed background of hydrogels and microgels. Chapter 2 describes the use of microgels in thin films, where it is observed that higher the concentration of microgels in the film, faster the stabilization is observed at high temperatures. Chapter 3 describes the process of preparing photoresponsive microgels. In this chapter the microgels are conjugated with malachite green, which is a photon-to-heat converter. The microgels deswell on irradiation with HeNe laser. Chapter 4 contains the process of synthesizing and characterizing degradable microgels and then using them to prepare hollow microgels. Chapter 5 includes the synthesis of zwitterionic microgels. These microgels go from a positively charged state to zwitterionic to negatively charged state on increasing the pH. Chapter 6 discusses the use of microgels for targeting cancer cells. Folic acid is used as the targeting ligand. The microgels are conjugated with folic acid and are able to target cells that overexpress folate receptors. In Chapter 7 microgels with a degradable shell are synthesized. These microgels exhibit pore-size dependent permeation of proteins. Chapter 8 lists the future outlook experiments, which can be done for the projects described in the previous chapters.

CHAPTER 1

INTRODUCTION TO HYDROGELS AND MICROGELS

This chapter deals with the basics of hydrogel materials with a particular emphasis towards responsive hydrogels prepared from *N*-isopropylacrylamide (NIPAm). Microgels, which are colloidal hydrogel dispersions, are also discussed in this chapter.

1.1 Definition of Hydrogels

Hydrogels are defined as a polymeric network that can swell in water. On the basis of rheology, hydrogels are defined as cross-linked polymers that exhibit visco-elastic or pure elastic behavior. The swelling capacity of hydrogels is enormous, they can absorb water about thousand times more than their dry weight.[1-3] This water-absorbing property of the hydrogels has made them useful for contact lenses,[4] drug delivery,[2,5] protein separation,[6] tissue engineering[7-9] and catalysis.[10-12]

1.2 Classification of Hydrogels

Hydrogels can be classified in many ways but in this chapter we will deal mostly with the classification based on type of cross-links. Cross-links are important to maintain the 'network' structure of the hydrogels and to prevent dissolution of the hydrophilic chains. Based on the type of cross-links there are two classes of hydrogels.[13]

1.2.1 Physically Cross-Linked Hydrogels

The hydrogels in this class have been inspired by the idea of making degradable hydrogels that can easily go from the three-dimensionally stable structure to the polymer solution, and do this reversibly. Most often these hydrogels have been used in encapsulating proteins,[14] cells[15] or drugs[2,16] and release them by dissolving the structure. The cross-links in this class of hydrogels are due to non-covalent attractive forces between the polymer chains. These forces are usually hydrophobic or ionic interactions.

Alginate is a polymer that forms hydrogels in the presence of calcium ions. It is a polysaccharide composed of mannuronic acid and gluconic acid, which can be cross-linked by divalent calcium ions.[13,17] The hydrogel structure can be dissolved by using a chelating agent that binds to the ions. Hence alginate hydrogels have been used for encapsulating proteins and also as a cellular matrix. Another example of cross-linking by ions, is of dextran, which lacks charged region but it forms hydrogels in the presence of potassium ions. The reason for the cross-linking is that the ionic radius of potassium ions is such that it fits perfectly in the cage formed by six oxygen atoms of glucose units of three polymer chains.[18]

Poly(acrylic acid) and poly(methacrylic acid) form hydrogen bonds with poly(ethylene glycol), which results into formation of hydrogels. The hydrogen bond is formed between the oxygen of the poly(ethylene glycol) and carboxylic group of the poly acids. The hydrogen bonds are formed only when the acid groups are protonated, hence the hydrogel formation is pH dependent.[19,20] Oligonucleotides have also been used in the formation of hydrogels. Nagahara et al. coupled water soluble poly(*N,N*-

dimethylacrylamide-co-*N*-acryloylsuccinimide) to a single stranded DNA.[21] In presence of complimentary DNA, hydrogels are formed. The gels are formed at room temperature and can be dissolved at high temperature when the DNA is dehybridized.

1.2.2 Chemically Cross-Linked Hydrogels

These types of hydrogels are more stable than the physically cross-linked hydrogels because the cross-links are formed by covalent bonds.[13] The hydrogels formed by such cross-links usually have a permanent structure unless there is an intentionally added lability to the network.

Chemically cross-linked gels are most often formed by polymerizing monomers in the presence of cross-linking agents. Poly(2-hydroxyethyl methacrylate) is a well studied hydrogel. It is synthesized by polymerizing 2-hydroxy methacrylate with ethylene glycol dimethacrylate. Various physical properties, like the swelling capacity, of the hydrogels are controlled by the amount of cross-linker used.[13]

Hydrogels can also be formed by cross-linking of the various functional groups present on the polymer backbone.[13] Polymers containing hydroxyl, amine or hydrazide groups can be cross-linked by using glutaraldehyde, which forms covalent bonds with each of the above-mentioned functionalities.[13,22,23]

Enzymes can also be used in the formation of cross-linked hydrogels. Sperinde et al. used tetrahydroxy PEG functionalized with glutaminyl groups. This polymer forms hydrogels in the presence of an enzyme transglutaminase and poly(lysine-co-phenylalanine). The enzyme catalyses the reaction between the γ-carboxyamide group of the PEG-glutaminyl polymer and ε-amine group of the lysine to form an amide bond.[24,25]

1.2.3 Other Classifications

Hydrogels can also be classified based on their size as macrogels or microgels. Macrogels[26-30] are bulk gels where the size can be anywhere from millimeter and above, while microgels[31-39] are colloidally stable hydrogels and their size can vary from nanometer to micrometer. Microgels will be discussed in more detail later in the chapter.

Hydrogels can be further classified as stimuli-responsive or non-responsive gels. Non-responsive gels, as the name suggests, are merely materials that swell upon water absorption. On the other hand stimuli-responsive gels are considered to be "smart" materials because they respond to subtle changes in the environment. These hydrogels can be made responsive to temperature,[27] pH,[35,40] ionic strength,[41-43] light,[44-48] electric field[49] and biomolecules.[50-53] The "smart" behavior of the hydrogels is inherited from the type of the polymer that is used in making these gels.

1.3 Poly(*N*-isopropylacrylamide) (PNIPAm)

Due to its unusual thermal behavior in aqueous solutions, pNIPAm has been widely used to make responsive hydrogels. PNIPAm has been synthesized by a variety of techniques: redox initiation, free radical initiation, ionic initiation and also using radiation.[54] Various functional groups have also been added to the polymer by using comonomers.

1.3.1 Solution Behavior of PNIPAm

The behavior of a polymer in a solvent is a balance of solvent-solvent interactions, solvent-polymer interactions and polymer-polymer interactions. In water pNIPAm has water molecules hydrogen bonded to the amide side chains. Also there is

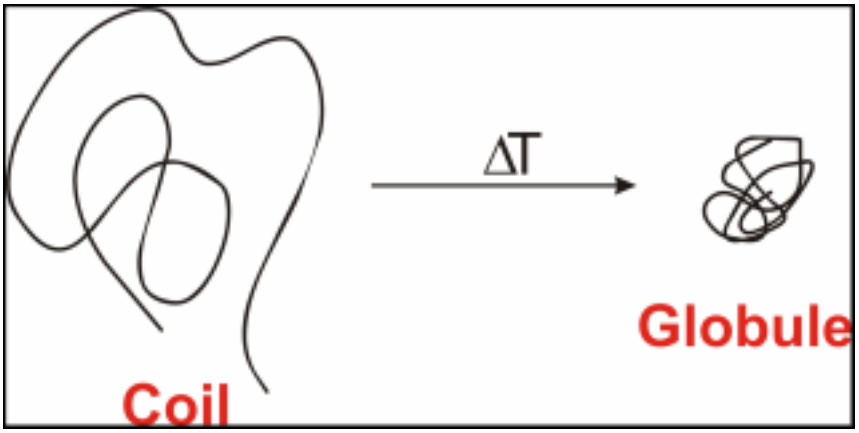

Figure 1-1. Coil to globule transition of pNIPAm chain

some structured water around the isopropyl group. This effect of structured water is known as hydrophobic effect.[54] In this case pNIPAm has a random coil structure because the solvent-polymer interactions are stronger than the polymer-polymer interactions. At higher temperatures the hydrogen bonds with the water molecules break and there is an entropically-favored release of water. In this case the polymer-polymer interactions become stronger than the polymer-solvent interactions and the polymer phase separates.

The temperature at which this phase separation occurs is called the lower critical solution temperature (LCST). Figure 1-1 shows the coil to globule transition of the pNIPAm polymer chain. This behavior of pNIPAm makes it a very attractive candidate for making stimuli-responsive hydrogels. The LCST behavior of the pNIPAm has been studied by a variety of techniques: UV-VIS, differential scanning calorimetry, light scattering, viscometry and fluorescence.[55-63] Wu et al. have studied the phase transition of pNIPAm, where they observed that the transition is not first order *i.e.* the polymer does not directly go from a random coil state to a globular state but there are other intermediate thermodynamically stable states.[61,63]

1.4 PNIPAm Macrogels

As mentioned above, pNIPAm due to its inverse solubility with increasing temperature, has been used in synthesizing stimuli-sensitive hydrogels. The thermoresponsivity of the parent polymer is inherited by the macrogels made from it. These hydrogels exhibit volume phase transition temperature (VPTT)[64] at around the LCST of pNIPAm. At temperatures higher than VPTT, the hydrogel goes from a swollen (hydrophilic) state to a deswollen (relatively hydrophobic) state. Figure 1-2 illustrates the molecular view of the process of VPT in cross-linked pNIPAm hydrogels. The VPTT of the gels is dependent on several factors: cross-linker density, hydrophobic-hydrophilic balance and solvent. Tanaka and coworkers have extensively studied the deswelling of pNIPAm gels.[26-30,49] They have shown that ionic gels have a discontinuous transition in comparison to nonionic gels, which have a continuous transition.[28,65] They have also shown that the deswelling rate of the gel is inversely proportional to the square of the

smallest dimension of the gel.[27,66] Hoffman et al. have shown that by polymerizing pNIPAm gels at temperatures higher than the LCST of the polymer results in gels having large pore size, which in turn have faster swelling rates.[67]

Thermosensitivity of pNIPAm gels have been used in controlling the activity of enzymes too. Hoffman et al. immobilized an enzyme to the gel and controlled the diffusion of the substrate to the enzyme by controlling the pore size of the gel, which depends on the temperature of the system. In this way they were able to switch the enzyme on or off by controlling the temperature.[68] Kim et al. have synthesized pNIPAm gels with peptide cross-links. These gels can be used as extracellular matrix where the peptide can be cleaved by a metalloproteinase and subsequently degrade the gel.[69]

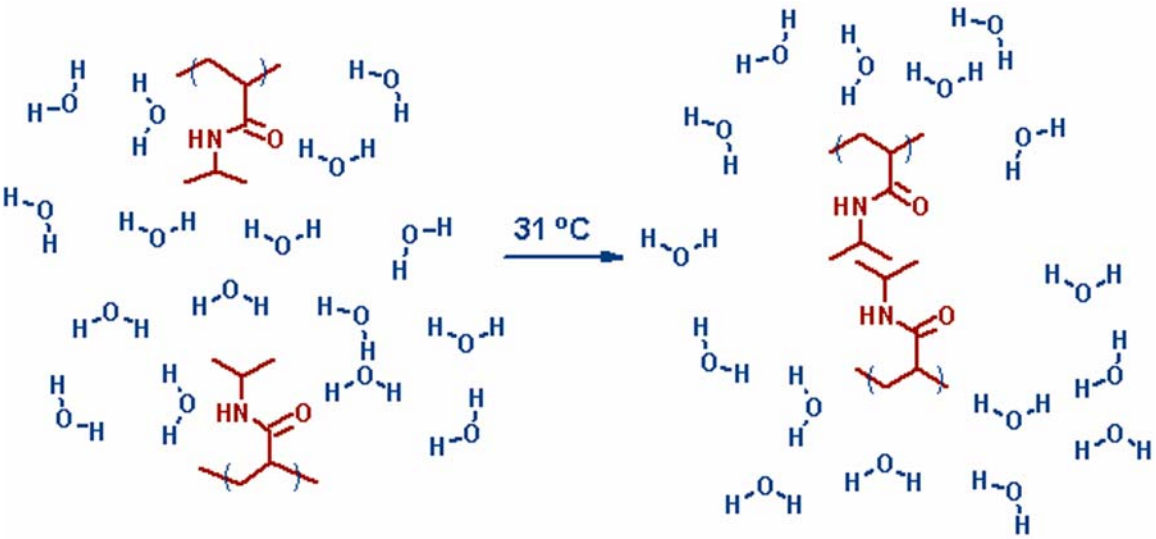

Figure 1-2. Volume phase transition in pNIPAm gels. At temperatures below the LCST of pNIPAM, which is ~ 31 °C, water is hydrogen bonded to the amide side chains of pNIPAm, there is also some structured water around the isopropyl group. Hence the gel is swollen due to strong polymer-solvent interactions. At temperatures above the LCST of pNIPAm there is an entropically-favored release of water from the interior of the gel and the polymer-polymer interactions become stronger, thereby deswelling the gel.

1.5 PNIPAm Microgels

Microgels are colloidally stable hydrogel particles. Their size ranges typically from 50 nm to 5 μm.[70] Microgels can be prepared from various monomers but in this chapter we will restrict our discussion to pNIPAm microgels. Microgels constructed from pNIPAm have similar properties as their macrogel counterparts i.e. they undergo volume phase transition (VPT) around the LCST of pNIPAm. The VPTT of the microgels is affected by cross-linking density,[38] solvents[71] and comonomer.[35] Microgels posses several advantages over bulk gels: small size and volume, high surface area, faster response to stimuli and high diffusivity.[72]

1.5.1 Microgel Synthesis

Microgels can be synthesized by a variety of techniques: precipitation polymerization, miniemulsion polymerization and microemulsion polymerization.[70,73-83] Since in this dissertation precipitation polymerization is used to prepare microgels, this method is discussed in detail.

In this method the major monomer, which is NIPAm, and the cross-linker *N,N'*-methylene bisacrylamide (BIS) are dissolved in water. Figure 1-3 shows the structures of the common monomers used in the synthesis of microgels. The solution is added to a three-necked round bottom flask and to it some surfactant, either cationic or anionic, (depending upon the requirement) is added. The concentration of the surfactant is kept below the critical micelle concentration (CMC). The solution is then purged with nitrogen to remove the dissolved oxygen because it retards the polymerization.

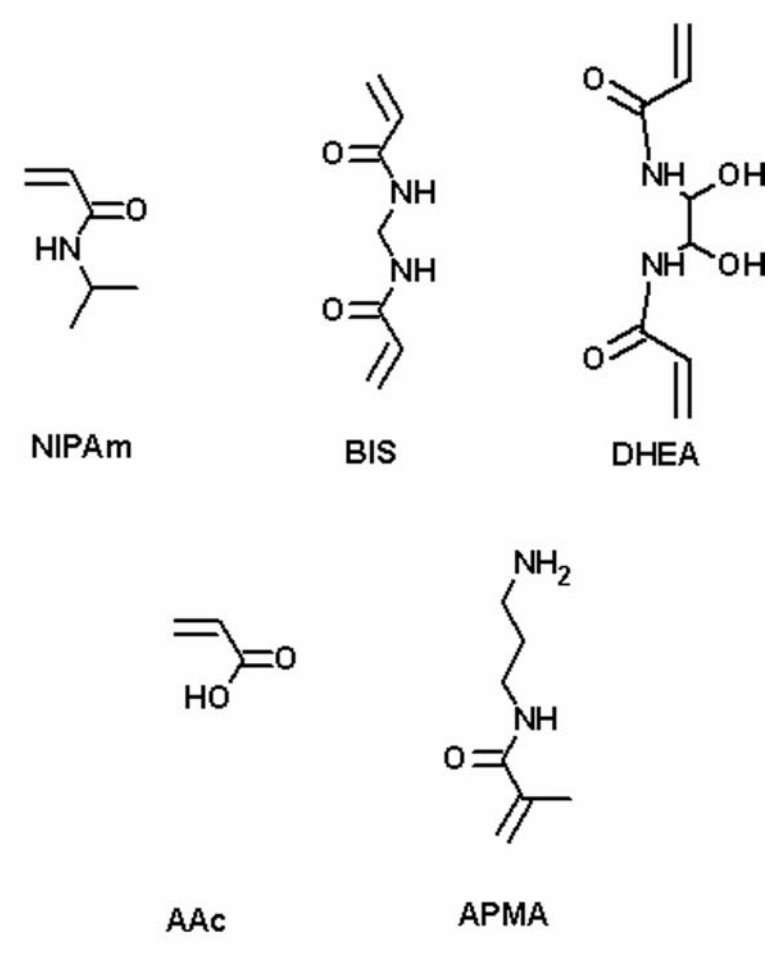

Figure 1-3. Common monomers used in the synthesis of microgels.
NIPAm – *N*-isopropylacrylamide
BIS – *N,N'*- methylenebisacrylamide
DHEA – *N,N'*-(1,2-Dihydroxyethylene)-bisacrylamide
AAc – Acrylic acid
APMA – *N*-(3-Aminopropyl)methacrylamide hydrochloride

The solution is heated to ~ 70 °C, under gentle stream of nitrogen gas. The initiator, ammonium persulfate (APS), is added to the heated solution and the reaction is allowed to proceed for ~ 4 h. At the end of the reaction the solution is cooled and filtered. Figure 1-4 depicts the synthetic scheme for preparation of microgels. This process usually gives monodisperse microgels. Depending upon the requirement of functional group, comonomers like acrylic acid or amine monomer can be added to the reaction mixture before polymerization. Presence of the cross-linker is essential to avoid dissolution of the polymer chains.

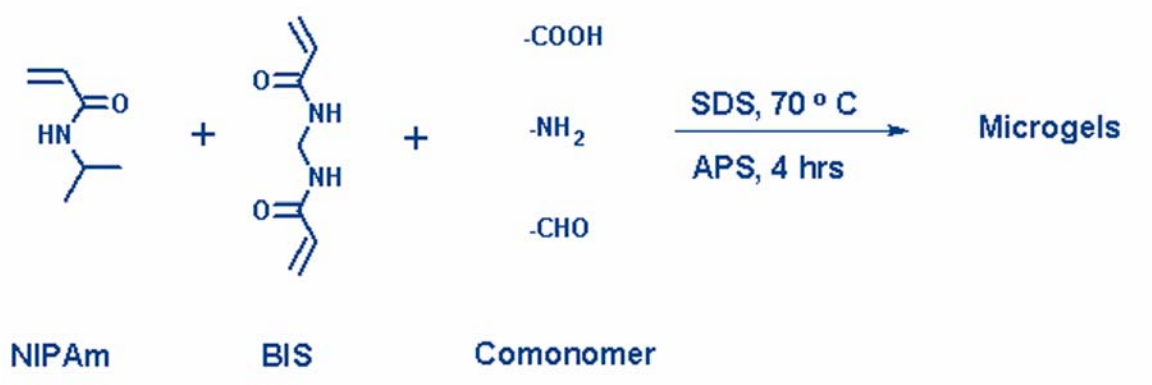

Figure 1-4. Microgel synthesis scheme. All the monomers are dissolved in water and the solution is heated to 70 °C with surfactant sodium dodecyl sulfate (SDS). The polymerization is initiated by a free-radical initiator ammonium persulfate (APS). Comonomers with different functionalities can also be polymerized in the microgel.

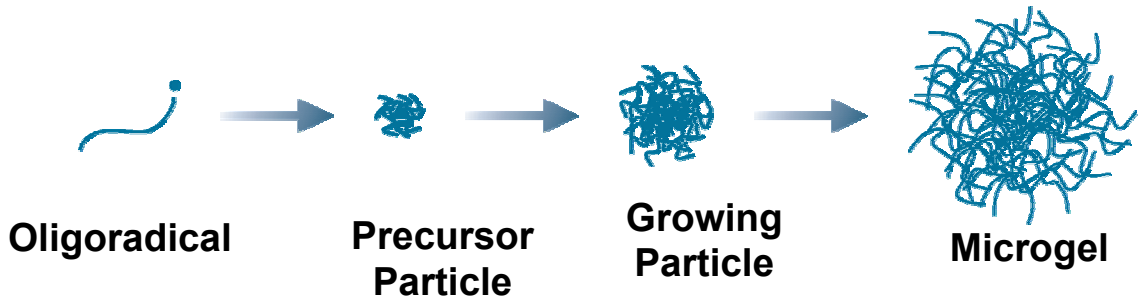

Figure 1-5. Precipitation polymerization. After initiation the oligoradical reaches a critical length and collapses on itself forming a precursor particle, which can then grow either by aggregating with other precursor particles or with growing oligomers.

Microgels are formed by homogenous nucleation.[70] Figure 1-5 illustrates the mechanism of precipitation polymerization. There are two reasons for the polymerization to be carried out at high temperature: one is formation of sulfate radicals, which initiate the polymerization. The second is, after initiation the NIPAm monomer polymerizes and the chain starts to grow, once the chain length reaches a certain critical length it collapses on itself giving precursor particles. The chain collapses because the polymerization temperature is higher than the LCST of the polymer and hence it phase separates. The precursor particles grow by two mechanisms: they either aggregate with the other precursor particles or are captured by existing colloidally stable particles. The charge imparted by the initiator stabilizes the microgels. To synthesize small microgels, the precursor particles have to be stabilized earlier in the reaction. Since there is not enough charge available to stabilize the small precursor particles, surfactant is used, which stabilizes the small precursor particles.

Depending on the application of the microgels, they can be modified by post-polymerization modification. In this method, the polymerized functional group on the microgels is used to attach further functionalities by a chemical reaction. These functionalities can range from small ligand molecules to large proteins.[84-94]

1.5.2 Properties of PNIPAm Microgels

PNIPAm microgels exhibit VPT behavior, where at T < VPTT the microgels are individually swollen with water and at T > VPTT the microgels decrease in size due to expulsion of water from the interior of the microgels.[31,32] This transition can be followed by detecting the scattered light. A dilute solution of microgel appears transparent because as mentioned above at T < VPTT the microgels are swollen with water and the difference between the refractive indices of the polymer and the solvent is not very high. At T > VPTT the water is expelled from the polymer resulting in an increase in refractive index contrast between the polymer and the solvent, which turns the solution turbid.

Wu et al. have shown that the VPTT of the microgels is higher than the LCST of pNIPAm and also that the transition region is less sharp than that of bulk gels.[95] The reason for this continuous transition is due to higher heterogeneity in the subchain lengths of the microgels. When the microgels are subjected to T > VPTT, the regions with longer subchains collapse before the regions with shorter subchains. Thus different regions undergo phase transition at different temperatures. This also explains the observation that the phase transition in microgels with higher BIS concentration is broader than the microgels with lesser cross-linker density because there is more heterogeneity in these samples.

PNIPAm microgels show interesting behavior in mixed solvents due to cononsolvency of pNIPAm.[96] The LCST of pNIPAm decreases with increase in concentration of methanol until 55% methanol, beyond that the LCST increases sharply.[97] The same effect is observed for microgels in mixed solvents and it was first observed by McPhee.[98] The mechanism for cononsolvency is explained by clatharate formation. Cosolvents like water and methanol form clatharate structures, which competes with pNIPAm for the water molecules that hydrate the polymer. Hence the deswelling of the polymer is observed as the water molecules are removed from the interior of the gel.[99]

Saunders et al. have studied the effect of electrolyte on the stability of the microgels.[99] It was observed that at a particular temperature particles flocculate at higher ionic strength. The swelling ability of the particles also depended on the ionic strength of the salt and its position in the Hoffmeister series.

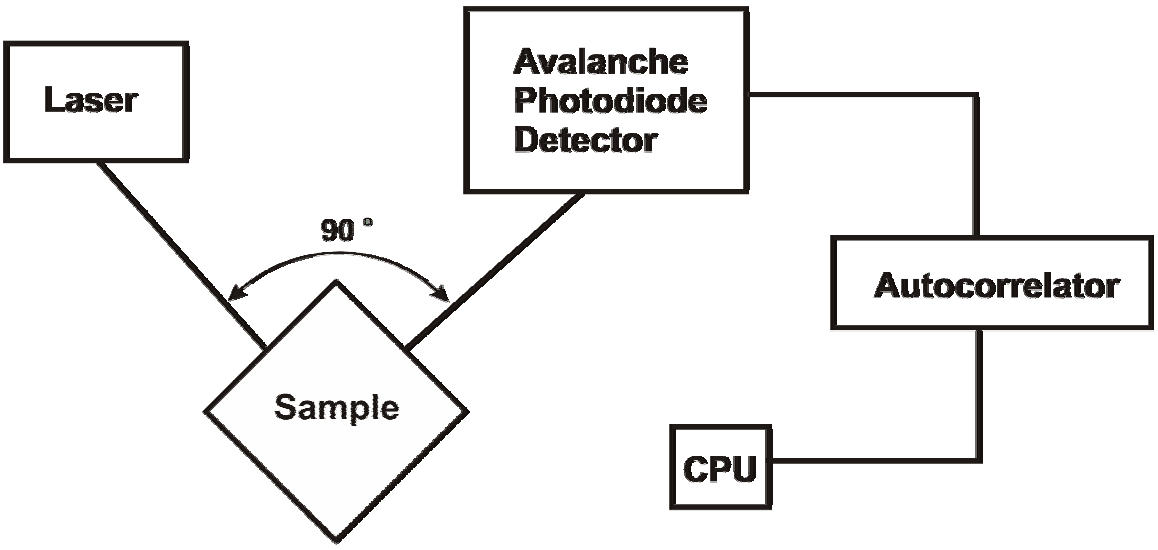

Figure 1-6. Schematic of Dynamic Light Scattering (DLS) setup. In this method the scattered light is detected at 90 ° from the light source and the signal from the detector is fed to the autocorrelator, which then gives the autocorrelation function, which is then used to calculate the diffusion coefficient of the particles

1.5.3 Characterization of Microgels

Several techniques have been used to characterize microgels.[70] Some of them are: light scattering, differential scanning calorimetry, fluorometry, small-angle neutron scattering, UV-VIS spectrophotometry, rheology and NMR. In our lab dynamic light scattering (DLS) has been used most often to study the solution behavior of the microgels, hence we will discuss this technique in some detail.[35,38]

All of the DLS experiments in this dissertation were carried out on a Protein Solutions DynaPro-MS/X. The schematic of the instrument layout can be found in Figure 1-6. The source is a semiconductor laser of λ = 784.8 nm. The light impinges on the sample through fiber optics and the scattered light at 90° to the source is collected by an

avalanche photodiode. The signal from the photodiode is fed to an autocorrelator board, from which the diffusion coefficient is calculated.

In DLS, the fluctuations in the scattered intensity are collected and these fluctuations are used to plot the autocorrelation function. The diffusion coefficient is then calculated from the decay of the autocorrelation function. Assuming that the particles have random Brownian motion the diffusion coefficient is used to calculate the hydrodynamic radius (R_h) of the particles from the Stoke-Einstein equation

$$R_h = \frac{k_b T}{6\pi\eta D} \qquad (1)$$

where k_b is the Boltzman constant, T is the temperature in Kelvin, η is the solvent viscosity and D is diffusion coefficient.[100] Figure 1-7 shows typical phase transition curve obtained for microgels by DLS.

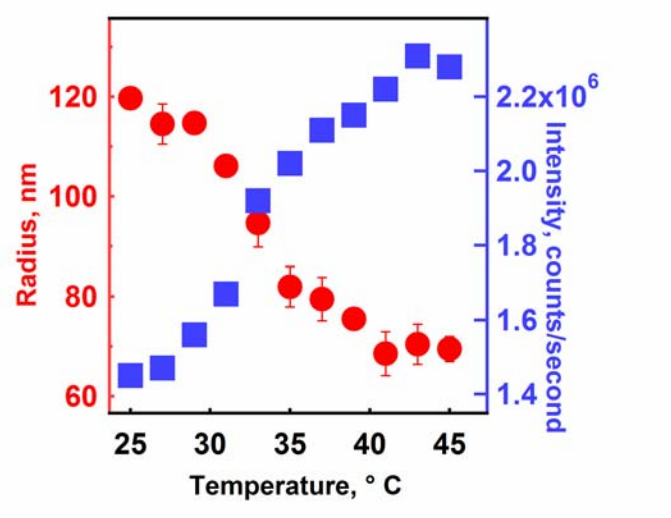

Figure 1-7. Volume phase transition curve obtained by DLS. As the R_h of the particle decreases the intensity of scattered light increases, due to the increase in refractive index contrast.

1.5.4 Applications of Microgels

Microgels made from "smart materials" have potential applications in several fields including drug delivery,[101-103] biosensing,[50,104] chemical separations,[105,106] catalysis[11,12] and optics.[36,37] Kawaguchi et al. have used thermoresponsive microgels in the field of biotechnology. In one system, pNIPAm bearing carboxyl groups at the end was polymerized, and then functionalized on to the microgels. The end carboxylic group was then used to attach an enzyme trypsin, resulting into a particle having two different kinds of pNIPAm chains on the surface one with trypsin and the other without it. The two different chains had different transition temperatures. The free chains collapsed at a lower temperature than the trypsin conjugated chains, hence exposing the enzyme for substrate

binding. Hence by this simple construct they were able to control the enzyme activity by controlling the temperature.[93]

In other example Choi et al. have used pNIPAm-co-acrylic acid microgels for targeting cells. In this case the acid groups were converted to amine groups by reacting the acid groups with ethylene diamine. The amine groups were then used for conjugating galactose to the particles. Hepatocytes have asialoglycoprotein receptors that recognize galactose and hence these galactosylated particles are internalized in these cells. This construct can be used for targeted delivery of drug carrier.[92]

1.5.5 Core/Shell Microgels

Our group has designed another method to prepare microgels with high concentration of the desired functionality on the surface of the particles. These particles are called core/shell microgels due to their morphology.[31-35,38] In this method a polymer shell, of same/different functionality as that of the core, is added on the preformed core particles thereby allowing control over the radial distribution of the functional groups in the particle.

In this synthesis, preformed pNIPAm core particles are taken in three-necked round bottom flask and heated to ~ 70 °C, followed by addition and initiation of the shell monomer solution. The reaction is carried out for ~ 4 h and then cooled and filtered. This method gives core/shell particles with no increase in polydispersity. To prevent heteronucleation there are several important parameters that should be controlled: concentration of the core, initiator, surfactant and the shell monomer.

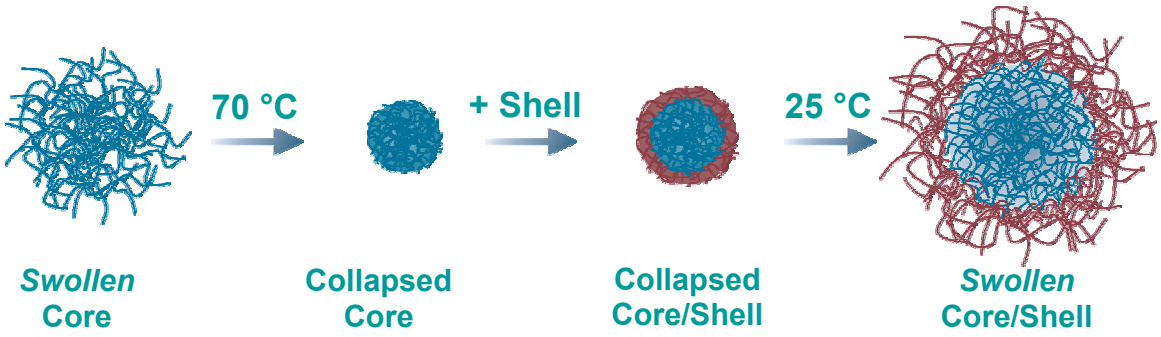

Figure 1-8. Scheme for core/shell particle synthesis. The collapsed core acts as a capturing entity for the growing shell polymer chains.

The mechanism with which this reaction takes place is somewhat similar to that for the core microgels. Since the reaction temperature is well above the VPTT of the core particles, the particles are in a collapsed state. The collapsed particles are hydrophobic and hence they tend to capture the growing oligomers, which results in formation of the shell.

Core/shell particles exhibit very interesting properties. Since the shell can have different comonomers the particles show multiple phase transition behavior with the increase in temperature.[35] Depending upon the cross-linker density of the shell, compression of the core is observed. Cross-linker density gradient is also observed in the shell.[34,38] Interpenetration of the polymer networks between the core and the shell is also

observed. All these properties make core/shell particles very complex and interesting materials.

This chapter dealt with the basic properties, synthesis, characterization and applications of thermoresponsive pNIPAm macrogels and microgels. The remaining chapters will deal with the synthesis and characterization of different types of microgels, which can potentially be used in different fields of biotechnology.

REFERENCES

(1) Yeomans, K. *Chem. Rev.* **2000**, *10*, 2-5.

(2) Hoffman, A. S. *Adv. Drug Deliv. Rev.* **2002**, *54*, 3-12.

(3) Gehrke, S. H. In *Advances in Polymer Science*; Springer-Verlag: Berlin, 1993; Vol. 110, pp 82-144.

(4) Compan, V.; Andrio, A.; Lopez-Alemany, A.; Riande, E.; Refojo, M. F. *Biomaterials* **2002**, *23*, 2767-2772.

(5) Kim, S. W.; Bae, Y. H.; Okano, T. *Pharm. Res.* **1992**, *9*, 283-290.

(6) Kim, J. J.; Park, K. *Bioseparation* **1998**, *7*, 177-184.

(7) Lee, K. Y.; Mooney, D. J. *Chem. Rev.* **2001**, *101*, 1869-1879.

(8) Drury, J. L.; Mooney, D. J. *Biomaterials* **2003**, *24*, 4337-4351.

(9) Nguyen, K. T.; West, J. L. *Biomaterials* **2002**, *23*, 4307-4314.

(10) Nagayama, H.; Maeda, Y.; Shimasaki, C.; Kitano, H. *Macromol. Chem. Phys.* **1995**, *196*, 611-620.

(11) Bergbreiter, D. E.; Case, B. L.; Liu, Y.-S.; Caraway, J. W. *Macromolecules* **1998**, *31*, 6053-6062.

(12) Bergbreiter, D. E.; Liu, Y.-S.; Osburn, P. L. *J. Am. Chem. Soc.* **1998**, *120*, 4250-4251.

(13) Hennink, W. E.; van Nostrum, C. F. *Adv. Drug Deliv. Rev.* **2002**, *54*, 13-36.

(14) Gombotz, W. R.; Wee, S. *Adv. Drug Deliv. Rev.* **1998**, *31*, 267-285.

(15) Goosen, M. F. A.; O'Shea, G. M.; Gharapetian, H. M.; Chou, S.; Sun, A. M. *Biotechnol. Bioeng.* **1985**, *27*, 146-150.

(16) Lutolf, M. P.; Raeber, G. P.; Zisch, A. H.; Tirelli, N.; Hubbell, J. A. *Adv. Mater.* **2003**, *15*, 888-892.

(17) Gacesa, P. *Carbohyd. Polym.* **1988**, *8*, 161-182.

(18) Watanabe, T.; Ohtsuka, A.; Murase, N.; Barth, P.; Gersonde, K. *Magnet. Reson. Med.* **1996**, *35*, 697-705.

(19) Eagland, D.; Crowther, N. J.; Butler, C. J. *Eur. Polym. J.* **1994**, *30*, 767-773.

(20) Mathur, A. M.; Hammonds, K. F.; Klier, J.; Scranton, A. B. *J. Control. Release* **1998**, *54*, 177-184.

(21) Nagahara, S.; Matsuda, T. *Polymer Gels and Networks* **1996**, *4*, 111-127.

(22) Peppas, N. A.; Benner, R. E., Jr. *Biomaterials* **1980**, *1*, 158-162.

(23) Dai, W. S.; Barbari, T. A. *J. Membrane Sci.* **2000**, *171*, 79-86.

(24) Sperinde, J. J.; Griffith, L. G. *Macromolecules* **1997**, *30*, 5255-5264.

(25) Sperinde, J. J.; Griffith, L. G. *Macromolecules* **2000**, *33*, 5476-5480.

(26) Li, Y.; Tanaka, T. *J. Chem. Phys.* **1989**, *90*, 5161-5166.

(27) Li, Y.; Tanaka, T. *J. Chem. Phys.* **1990**, *92*, 1365-1371.

(28) Tanaka, T.; Fillmore, D. J.; Sun, S.-T.; Nishio, I.; Swislow, G.; Shah, A. *Phys. Rev. Lett.* **1980**, *45*, 1636-1639.

(29) Tanaka, T. *Physica A* **1986**, *140A*, 261-268.

(30) Tanaka, T.; Wang, C.; Pande, V.; Grosberg, A. Y.; English, A.; Masamune, S.; Gold, H.; Levy, R.; King, K. *Faraday Discuss.* **1995**, *101*, 201-206.

(31) Gan, D.; Lyon, L. A. *J. Am. Chem. Soc.* **2001**, *123*, 7511-7517.

(32) Gan, D.; Lyon, L. A. *J. Am. Chem. Soc.* **2001**, *123*, 8203-8209.

(33) Gan, D.; Lyon, L. A. *Macromolecules* **2002**, *35*, 9634-9639.

(34) Gan, D.; Lyon, L. A. *Analytica Chimica Acta* **2003**, *496*, 53-63.

(35) Jones, C. D.; Lyon, L. A. *Macromolecules* **2000**, *33*, 8301-8306.

(36) Jones, C. D.; Serpe, M. J.; Schroeder, L.; Lyon, L. A. *J. Am. Chem. Soc.* **2003**, *125*, 5292-5293.

(37) Jones, C. D.; Lyon, L. A. *J. Am. Chem. Soc.* **2003**, *125*, 460-465.

(38) Jones, C. D.; Lyon, L. A. *Macromolecules* **2003**, *36*, 1988-1993.

(39) Jones, C. D.; McGrath, J. G.; Lyon, L. A. *J. Phys. Chem. B* **2004**, *108*, 12652-12657.

(40) Moselhy, J.; Wu, X. Y.; Nicholov, R.; Kodaria, K. *J. Biomater. Sci., Polym. Ed.* **2000**, *11*, 123-147.

(41) Duracher, D.; Sauzedde, F.; Elaissari, A.; Perrin, A.; Pichot, C. *Colloid Polym. Sci.* **1998**, *276*, 219-231.

(42) Duracher, D.; Sauzedde, F.; Elaissari, A.; Pichot, C.; Nabzar, L. *Colloid Polym. Sci.* **1998**, *276*, 920-929.

(43) Snowden, M. J.; Chowdhry, B. Z.; Vincent, B.; Morris, G. E. *J. Chem. Soc.-Faraday Trans.* **1996**, *92*, 5013-5016.

(44) Sershen, S. R.; Westcott, S. L.; Halas, N. J.; West, J. L. *J. Biomed. Mater. Res.* **2000**, *51*, 293-298.

(45) Sershen, S. R.; Westcott, S. L.; West, J. L.; Halas, N. J. *Appl. Phys. B* **2001**, *73*, 379-381.

(46) Sershen, S. R.; Westcott, S. L.; Halas, N. J.; West, J. L. *Applied Physics Letters* **2002**, *80*, 4609-4611.

(47) Suzuki, A.; Tanaka, T. *Nature* **1990**, *346*, 345-347.

(48) Suzuki, A.; Ishii, T.; Maruyama, Y. *J. Appl. Phys.* **1996**, *80*, 131-136.

(49) Tanaka, T.; Nishio, I.; Sun, S. T.; Ueno-Nishio, S. *Science (Washington, DC, United States)* **1982**, *218*, 467-469.

(50) Miyata, T.; Asami, N.; Uragami, T. *Nature* **1999**, *399*, 766-769.

(51) Ogawa, K.; Wang, B.; Kokufuta, E. *Langmuir* **2001**, *17*, 4704-4707.

(52) Ogawa, Y.; Ogawa, K.; Wang, B.; Kokufuta, E. *Langmuir* **2001**, *17*, 2670-2674.

(53) Ogawa, K.; Nakayama, A.; Kokufuta, E. *Langmuir* **2003**, *19*, 3178-3184.

(54) Schild, H. G. *Prog. Polym. Sci.* **1992**, *17*, 163-249.

(55) Winnik, F. M. *Macromolecules* **1990**, *23*, 1647-1649.

(56) Winnik, F. M. *Langmuir* **1990**, *6*, 522-524.

(57) Winnik, F. M. *Macromolecules* **1990**, *23*, 233-242.

(58) Wu, C.; Zhou, S. *Macromolecules* **1995**, *28*, 8381-8387.

(59) Wu, C.; Zhou, S. *Macromolecules* **1995**, *28*, 5388-5390.

(60) Wu, C.; Zhou, S. *Macromolecules* **1996**, *29*, 1574-1578.

(61) Wu, C. *Polymer* **1998**, *39*, 4609-4619.

(62) Wu, C.; Qiu, X. *Phys. Rev. Lett.* **1998**, *80*, 620-622.

(63) Wu, C.; Wang, X. *Phys. Rev. Lett.* **1998**, *80*, 4092-4094.

(64) Shibayama, M.; Tanaka, T. In *Advances in Polymer Science*; Springer-Verlag: Berlin, 1993; Vol. 109, pp 1-62.

(65) Matsuo, E. S.; Tanaka, T. *J. Chem. Phys.* **1988**, *89*, 1695-1703.

(66) Tanaka, T.; Fillmore, D. J. *J. Chem. Phys.* **1979**, *70*, 1214 - 1218.

(67) Yan, Q.; Hoffman, A. S. *Poly. Commun.* **1995**, *36*, 887-889.

(68) Park, T. G.; Hoffman, A. S. *J. Biomed. Mater. Res.* **1990**, *24*, 21-38.

(69) Kim, S.; Healy, K. E. *Biomacromolecules* **2003**, *4*, 1214-1223.

(70) Pelton, R. *Adv. Colloid. Interface Sci.* **2000**, *85*, 1-33.

(71) Pelton, R.; Richardson, R.; Cosgrove, T.; Ivkov, R. *Langmuir* **2001**, *17*, 5118-5120.

(72) Kawaguchi, H. *Prog. Polym. Sci.* **2000**, *25*, 1171-1210.

(73) Braun, O.; Selb, J.; Candau, F. *Polymer* **2001**, *42*, 8499-8510.

(74) Dowding, P. J.; Vincent, B.; Williams, E. *J. Colloid Interf. Sci.* **2000**, *221*, 268-272.

(75) Guo, Z. L.; Wang, J. T.; Zhu, H. J. *Acta Polym. Sin.* **2001**, 489-493.

(76) HernandezBarajas, J.; Hunkeler, D. *Polymer* **1997**, *38*, 5623-5641.

(77) Landfester, K.; Willert, M.; Antonietti, M. *Macromolecules* **2000**, *33*, 2370-2376.

(78) Ming, W. H.; Zhao, Y. Q.; Cui, J.; Fu, S. K.; Jones, F. N. *Macromolecules* **1999**, *32*, 528-530.

(79) Neyret, S.; Vincent, B. *Polymer* **1997**, *38*, 6129-6134.

(80) Platkowski, K.; Pross, A.; Reichert, K. H. *Polym. Int.* **1998**, *45*, 229-238.

(81) Pross, A.; Platkowski, K.; Reichert, K. H. *Polym. Int.* **1998**, *45*, 22-26.

(82) Wu, C.; Zhou, S. Q. *J. Macromol. Sci. Phys.* **1997**, *B36*, 345-355.

(83) Glukhikh, V.; Graillat, C.; Pichot, C. *J. Polym. Sci. Pol. Chem.* **1987**, *25*, 1127-1161.

(84) Delair, T.; Meunier, F.; Elaissari, A.; Charles, M. H.; Pichot, C. *Colloid. Surf. A* **1999**, *153*, 341-353.

(85) Fujimoto, K.; Nakajima, Y.; Kashiwabara, M.; Kawaguchi, H. *Polym. Int.* **1993**, *30*, 237-241.

(86) Fujimoto, K.; Nakahama, K.; Shidara, M.; Kawaguchi, H. *Langmuir* **1999**, *15*, 4630-4635.

(87) Kasuya, Y.; Fujimoto, K.; Kawaguchi, H.; Miyamoto, M. *Biomaterials* **1994**, *15*, 570-576.

(88) Makino, K.; Yamamoto, S.; Fujimoto, K.; Kawaguchi, H.; Ohshima, H. *J. Colloid Interf. Sci.* **1994**, *166*, 251-258.

(89) Shiroya, T.; Tamura, N.; Yasui, M.; Fujimoto, K.; Kawaguchi, H. *Colloid. Surface. B* **1995**, *4*, 267-274.

(90) Yasui, M.; Shiroya, T.; Fujimoto, K.; Kawaguchi, H. *Colloid. Surface. B* **1997**, *8*, 311-319.

(91) Zhou, G.; Elaissari, A.; Delair, T.; Pichot, C. *Colloid Polym. Sci.* **1998**, *276*, 1131-1139.

(92) Choi, S. H.; Yoon, J. J.; Park, T. G. *J. Colloid Interf. Sci.* **2002**, *251*, 57-63.

(93) Kawaguchi, H.; Kisara, K.; Takahashi, T.; Achiha, K.; Yasui, M.; Fujimoto, K. *Macromol. Symp.* **2000**, *151*, 591-598.

(94) Kawaguchi, H.; Fujimoto, K.; Nakazawa, Y.; Sakagawa, M.; Ariyoshi, Y.; Shidara, M.; Okazaki, H.; Ebisawa, Y. *Colloid Surf. A-Physicochem. Eng. Asp.* **1996**, *109*, 147-154.

(95) Wu, C.; Zhou, S. *Macromolecules* **1997**, *30*, 574-576.

(96) Crowther, H. M.; Vincent, B. *Colloid Polym. Sci.* **1998**, *276*, 46-51.

(97) Winnik, F. M.; Ringsdorf, H.; Venzmer, J. *Macromolecules* **1990**, *23*, 2415-2416.

(98) McPhee, W.; Tam, K. C.; Pelton, R. *J. Colloid Interface Sci.* **1993**, *156*, 24-30.

(99) Daly, E.; Saunders, B. R. *Langmuir* **2000**, *16*, 5546-5552.

(100) Pecora, R. *Dynamic Light Scattering*; Plenum Press: New York, 1985.

(101) Jeong, B.; Bae, Y. H.; Lee, D. S.; Kim, S. W. *Nature* **1997**, *388*, 860-862.

(102) Kurisawa, M.; Terano, M.; Yui, N. *Macromol. Rapid Commun.* **1995**, *16*, 663-666.

(103) Brondsted, H.; Kopecek, J. *Pharm. Res.* **1992**, *9*, 1540-1545.

(104) Holtz, J. H.; Asher, S. A. *Nature* **1997**, *389*, 829-832.

(105) Umeno, D.; Kawasaki, M.; Maeda, M. *Bioconj. Chem.* **1998**, *9*, 719-724.

(106) Kawaguchi, H.; Fujimoto, K. *Bioseparation* **1998**, *7*, 253-258.

CHAPTER 2

NANOCOMPOSITE THIN FILMS

In this chapter the deswelling behavior of nanocomposite hydrogel films composed of poly(*N*-isopropylacrylamide) (pNIPAm) is discussed. These films were synthesized first by formation of pNIPAm microgel particles via precipitation polymerization, followed by polymerization of these particles into a pNIPAm thin film gel matrix immobilized on a glass slide. The deswelling behavior of these composite films was studied by temperature-dependent light scattering (i.e. turbidity). In conventional (not microstructured) films the scattering increases and plateaus as the temperature is increased beyond the lower critical solution temperature (LCST) of pNIPAm. In contrast to these conventional films, microgel composite films display an increase in turbidity until the LCST, followed by a rapid turbidity decrease beyond the LCST. It is also observed that the rate at which scattering decreases depends on the concentration of the hydrogel particles in the film. Together, these results offer insight into the morphological changes occurring during the deswelling processes in composite hydrogel thin films.

2.1 Introduction

Monolithic hydrogels reach equilibrium slowly, with swelling times in many cases ranging from few hours to days.[1,2] Such sluggish kinetics may make such materials inappropriate for many applications. To use these hydrogels for drug delivery, chemical

separations, and fluidics,[3-5] it is often essential that these hydrogels display fast responses to the selected stimuli. Several methods have been employed to decrease the response time of hydrogels. Hoffman et al.[6] have made fast responding macroporous hydrogels by synthesizing them at temperatures above the LCST, wherein the polymer phase separates as it is formed. Crosslinking between the aggregated polymer chains results in hydrogels with a macroporous structure, which then facilitated the rapid delivery of macromolecules. Serizawa et al.[7] have synthesized porous hydrogels by incorporating spherical silica particles into gels, followed by removal of the silica particles. The hydrogels obtained by this method had porous structure and exhibited a rapid deswelling rate, which increased with an increase in the number of silica particles in the gel. Chen et al.[8] have made superporous hydrogels by polymerization of various vinyl monomers in the presence of gas bubbles formed by aqueous $NaHCO_3$. These bubbles were trapped inside the hydrogels during polymerization, thereby providing a fast responding superporous hydrogel. Cai et al.[9] have made fast responding bulk hydrogels by crosslinking poly(*N*-isopropylacrylamide-*co*-acrylic acid) microgels in a pNIPAm polymer network; these hydrogels have very high swelling ratios and faster swelling rates, which was attributed to the presence of ionic microgels in the bulk gel. Finally, Kato et al.[10] have made fast responsive hydrogels first by freeze-drying the hydrogels and then reswelling them in water. In comparison to conventional hydrogels, the freeze-dried hydrogels collapsed about two orders of magnitude faster when subjected to temperature jump.

In this chapter the preparation of composite hydrogel films and studies of their deswelling and equilibration behavior are reported. In contrast to the work described

above, the main focus is not on the traditional dimensional deswelling rates (thickness vs. time), but rather the long timescale, internal restructuring of the thin films (light scattering vs. time). It has been demonstrated that hydrogels continue to redistribute water and polymer aggregates long after the macroscopic dimensional changes of the gel have ceased.[1] The influence of added microstructure in the form of pNIPAm microgels,[11] contributes to the long timescale equilibration of pNIPAm thin films, as shown by light scattering measurements. Composite films are synthesized by crosslinking pNIPAm microgels into a pNIPAm polymer network and the deswelling behavior of these films is studied by light scattering. It is observed that these films reach their light scattering equilibrium much faster than their non-nanostructured counterparts, suggesting the morphological equilibration of the deswollen film is facilitated by the presence of the microgels. It is also observed that the rate at which these films equilibrate increases with the concentration of the microgels in the film.

2.2 Experimental Section

Materials

N-Isopropylacrylamide (NIPAm, Aldrich) was purified by recrystallization from hexane (J. T. Baker) prior to use. *N, N'*-Methylenebis(acrylamide) (BIS), ammonium persulfate (APS), 2,2-diethoxyacetophenone were purchased from Aldrich and used as received. 3-Acryloylpropyltrimethoxy silane was purchased from United Chemical Technologies. Water was purified with Barnstead E-Pure system to a resistance of 18 MΩ and then filtered through a 0.2 μm filter to remove particulate matter.

Particle Synthesis

PNIPAm particles were synthesized by precipitation polymerization as described previously.[11-15] NIPAm (1.5 g) and BIS (0.03 g) were dissolved in 100 mL of water and filtered through a 0.2 μm membrane filter (Pall Gelman Metricel) to remove any particulate matter. The reaction mixture was transferred into 250 mL round bottom flask, after which it was heated to and kept at 70 °C under gentle nitrogen stream for 40 minutes. APS (0.05 g) was added to initiate reaction. The reaction mixture was kept at 70 °C under nitrogen for at least 4 h to complete the reaction. After synthesis, the hydrogel solution was filtered using fine porosity filter paper (Fisher Scientific) to remove any aggregated material. The particles were then purified by dialysis (Spectra/Por 7 dialysis membrane, MWCO 10,000) against daily changes of water for at least 7 days. Particles were freeze-dried (Freezone 4.5 Labconco, Missouri) before using them in preparation of films.

Glass Slide Preparation

Microscope slides were cut in such a fashion that they would fit diagonally (for scattering measurements) and laterally (for microscope experiments) in standard 1-cm path-length plastic cuvettes (Fisher Scientific). The cut glass slides were cleaned in piranha solution (1:4 H_2O_2: H_2SO_4) at 70 °C for one hour (**Caution**: Piranha solutions react violently in the presence of many organic compounds and should be handled with extreme caution), after which they were rinsed thoroughly with water and dried in an oven. For silanization, a 1% ethanolic solution of 3-acryloylpropyltrimethoxy silane was poured in a Copeland jar containing cleaned glass slides. Silanization was carried out for

2 h, after which the glass slides were removed and washed thoroughly with 95% ethanol. The slides were stored in ethanol until use.

Preparation of film solutions

To prepare solutions for film polymerization, 0.9 g of NIPAm and 0.1 g of the crosslinker (BIS) were dissolved in 5 ml water. To this solution, 2 μL of the photoinitiator 2,2- diethoxyacetophenone was added. Separately, 50 mg of the freeze-dried particles was dissolved in 5 ml of water. This solution was homogenized for one day to allow the particles to resuspend and re-swell completely. For polymerization, several solutions were made with varying ratios of the monomer solution and the polymer solution according to Table 2-1. Note that these preparations all contain the same total solids concentration and total volume. Thus, the results presented below should not be attributable to changes in the film density brought about by differences in the total solids content.

Film Photopolymerization

The method of film preparation is summarized in Figure 2-1. Silanized glass slides were dried under nitrogen and covered with a sheet of parafilm. A small rectangular region of the parafilm was cut in order to form a well on the glass slides. This structure is designed to provide a film of the approximate thickness of the parafilm. A few drops of the microgel/monomer/initiator solution were put in the parafilm well and the solution was squeezed with a second (unsilanized) glass cover slip. This "sandwich" structure was kept on an ice jacket, and the solution was photopolymerized using a UV arc lamp (Oriel Corporation, Connecticut) for 40 minutes. After photopolymerization, the cover slip and the parafilm were removed and the film-modified glass slides were stored

in water. The water was changed every day for two weeks to remove unreacted monomer and initiator.

Table 2-1. Solution compositions used for film preparation.

Sample #	Particle solution volume[a] (ml)	Monomer solution volume[b] (ml)	Total volume[c] (ml)
0	0.00	0.200	1
1	0.05	0.197	1
2	0.20	0.190	1
3	0.35	0.182	1
4	0.50	0.175	1
5	0.65	0.167	1
6	0.80	0.160	1

[a]The particle solution was 0.01 g/ml; [b]monomer solution was 0.2 g/ml plus 2µl of the photoinitiator; [c]each sample was diluted to 1 ml with deionized water.

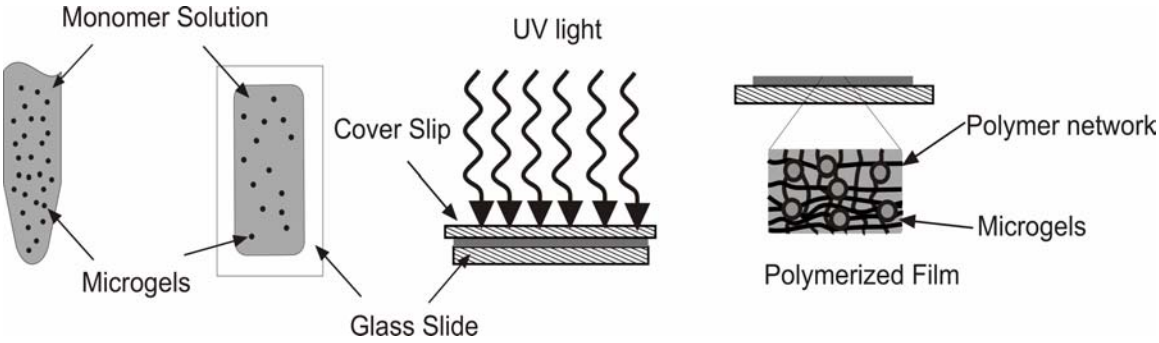

Figure 2-1. Preparation of nanocomposite films.

Temperature-dependent scattering measurements

A steady-state fluorescence spectrophotometer (Photon Technology International) equipped with a Model 814 PMT photon-counting detector was used to record scattering as a function of temperature. The temperature was controlled using a PE 60 Temperature Controller and Peltier Stage (Linkam Scientific Instruments Ltd., Surrey, UK). The slides with the polymerized films were kept diagonally in the cuvettes such that the scattered light was collected by the detector at 90° to the incident beam (Figure 2-2). The slit widths were set to a bandwidth of 1 nm and the excitation and emission monochromators were set to pass 600 nm. The solution temperature was measured with a platinum resistor immersed in the solution; the temperature accuracy was ± 0.1 °C, as specified by the manufacturer. For temperature ramp experiments the films were heated at a particular

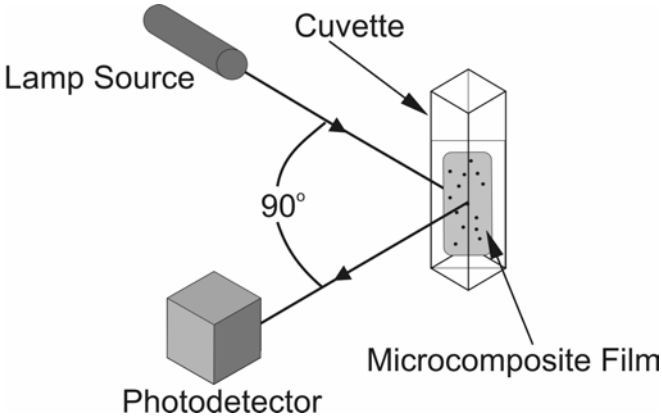

Figure 2-2. Experimental setup for measurement of light scattering from microcomposite films.

rate and the scattered light intensity was recorded as a function of temperature. For equilibrium measurements the films were heated to a certain temperature at a constant rate and held at that temperature until the scattering intensity stabilized. Scattering ratio was plotted as function of temperature for comparison of scattering plots for different heating rates and also for equilibrium plots

$$Scattering\ Ratio = \frac{I_T - I_0}{I_0}$$

where I_0 is the scattering intensity at 26 °C and I_T is the scattering intensity at each respective temperature.

Optical Microscopy

Brightfield microscopy images were obtained with an Olympus IX-70 inverted microscope using standard brightfield optics. The film-modified slides were attached to the wall of the cuvette with a double-sided tape. The cuvette was filled with water and sealed with a cuvette lid. The cuvette was placed on the stage such that the film could be observed in profile. The film temperature was controlled using a Peltier-controlled temperature stage (Physitemp). Images were obtained using a color CCD camera (Coolsnap, Photometrics).

2.3 Results and Discussion

Particle Characterization

The particles were synthesized by a standard precipitation polymerization technique, as described above.[11-15] Photon Correlation Spectroscopy (PCS) was used to determine the hydrodynamic diameter (D_h) of the particles as described previously.[12-16] The D_h of the particles was found to be ~600 nm with polydispersity of 16%.

Preparation of Films

Solutions containing varying feed ratios of microgel solution to monomer solution were made according to Table 2-1, where Sample 0 contains no microgels, while Sample 6 contains the highest concentration of microgels. These solutions were photopolymerized on silanized glass having acrylate groups on the surface to obtain strong adhesion of the film to the glass surface. Since the films are on the order of 100 μm thick, this supported film format facilitates the positioning of the film for the measurement of the optical properties. Formation of the composite film is shown in

Figure 2-1. It should be noted that others have recently studied the influence of the substrate and film pinning on the deswelling characteristics of hydrogel films and have shown profound dependencies of film thickness on the deswelling properties due to the presence of the substrate.[17,18] However, the films discussed in this contribution are many orders of magnitude thicker than the critical thickness for strong substrate effects determined by those researchers.[17] Thus, we expect the influence of the substrate to be minimal in these studies.

Scattering measurements

The films were characterized by light scattering (turbidity) measurements as illustrated in Figure 2-2. Films were placed diagonally in a plastic cuvette filled with water and were heated at a constant rate. The scattered light was then detected at 90° with respect to the incident radiation as a function of temperature. Since these films are composed of thermoresponsive pNIPAm, they show a volume phase transition at or near the LCST of the polymer (~32 °C). Figure 2-3 depicts the various stages of the process of the deswelling of the film. Initially the film is swollen and transparent as water-polymer interactions dominate due to hydrogen bonding between water and the amides of the polymer side chains. On heating, polymer-polymer hydrophobic interactions tend to become stronger than water-polymer interactions, thus resulting in the formation of polymer aggregates in the film. Due to the inherent inhomogeneity in the film, certain regions in the film have a higher tendency to expel water and aggregate resulting in the formation of microheterogeneities on the surface and in the bulk of the film. This effect is typically referred to as spinodal decomposition.[1,19]

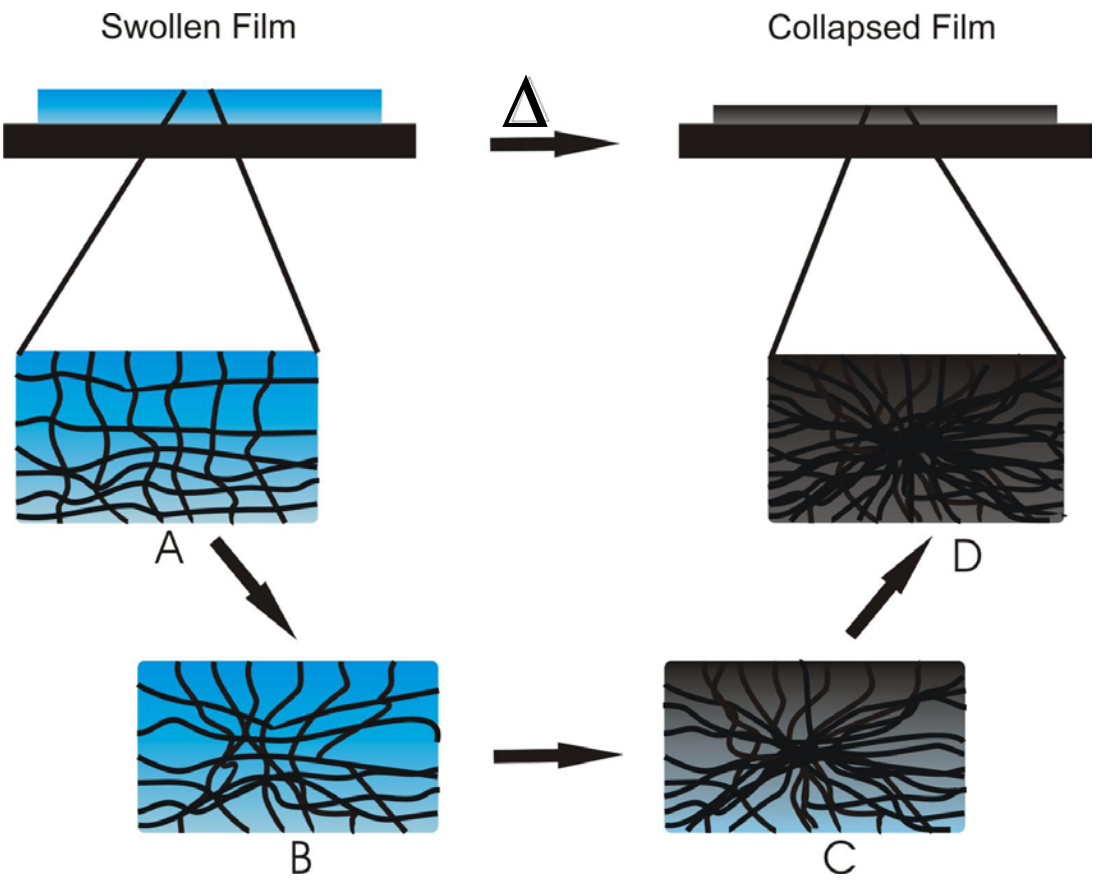

Figure 2-3. Deswelling of non-composite films.

A- Swollen film solvent-polymer interactions dominate

B- Formation of microheterogeneity (spinodal decomposition) polymer-polymer interactions get stronger than solvent –polymer interaction

C- Polymer-polymer interaction dominate expelling water resulting in skin layer and trapping water in the film

D- Completely deswollen film

Due to the formation of microheterogeneities, the scattering intensity rises due to increase in the difference between the refractive indices of the collapsed regions (high polymer concentration) and the surrounding regions (low polymer concentration). On further heating, the size of the microheterogeneities grows due to further aggregation of the polymer network, while the less concentrated regions become more dilute due to an increase in local water content. The scattering intensity grows with the increase in the size of the microheterogeneities until those heterogeneities become significantly larger than the wavelength of light. Further increase in the size of microheterogeneities does not bring about any increase the scattering intensity. For complete homogenization of the film to occur, the water must be expelled uniformly from the gel. By comparison, when low cross link density monolithic gels are heated, they undergo shrinking in two steps with the first step being rapid release of water from weakly densified regions close to the surface of the gel. This results in the formation of a densified skin layer on the surface of the gel, which traps water in the interior.[20-22] Thus, the second step is slow expulsion of water from the interior of the gel through the skin layer.

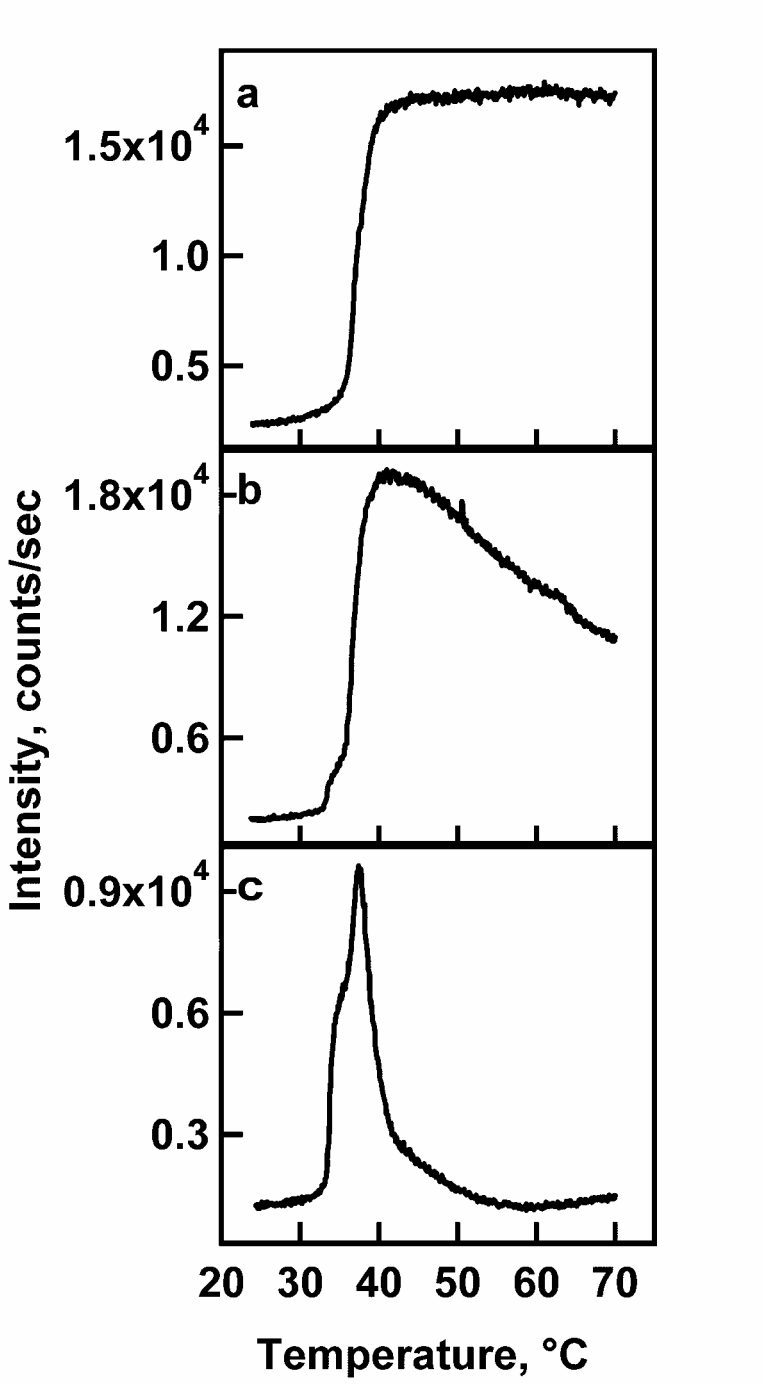

Figure 2-4. Scattering intensity of microgel composite films as a function of temperature at a scan rate of 1 °C/min. (a) Sample 0, (b) Sample 2, (c) Sample 6. See Table 2-1 for film preparation conditions.

Figure 2-4 shows the scattering intensity of the films as a function of temperature when the films are heated at 1 °C/min. For Sample 0 (no microgels added) the scattering intensity increases beyond the LCST of pNIPAm and then stabilizes at higher temperature. However, for Samples 2 through 6 it is observed that the scattering intensity decreases at higher temperature while the rate at which scattering decreases depends on the concentration of the microgels in the film. Hu et al. have shown that gels without any purposely-added nanostructure display a turbidity decrease at high temperatures (above the VPTT) when the system is completely equilibrated at each temperature.[1] The proposed reason for this phenomenon is attributed to the uniform and complete expulsion of water from the network when gels are heated at a rate that approximates the equilibration rate. In case of Samples 2 and 6, where the scattering decreases at high temperature, it appears that the particles facilitate release of water from the interior of the films even for heating rates far from the equilibrium heating rate. Samples 2 and 6 also show a small shoulder on the scattering peak during the initial stages of deswelling that is absent for Sample 0. The shoulder is larger for Sample 6 in comparison to Sample 2 indicative that the shoulder is due to particle deswelling in the film and also that the particles collapse at a faster rate and/or at a lower temperature than the bulk film.

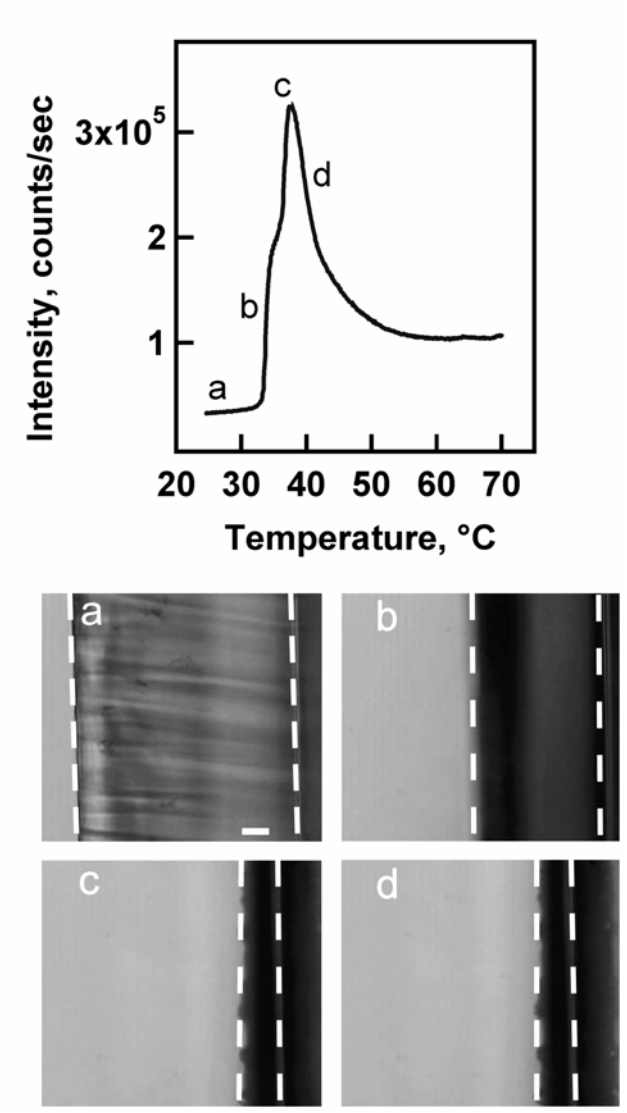

Figure 2-5. Brightfield optical microscopy images of Sample 5 at the temperatures indicated on the scattering intensity plot. The film was heated on the microscope stage at a rate of 1 °C/min. The dashed white lines indicate the water/film and film/glass interfaces, with the film deswelling from the left to the right. Scale bar = 20 μm.

Microscopic observation of film deswelling

The deswelling of the films was observed visually by heating the films while observing the film in cross-section on a light microscope as described in the experimental section. Figure 2-5 shows the scattering plot for Sample 5 and the corresponding state of the film at the indicated temperatures. It is observed that the film deswells ~10-fold in thickness from 25 °C to 40 °C. Beyond that temperature there is no observable change in the thickness of the film despite the observed decrease in the scattering at those temperatures. This suggests that decreases in the scattering of the film above 40 °C are due to the internal rearrangement of solvent and polymer in the film, and are not associated with gross changes in the film dimensions.

Scan Rate Dependence on Deswelling

The films were heated at three different scan rates to elucidate the contribution of film deswelling kinetics to the observed behavior. Figure 2-6 shows the scattering ratios of Samples 0, 2, 4 and 6 as a function of temperature, where each film is heated at three different rates: 1 °C/min, 2.5 °C/min and 4 °C/min. All scan rates shown here are faster than the characteristic deswelling rate of the films and are thus non-equilibrium scans. As expected given the above discussion, it is observed that the heating rate has a significant impact on the observed scattering intensity curves of the films. The scattering intensity for a given film at a given temperature depends on the rate at which the film was heated to that temperature, which is consistent with the effect observed by Hu et. al.[1] However, for Sample 6 it is observed that the scattering intensity above the VPTT reaches about the same level irrespective of the heating rate. This effect can again be attributed to the

ability of the films with higher particle loading to facilitate release of water from the interior of the film as compared to films with low (or no) particle loading.

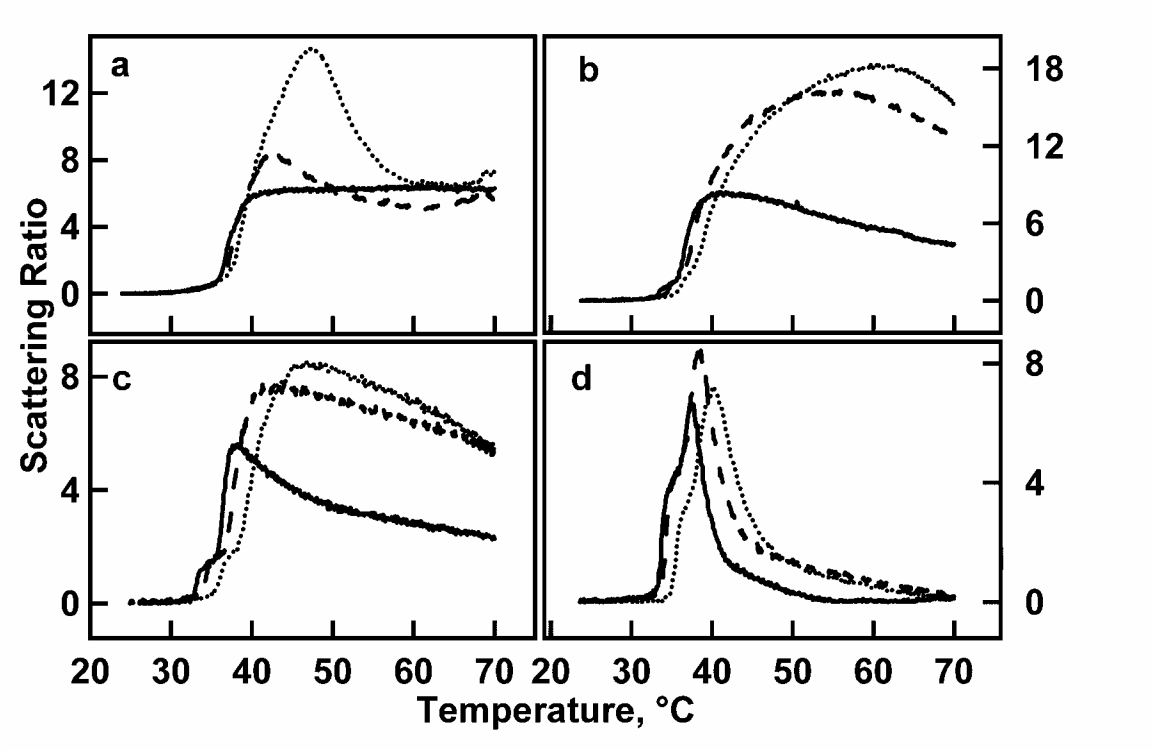

Figure 2-6. Scattering intensity ratios as a function of heating rate: 1 °C/min (solid line), 2.5 °C/min (dashed), and 4 °C/min (dotted). (a) Sample 0, (b) Sample 2, (c) Sample 4, and (d) Sample 6.

Relaxation Plots

To deconvolute the kinetic and thermodynamic contributions to the observed behavior and also to characterize the time scale for film equilibration, relaxation plots were obtained. The films were rapidly heated to 50 °C, which is higher than the critical phase transition temperature, at different rates and were then held at that temperature. The scattering intensity was then recorded as a function of time to observe the equilibration of the film. For each film the scattering was recorded for 8000 seconds. Figure 2-7 shows relaxation plots for Samples 0, 2, 5, and 6. It was observed that for all films the scattering intensity for different heating rates approach to the same final value but have scan rate dependent peak intensities and relaxation rates. This suggests that for different heating rates the films have the same thermodynamic minimum but reach those states via different pathways. This is expected, as faster heating rates should take the system further from equilibrium, thus increasing the time required for homogenization, *i.e.* removal of water. Samples 0 and 2 do not reach a stable scattering intensity even after a time window of 8000 seconds. However, for all heating rates Samples 5 and 6 reach stable scattering intensities at ~ 4000 and 2000 seconds, respectively. This observation confirms the hypothesis that the particles in the film facilitate the long timescale homogenization of the films.

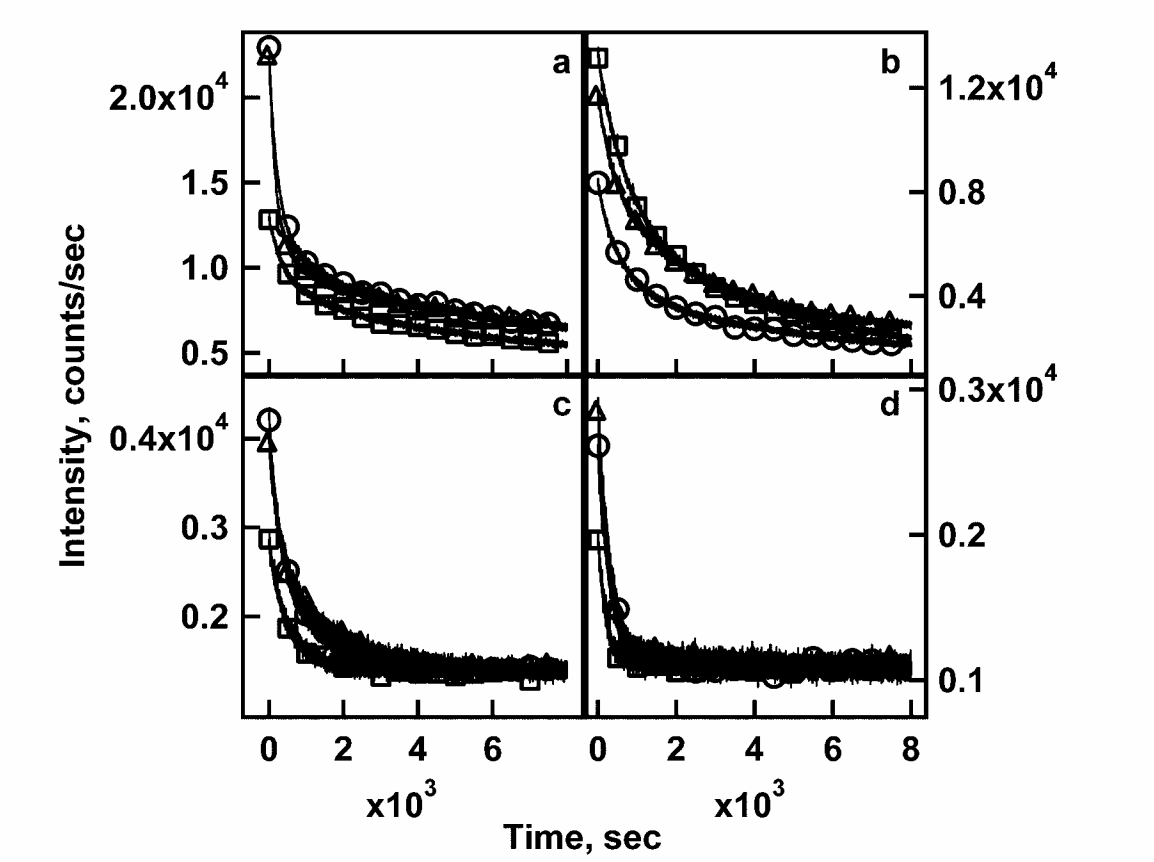

Figure 2-7. Relaxation plots following heating to 50 °C at the following heating rates: 1 °C/min (squares), 2.5 °C/min (triangles), and 4 °C/min (circles). (a) Sample 0, (b) Sample 2, (c) Sample 5, and (d) Sample 6. Time=0 is defined as the time when the solution surrounding the film attains a temperature of 50 °C. The symbols are meant to differentiate between the curves and do not represent actual data points.

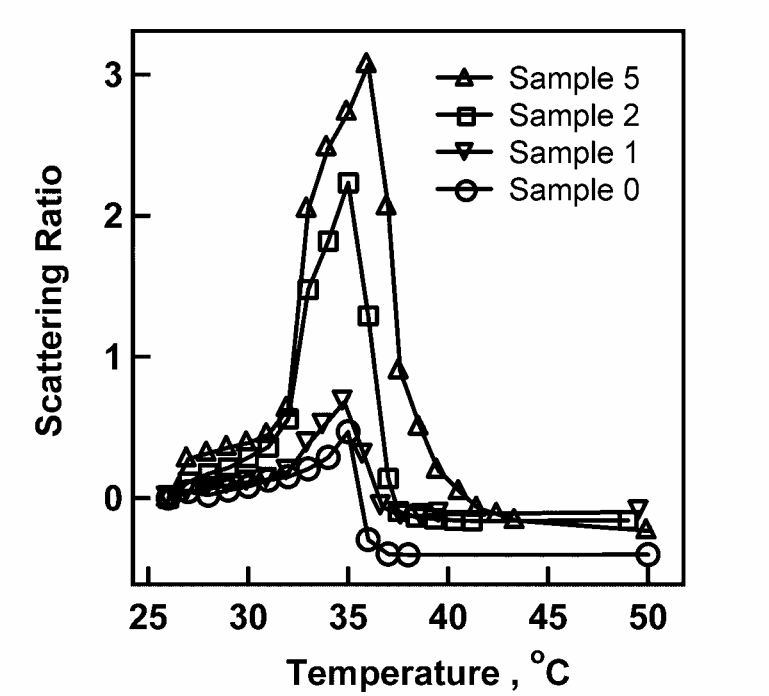

Figure 2-8. Equilibrium scattering intensity plots as a function of temperature for the indicated Samples. Lines are drawn to guide the eye.

Equilibrium Deswelling

Pure equilibrium plots were obtained for the films by heating the films to each temperature and then allowing the scattering intensity to stabilize. Figure 2-8 shows pure equilibrium plots where the final stable scattering intensity, which is normalized with respect to the initial scattering intensity at 26 °C, is plotted as a function of temperature. It is observed that higher particle concentrations lead to higher peak intensities and also larger shoulders near the deswelling temperature. For Sample 0 the scattering intensity above the deswelling temperature decreases to a value much lower than the value recorded at 25 °C. This is in agreement with the effect observed by Hu et al., where the gel was observed to be transparent at equilibrium both above and below the critical phase transition temperature.[1] It is interesting to note that the shoulder observed during the initial stages of deswelling is present both in the non-equilibrium (Figure 2-4) and equilibrium (Figure 2-8) scans. This suggests that the shoulder, which is most likely due to particle deswelling, is not solely due to the dynamics of the system (e.g. faster particle deswelling) but is due also to a thermodynamic preference for particle deswelling at temperatures below that of the photopolymerized film. Cohen et al.[23] have shown that gels with higher crosslinking density scatter more light in comparison to low crosslinked gels when they undergo phase transition. This was attributed to a larger number of inherent heterogeneities in the gels with higher crosslinking density. This phenomenon is analogous to the one observed for these nanostructured films, where the inherent heterogeneities are due to the particles in the film and the crosslinking in the bulk gel. When these films are heated, the particles collapse first and form microheterogeneities in the film, which cause an increase in the scattering intensity due to difference in refractive

indices of the collapsed particle and the surrounding bulk gel. Thus one would expect higher particle concentrations to yield higher overall scattering intensities at the VPTT.

Deswelling Mechanism for Composite Films

It is observed from the pure equilibrium and dynamic scattering experiments that during the initial periods of deswelling of the films with microgels there is a pronounced shoulder. This shoulder is attributed to the deswelling of the particles. It is also observed that the size of the shoulder depends on the concentration of the particles in the film. From Figures 2-4 and 2-8 it can be seen that for the same heating rate, the temperature at which the particles collapse is the same for all the films. This indicates that the particles collapse independently of the surrounding polymer network both in a thermodynamic and dynamic fashion. This can to a first approximation be understood by considering that the microgel particles have a 2% (mol-%) crosslink density while the bulk gel is 10% crosslinked. Since it is generally understood that pNIPAm gels with lower crosslinking densities have a lower VPTT,[24-28] it is proposed that when the particles deswell they may be forming a void around them into which they expel water. When the surrounding bulk gel undergoes its VPT, the regions in the film that have a higher tendency to collapse may expel water in these voids. This, in turn, may result into formation of channels which aid the expulsion of water and hence homogenization of the film. The probability of these films forming enough of these channels increases with the increase in the concentration of the particles in the film, hence the observation of faster homogenization in films with higher particle concentrations.

2.4 Conclusions

The deswelling behavior of microstructured hydrogel films has been studied using temperature dependent light scattering measurements (turbidity). Following the film volume phase transition, it is observed that a slow restructuring of the film occurs, which is due to solvent and polymer aggregate redistribution. This restructuring occurs on the timescale of hours, while the actual film thickness changes occur in minutes for the 100 μm thick films studied here. When microgels prepared by precipitation polymerization are co-polymerized into the thin film, it is observed that such films homogenize faster than those without added microstructure, as evidenced by the rate of long timescale equilibration of film turbidity. Microgels present in the film play a major role in this observed phenomenon, as they collapse at a lower temperature and at a faster rate than the bulk gel, which in turn facilitates the restructuring and expulsion of water from the films. It is expected that such constructs may form the basis for fast-responding hydrogel films, which are of interest in applications such as microfluidic valves and controlled release.

REFERENCES

(1) Hu, Z.; Wang, C.; Chen, Y.; Zhang, X.; Li, Y. *J. Polym. Sci., Part B: Polym. Phys.* **2001**, *39*, 2168-2174.

(2) Takigawa, T.; Yamawaki, T.; Takahashi, K.; Masuda, T. *Polym. J. (Tokyo)* **1999**, *31*, 595-598.

(3) Beebe, D. J.; Moore, J. S.; Bauer, J. M.; Yu, Q.; Liu, R. H.; Devadoss, C.; Jo, B. H. *Nature* **2000**, *404*, 588-590.

(4) Beebe, D. J.; Moore, J. S.; Yu, Q.; Liu, R. H.; Kraft, M. L.; Jo, B.-H.; Devadoss, C. *Proc. Natl. Acad. Sci. U. S. A.* **2000**, *97*, 13488-13493.

(5) Yu, Q.; Bauer, J. M.; Moore, J. S.; Beebe, D. J. *Appl. Phys. Lett.* **2001**, *78*, 2589-2591.

(6) Yan, Q.; Hoffman, A. S. *Poly. Commun.* **1995**, *36*, 887-889.

(7) Serizawa, T.; Wakita, K.; Kaneko, T.; Akashi, M. *Journal of Polymer Science Part a-Polymer Chemistry* **2002**, *40*, 4228-4235.

(8) Chen, J.; Park, H.; Park, K. *J. Biomed. Mater. Res.* **1999**, *44*, 53-62.

(9) Cai, W. S.; Gupta, R. B. *J. App. Polym. Sci.* **2002**, *83*, 169-178.

(10) Kato, N.; Sakai, Y.; Shibata, S. *Macromolecules* **2003**, *36*, 961-963.

(11) Pelton, R. *Adv. Colloid. Interface Sci.* **2000**, *85*, 1-33.

(12) Debord, J. D.; Eustis, S.; Debord, S. B.; Lofye, M. T.; Lyon, L. A. *Adv. Mater.* **2002**, *14*, 658-661.

(13) Gan, D.; Lyon, L. A. *J. Am. Chem. Soc.* **2001**, *123*, 7511-7517.

(14) Gan, D.; Lyon, L. A. *J. Am. Chem. Soc.* **2001**, *123*, 8203-8209.

(15) Gan, D.; Lyon, L. A. *Macromolecules* **2002**, *35*, 9634-9639.

(16) Jones, C. D.; Lyon, L. A. *Macromolecules* **2000**, *33*, 8301-8306.

(17) Harmon, M. E.; Kuckling, D.; Frank, C. W. *Macromolecules* **2003**, *36*, 162-172.

(18) Kuckling, D.; Harmon, M. E.; Frank, C. W. *Macromolecules* **2002**, *35*, 6377-6383.

(19) Li, Y.; Wang, G.; Hu, Z. *Macromolecules* **1995**, *28*, 4194-4197.

(20) Kaneko, Y.; Yoshida, R.; Sakai, K.; Sakurai, Y.; Okano, T. *J. Membr. Sci.* **1995**, *101*, 13-22.

(21) Yoshida, R.; Sakai, K.; Okano, T.; Sakurai, Y.; Bae, Y. H.; Kim, S. W. *J. Biomater. Sci., Polym. Ed.* **1991**, *3*, 155-162.

(22) Yoshida, R.; Sakai, K.; Okano, T.; Sakurai, Y. *J. Biomater. Sci., Polym. Ed.* **1992**, *3*, 243-252.

(23) Cohen, Y.; Ramon, O.; Kopelman, I. J.; Mizrahi, S. *J. Polym. Sci. B* **1992**, *30*, 1055-1067.

(24) Wu, C.; Zhou, S. *Macromolecules* **1997**, *30*, 574-576.

(25) Wu, C. *Polymer* **1998**, *39*, 4609-4619.

(26) Woodward, N. C.; Chowdhry, B. Z.; Leharne, S. A.; Snowden, M. J. *Eur. Polym. J.* **2000**, *36*, 1355-1364.

(27) Shibayama, M.; Tanaka, T. In *Advances in Polymer Science*; Springer-Verlag: Berlin, 1993; Vol. 109, pp 1-62.

(28) Jones, C. D.; Lyon, L. A. *Macromolecules* **2003**, *36*, 1988-1993.

CHAPTER 3

PHOTORESPONSIVE MICROGELS

In this chapter we will discuss the synthesis and the properties of photoresponsive microgels. They have been prepared by precipitation polymerization of the thermoresponsive polymer poly(N-isopropylacrylamide) followed by covalent conjugation of the temperature-jump dye malachite green. The photoresponsivity of these dye-labeled microgels was characterized by a pump-probe optical setup. A HeNe laser is used for exciting the dye molecules and a near IR-diode laser is used to simultaneously measure the turbidity of the colloidal dispersion. Irradiation of malachite green increases the temperature of the sample through rapid non-radiative decay, thereby causing the polymer chains to aggregate. On deswelling, a decrease in the intensity of transmitted light is observed due to scattering. It is also observed that the photoresponsive behavior of the microgels is dependent on the concentration of the dye, intensity of the laser and bath temperature. These microgels can potentially be used in the field of photodynamic therapy.

3.1 Introduction

Photoresponsive polymers have found uses in many real world applications such as drug delivery,[1-3] photopatterning,[4] holographic sensors[5] and mechanochromic materials.[6] A common material that has been used for devising photoresponsive gels is the thermoresponsive polymer poly(*N*-isoprylacrylamide) (pNIPAM), which belongs to a

class of polymers that show an abrupt change in their solubility in response to a change in environmental conditions.

Photoresponsive gels have traditionally been made by one of several methods. The first method was pioneered by Irie and coworkers, wherein an azobenzene moiety was incorporated into the gel.[7] Under UV irradiation, the azobenzene group undergoes a trans to cis photoisomerization, which changes the free energy of mixing in the gels and hence the VPTT. Another interesting example of photoresponsive gels belonging to the above-mentioned class was reported by Ikeda et al.,[6] where a liquid crystalline gel containing an azobenzene moiety was constructed. In presence of UV light the gel folds in one direction and in presence of visible light, the reverse cis-to-trans isomerization takes place and the gel unfolds. Kamenjicki et al. have made polymerized colloidal crystal array that have azobenzene moieties in them.[8] Following irradiation with either UV or visible light the photonic crystal diffraction is shifted. Irie et al. have also made photoresponsive gels by copolymerizing triphenylmethane leuco dyes in the gels, which photodissociate in presence of UV light resulting in a charged species.[9,10] The gel then undergoes osmotic swelling due to formation of these charged species. Gels that are responsive to light via photothermal processes have also been reported previously. Tanaka and coworkers synthesized monolithic gels of pNIPAM containing the trisodium salt of chlorophyllin.[11,12] This dye acts as a photon antenna and locally heats the gel in presence of light of an appropriate wavelength. This increase in temperature causes the thermosensitive pNIPAM gel to collapse locally in the region being irradiated. Unfortunately, these studies did not study the photothermal effects or the optical properties of chlorophyllin in detail. Wen et al. have used an IR-absorbing dye in a

poly(methyl methacrylate) (PMMA) matrix to heat the polymer.[13] Halas and coworkers have made pNIPAM gels that release drugs or macromolecules in presence of IR radiation.[1-3] The photoresponsive moiety used in that work is a nanoparticle having a dielectric core surrounded by a gold nanoshell. These designer nanoparticles absorb IR radiation and then give off heat via nonradiative relaxation, thus deswelling the polymer and subsequently releasing the entrapped material. Finally, our group has made photonic crystals doped with gold nanoparticles. These crystals can be patterned photothermally using a frequency doubled Nd-YAG laser, which heats up the gold nanoparticles and subsequently melts or anneals the colloidal crystals in a spatially confined manner.[14]

In this work we use colloidally stable hydrogel nanoparticles, or microgels, as our polymeric material.[15-18] These microgels are composed of lightly crosslinked pNIPAM copolymerized with an amine-containing co-monomer, which is then used to attach a malachite green derivative to the network. In all previously cited examples of photoresponsive gels, the responsive material was in the physical form of a monolithic gel. Figure 3-1 illustrates the process of forming photoresponsive microgels. Microgels made from "smart materials" have potential applications in several fields[19] including drug delivery,[20-23] biosensing,[24-26]chemical separations,[27,28] catalysis[29-31] and optics.[14,32-34] The temperature jump dye used in the work described below is malachite green, which belongs to the class of triphenylmethane dyes. The photophysics of this dye have been well studied.[35-37] Due to the rapid nonradiative decay and large extinction coefficient of the dye, it has been used as a photon-to-heat converter for many studies.[38-42] In this study we label the microgels with this dye and study their deswelling behavior as a function

light intensity in order to ascertain the utility of such a system in the design of photoresponsive materials.

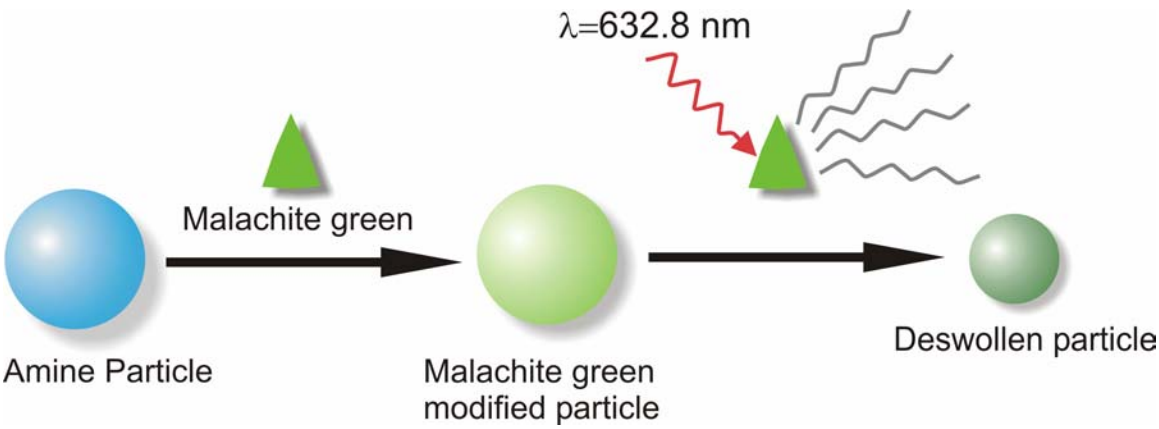

Figure 3-1. Schematic for preparation of photoresponsive microgels.

3.2 Experimental Section

Materials

N-isopropylacrylamide (NIPAm, Aldrich) was purified by recrystallization from hexane (J. T. Baker) prior to use. *N,N′*-methylenebis(acrylamide) (BIS), ammonium persulfate (APS), sodium dodecyl sulfate (SDS) and malachite green oxalate were purchased from Aldrich and used as received. *N*-(3-Aminopropyl)methacrylamide hydrochloride (APMA) was purchased from Polysciences. Malachite green isothiocyanate (MALG) was purchased from Molecular Probes (Eugene, OR). Water was purified with Barnstead E-Pure system to a resistance of 18 MΩ and then filtered through a 0.2-μm filter to remove particulate matter.

Microgel Synthesis

A detailed procedure for preparation of microgels by free radical precipitation polymerization is described elsewhere.[15] The total monomer concentration in the pregel solution was kept constant at 70 mM, out of which 1 mol-% was BIS and 1 mol-% was APMA, with the remaining 98 mol-% being NIPAm. All the monomers and 70 mg of SDS were dissolved in 250 mL of water and the resulting solution was filtered through a 0.2-μm-membrane filter (Pall Gelman Metricel) to remove particulate matter. The reaction mixture was heated in a 3-neck round bottom flask equipped with a condenser and inlet for nitrogen. The mixture was heated to 70 °C under a gentle stream of nitrogen for 1 h, after which 60 mg of APS dissolved in 1 mL of water was added to initiate the reaction. The reaction mixture was kept at 70 °C for 4 h to complete the reaction. After synthesis, the microgel solution was filtered using fine porosity filter paper (Fisher Scientific) to remove aggregated material, if any. The particles were then purified by

dialysis (Spectra/Por 7 dialysis membrane, MWCO 10,000) against daily changes of water for at least three weeks.

Conjugation of malachite green

The dialyzed microgel solution was lyophilized and rehydrated in 250 mL of pH 9.8 bicarbonate buffer. Five 20 mL portions of the microgel solution were removed. To each portion, varying amounts of malachite green isothiocyanate were added as shown in Table 3-1. The samples were let to react overnight at 4 °C and then dialyzed at 4 °C in the dark with daily changes of water for three weeks to remove unreacted dye. After dialysis, each sample was lyophilized separately and then rehydrated in deionized water to give a 50 mg/mL solution of the particles. Note that the amount of amine that is used for calculating the reaction stoichiometries is the amount that was present in the pregel solution. In Table 3-1, the actual amount of MALG that is conjugated to the particles is calculated from the Beer's Law plot in Figure 3-6.

UV-Vis characterization

The absorption spectra of the dye and the dye-conjugated microgels were obtained using a Shimadzu UV 1601 spectrophotometer.

Table 3-1: Particle conjugation with malachite green isothiocyanate

Sample #	Reaction Stoichiometry[a] [MALG] : [NH_2]	Malachite green isothiocyanate conjugated per gram of the polymer[b] (μmoles/g)
MAL1	0.01	4.8
MAL2	0.05	7.2
MAL3	0.10	9.6
MAL4	0.50	12.0
MAL5	1.00	26.4

[a] Reaction stoichiometries are calculated by taking the amount of APMA in the pregel solution.
[b] Amount of malachite green isothiocyanate conjugated to per gram of polymer is calculated from the Beer's plot shown in Figure 3-6.

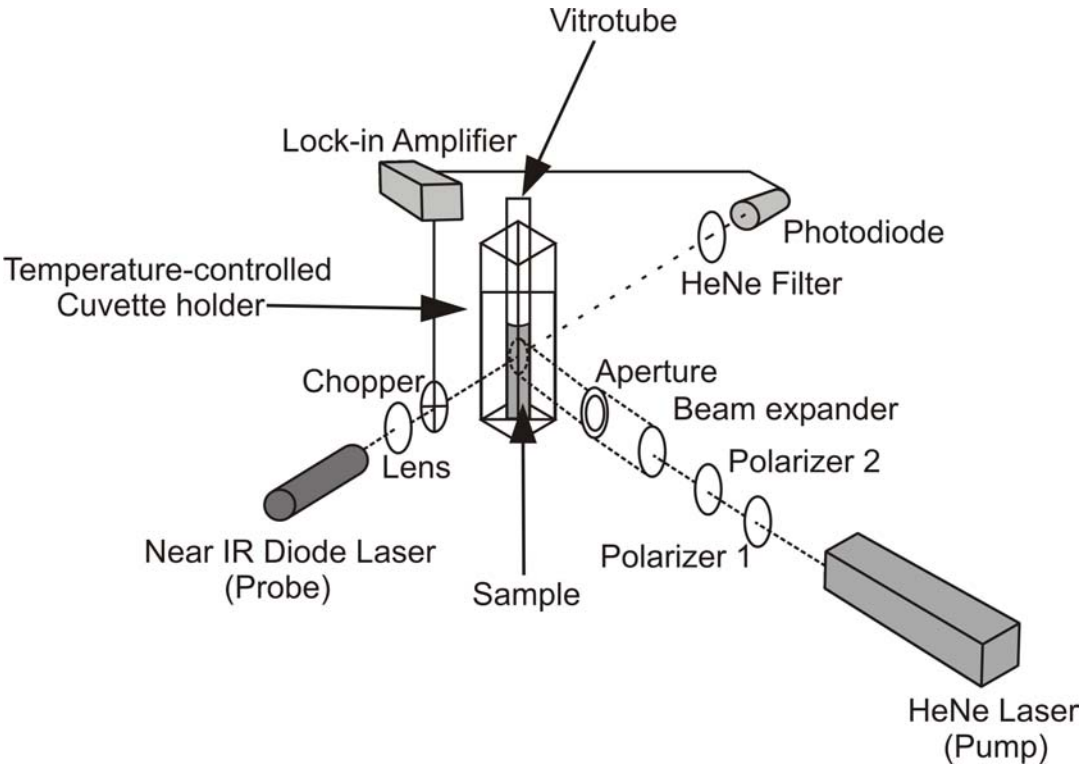

Figure 3-2. Pump-probe instrumental setup.

Pump-Probe Instrument

To measure the turbidity of the sample as a function of pump laser power, a pump-probe instrument was built. The schematic of the setup is shown in Figure 3-2. The excitation arm of this instrument consists of a Helium Neon laser (HeNe; λ=632.8 nm; Spectra Physics) pump laser, which is nearly resonant with the S0-S1 transition of malachite green (λ_{max}=620 nm), making it appropriate for excitation of the dye. The laser is passed through two polarizers. The second polarizer is fixed to pass p-polarized radiation, while the first can be rotated to control the total transmitted laser intensity. The beam is then expanded and impinged on the sample through an aperture. The sample is housed in a temperature-controlled cuvette holder (Quantum Northwest, WA). To interrogate the sample turbidity, a near-IR diode laser (Thor Labs, λ=820 nm) is oriented 90° relative to the pump arm. This beam is focused on the sample through an aperture and a chopper (Stanford Research Systems) and the transmitted light intensity is measured at a silicon photodiode. A HeNe interference filter is placed in front of the detector to eliminate stray or scattered pump laser light. The chopper (1 KHz) and detector are interfaced with a lock-in amplifier (SRS530, Stanford Research Systems) and the transmitted intensity was detected at the chopper frequency to eliminate contributions from stray light. Note that the apertures were chosen such that the pump illumination area was ~4-fold larger than the probe area and the beams were aligned to be concentric at the sample. This should provide pseudo-steady state conditions during the measurement. Figure 3-3 shows the variation in the laser power as a function of the angle of the polarizer.

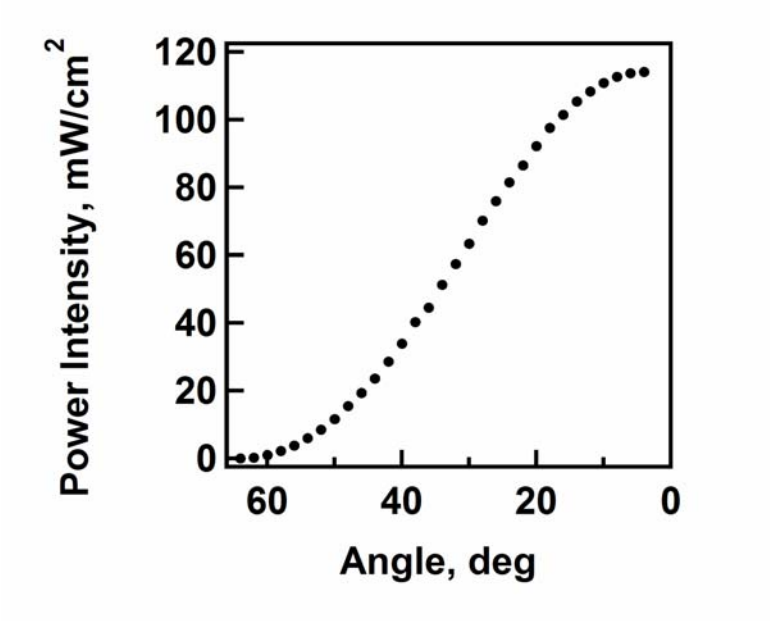

Figure 3-3. Variation in laser power intensity as a function of rotation of the polarizers.

Sample Preparation

For the pump-probe experiments, the sample was contained in a rectangular glass capillary tube, or vitrotube (0.2 X 4.0 mm,Vitrocom). To directly compare data from different samples, the same volume of sample is held in each vitrotube, which is achieved by allowing the sample to rise by capillary action to the same height in the vitrotubes. The tubes containing the sample were then attached to a glass coverslip (Fisher Scientific) that had been cut to fit diagonally in a standard 1-cm plastic cuvette. The cuvette is placed in the cuvette holder in such a fashion that the sample is at a 45° angle to the pump and probe beams, see Figure 3-2.

Photon Correlation Spectroscopy

Particle sizes were determined via photon correlation spectroscopy (PCS, Protein Solutions Inc.) equipped with an integrated Peltier temperature control device (± 0.1 °C), as previously reported.[15,16] The hydrodynamic radii of the particles were calculated from the diffusion coefficient using the Stoke-Einstein equation. The sample was allowed to equilibrate at the proper temperature for 10 minutes before data collection. Scattered light from the fiber-coupled diode laser (798 nm) was collected at 90° with a fiber-coupled avalanche photodiode detector connected to a 248-channel autocorrelator board. The data was analyzed with Protein Solutions' Dynamics Software Version 5.25.44.

3.3 Results and Discussion

Thermoresponsive pNIPAm hydrogel particles having primary amines were synthesized as described in the experimental section. These particles are found to have a hydrodynamic radius of ~700 nm, with a polydispersity of 14%, as determined by PCS in water at 25 °C and ~270 nm with a polydispersity of 6% at 41 °C, where polydispersity represents one standard deviation about the intensity-weighted average particle size. An isothiocyanate derivative of malachite green was used to react with the amines in the microgel to form an isothiourea bond. Figure 3-4 shows structure of malachite green isothiocyanate. The particles were conjugated with malachite green to varying degree, as shown in Table 3-1.

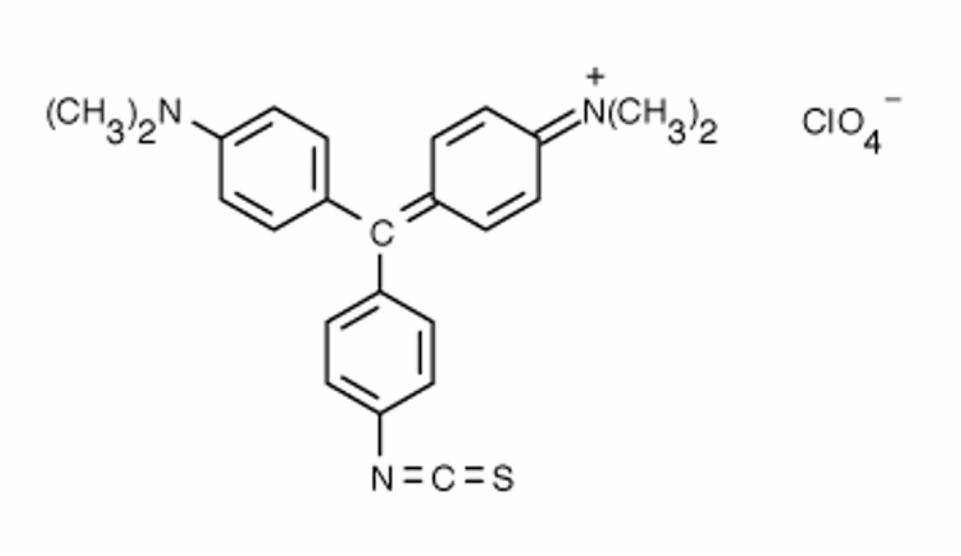

Figure 3-4. Structure of malachite green isothiocyanate.

Figure 3-5 shows the absorption spectra of sample MAL3 and an unconjugated sample, which is simply a mixture of particles and free dye. The unconjugated sample was prepared to contain the same concentration of particles and malachite green as in sample MAL3. The free dye used to make the unconjugated sample is an oxalate salt of malachite green, which has similar spectral properties as malachite green isothiocyanate. The rationale for using malachite green oxalate was to avoid any reaction between the amine and the malachite green during the measurement. As can be seen from the spectra, the peak associated with the S0 to S1 transition for the conjugated sample is slightly red shifted as compared to the free dye plus microgel spectrum, while there is large red shift for the S0 to S2 peak. Similar shifts have been observed previously by Indig et al,[40]

where they conjugated malachite green to bovine serum albumin (BSA). Also it can be seen that the S0 to S1 peak has an exaggerated shoulder on the blue side of the band.

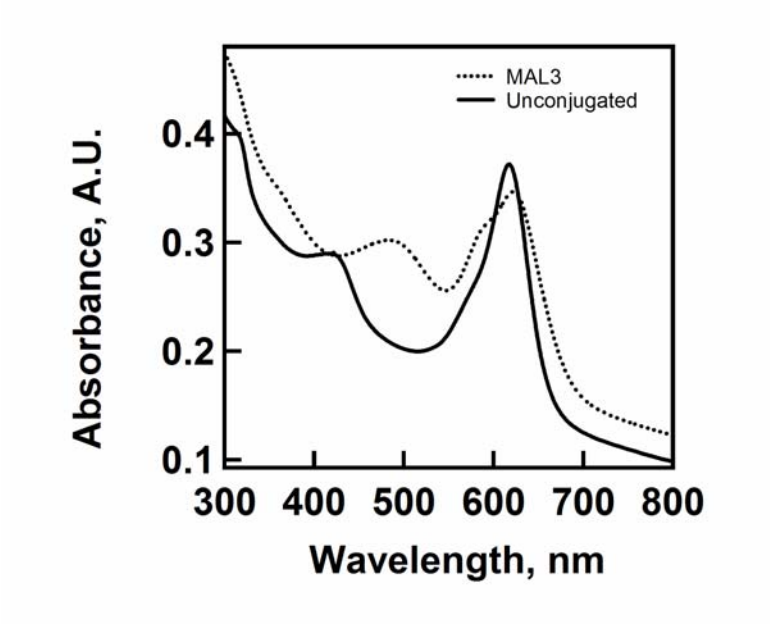

Figure 3-5. Absorption spectra of MAL3 and an unconjugated sample having same concentration of the particles and dye as in MAL3.

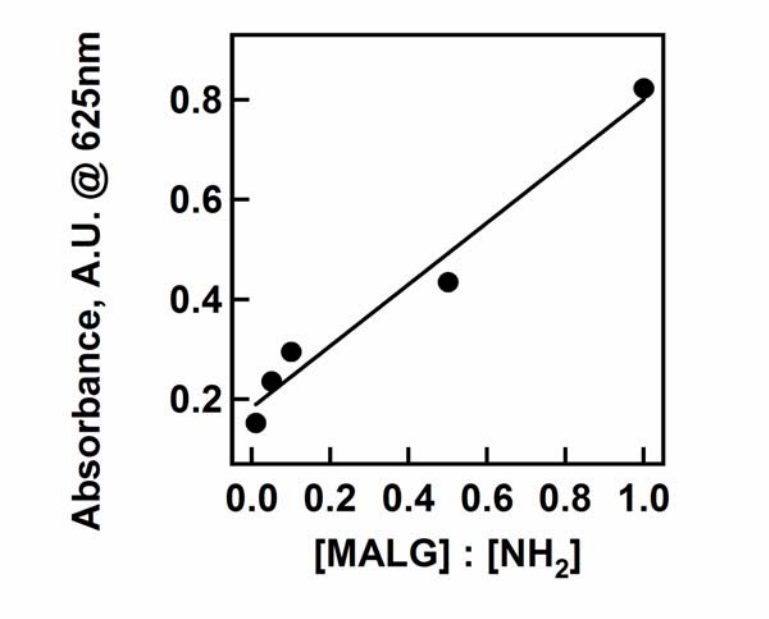

Figure 3-6. Absorbance of malachite-green modified particles at 625 nm as a function of reaction stoichiometry.

In free dye solutions this shoulder has been assigned to the presence of more than one stable ground state dye conformation.[36] The shoulder may be exaggerated when conjugated to the particles due to the presence of different dye environments that cause shifts in the conformational equilibria of the dye. To test the efficiency of malachite green conjugation, the electronic spectra of the particles were measured as a function of dye loading. These data are shown in Figure 3-6, which is a plot of the absorbance at 625 nm for samples conjugated with different ratios of MALG to APMA. The nonzero absorbance at zero concentration indicates that the reaction may become less efficient at higher dye concentrations. This maybe due to instability of isothiocyanates in water, hence at high dye concentration not all the dye molecules are able to incorporate in the microgels covalently. Nonetheless, the linear trend that is observed suggests that by simply controlling the particle to dye stoichiometry in the range studied here, one can control the amount of dye loaded on the particle.

As described in the Experimental Section, a two-polarizer configuration is used in the pump-probe instrument to control the pump laser power. Using this method to control laser intensity, we interrogated the photothermally induced deswelling of malachite green modified pNIPAm microgels. As stated above, the HeNe acts to excite the dyes, which then relax nonradiatively, causing local heating of the surroundings. If this laser-induced increase in temperature causes the VPTT of the particles to be traversed, one should observe particle deswelling. Particle deswelling can be observed as a change in solution transmittance, as the entropically favored expulsion of water from the network and the associated polymer phase separation is accompanied by an increase in particle scattering and hence an increase in solution turbidity.

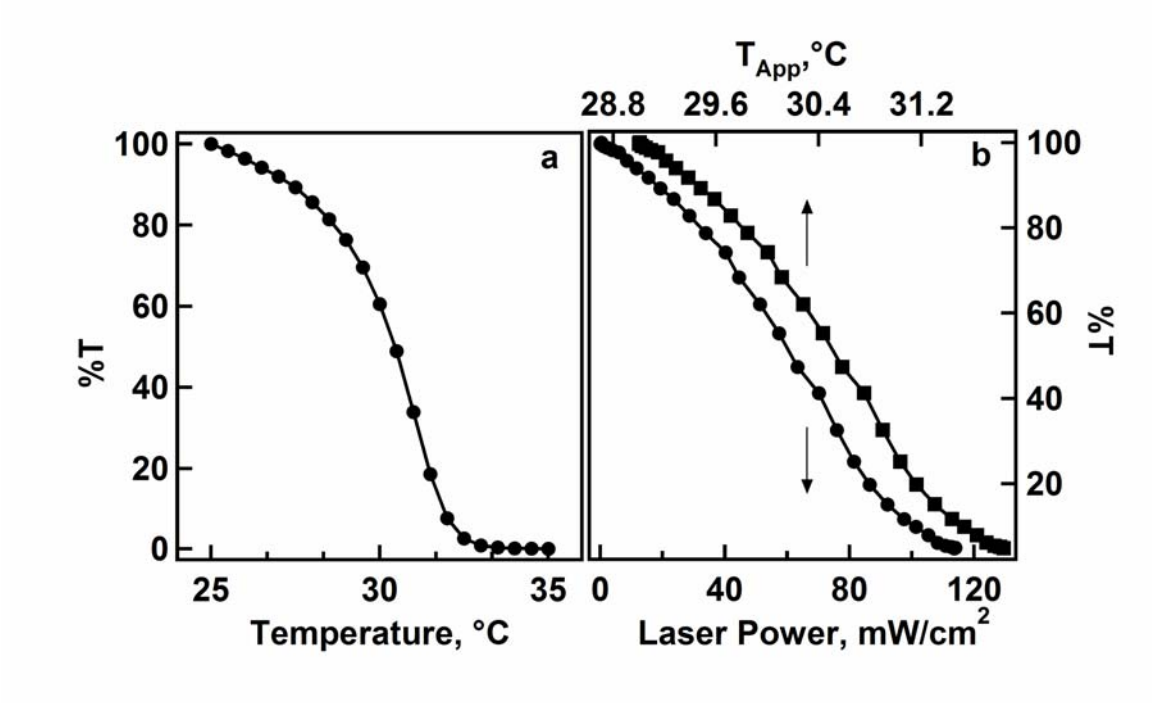

Figure 3-7. a) Percent transmitted light as a function of temperature for MAL3. b) Percent transmitted light as a function of laser power for MAL3 at 29 °C (circles) and percent transmitted light as a function of apparent temperature (T_{App}) (squares). See text for explanation.

Figure 3-7a shows the change in turbidity of sample MAL3 as a function of bath temperature and Figure 3-7b shows the change in relative transmittance *%T* as a function of laser power (circles) for MAL3 at a bath temperature of 29 °C.

$$\%T = \left(\frac{V_{Final}}{V_{Initial}} \right) \times 100 \qquad (1)$$

The change in solution turbidity is calculated using Equation 1, where *%T* is the relative percent transmitted light for each measurement, $V_{Initial}$ is the detector voltage before HeNe illumination and V_{Final} is detector voltage reached following equilibration of the system under HeNe illumination. It typically takes about 300 to 500 seconds for the transmitted intensity to reach a stable value during irradiation. In Figure 3-7b,

$$T_{App} = 29.0 + \Delta T \qquad (2)$$

where, 29 °C is the temperature of the bath and ΔT is the increase in temperature brought about by the laser at each laser power value. ΔT is calculated by determining the *%T* value at 31 °C from Figure 3-7a and then determining the corresponding laser power value from the photothermal curve at 29 °C. Application of this single point calibration to the entire photothermal deswelling curve gives the data in Figure 3-7b, where the *%T* values for MAL3 are plotted as a function of T_{App} (squares). As expected, both curves in Figure 3-7b have the same shape, suggesting a linear increase in the photothermal effect with laser power. A table showing the effective increase in temperature as function of laser power is provided in Table 3-2.

Table 3-2. Table for increase in temperature as a function of laser power calculated from Figure 3-7.

Laser Power mW/cm^2	Increase in temperature ΔT °C
0.04	0.00
0.25	0.01
0.96	0.02
2.22	0.06
3.81	0.10
5.97	0.15
8.51	0.21
11.63	0.29
15.43	0.39
19.32	0.48
23.56	0.59
28.62	0.72
33.91	0.85
40.21	1.01
44.53	1.11
51.27	1.28
57.41	1.44
63.35	1.58
70.21	1.76
75.95	1.90
81.46	2.04
86.51	2.16
92.21	2.31
97.54	2.44
101.39	2.53
105.37	2.63
108.31	2.71
110.86	2.77
112.63	2.82
113.68	2.84
114.07	2.85

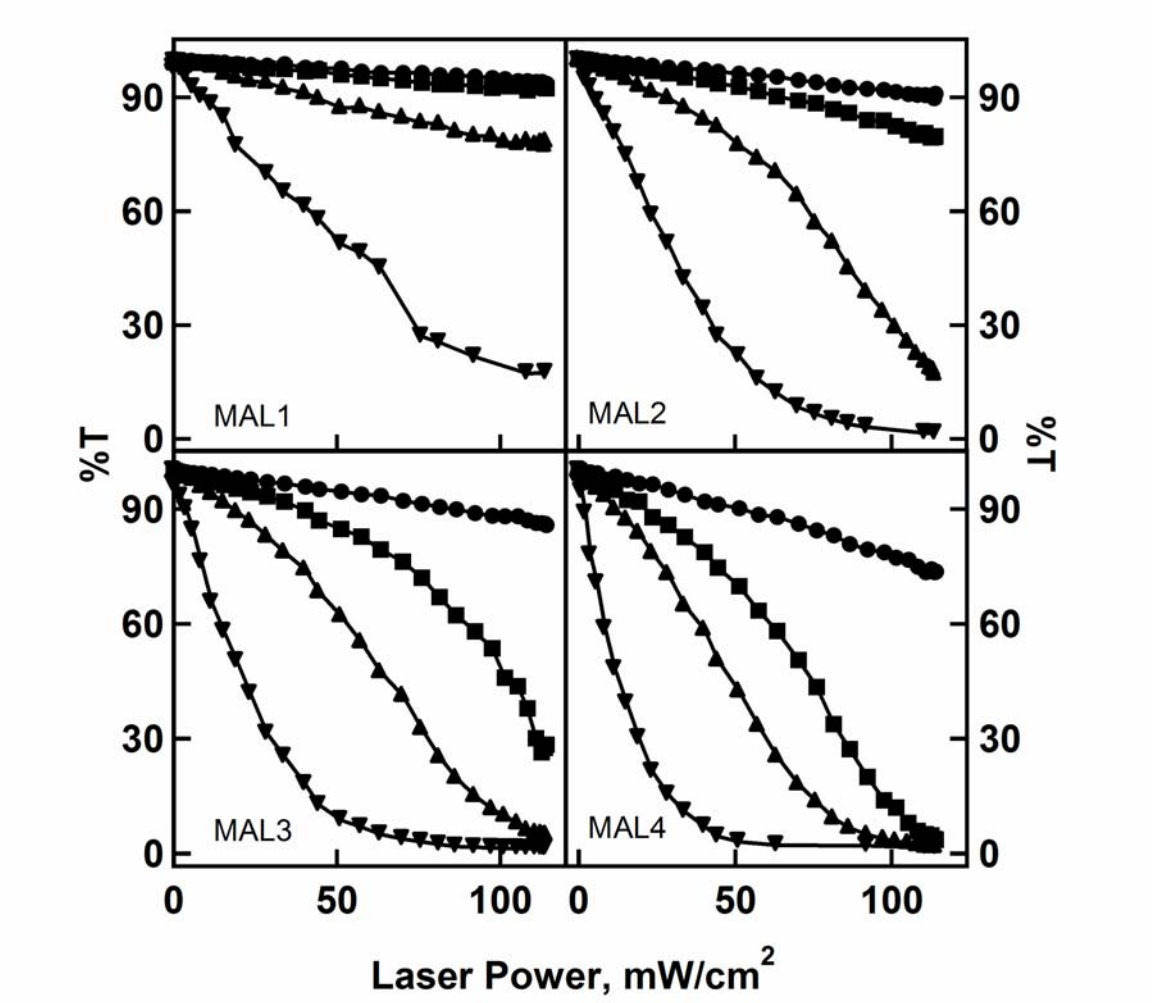

Figure 3-8. Percent transmitted light as a function of laser power intensity for samples MAL1, MAL2, MAL3 and MAL4 at 25 °C (circles), 27 °C (squares), 29 °C (triangles) and 31 °C (inverted triangles).

Figure 3-8 shows the change in transmittance as a function of the pump laser power for samples MAL1, MAL2, MAL3 and MAL4 at different bath temperatures (25 °C, 27 °C, 29 °C and 31 °C). In all the cases in Figure 3-8 the *%T* decreases with the increase in laser power intensity. In these experiments there are two sources of heat. One source is the temperature controlled cuvette holder, which we will refer to as the "bath". This temperature is held constant for each measurement performed as a function of laser power. The second source of heat is the radiation absorbed and released by the malachite green. By increasing the laser power one is increasing the number of dye molecules being excited and hence a higher laser power increases the photothermal heating, which in turn results in more microgel deswelling. In Figure 3-8 for all the samples it is observed that higher bath temperatures result in faster decreases in transmittance with laser power. In other words, for the same photon flux more deswelling is observed for the samples that are at higher bath temperatures. This is expected since as the bath temperature gets closer to the VPTT of the particles, a smaller photothermal effect is required to deswell the particles. It is also observed that as the concentration of the conjugated dye is increased in the sample it becomes easier to deswell the particles at a given bath temperature and at a given laser intensity. Again this can be explained as the conjugation of the dye to the particles is increased, the number of molecular heaters in the sample increases and hence at a given temperature fewer photons are needed to cause deswelling of the particles. For example, in the case of MAL1 it is observed that only at a bath temperature of 31 °C is significant deswelling is observed during irradiation at the highest laser power, while for MAL2, MAL3 and MAL4 almost complete deswelling is observed for a bath temperature of 31 °C at that laser power. Together, these data show the expected trends; higher bath

temperatures and higher dye loadings decrease the laser power required for particle deswelling.

In order to determine the photothermal efficiency of the dye as a function of particle conformation or solvent content, we performed an experiment involving subtle photo-induced temperature jumps as a function of bath temperature. This was investigated in order to determine if particle deswelling impacts the relative contributions of radiative and non-radiative pathways in malachite green, and hence the photothermal efficiency. Others have shown that the photoemission quantum yield of malachite green is dependent in some cases on the rigidity of its environment,[43,44] which may be expected to change as the microgel deswells. For this experiment MAL3 was chosen and the transmitted intensity was determined as a function of temperature without using the pump laser, which is denoted by the thermal curve in Figure 3-9a. At each bath temperature after the transmitted intensity had stabilized, the sample was irradiated with pump laser intensity of 3.81 mW/cm^2 and the decrease in transmitted intensity was measured. This intensity decrease is plotted as the photothermal curve in Figure 3-9a. The difference between the thermal and photothermal curve as a function of temperature is also plotted in Figure 3-9a, where,

$$\Delta V = V_{photothermal} - V_{thermal} \tag{3}$$

$V_{photothermal}$ is the detector voltage during illumination, while $V_{thermal}$ is the detector voltage in the absence of HeNe illumination. Here ΔV is taken as a measure of photothermal efficiency, where the photothermal efficiency is the ability of the dye molecules to bring about aggregation of the polymer chains at a fixed laser flux. From Figure 3-9a it is found that the maximum ΔV is obtained at 31 °C, which is the VPTT of the hydrogel particles.

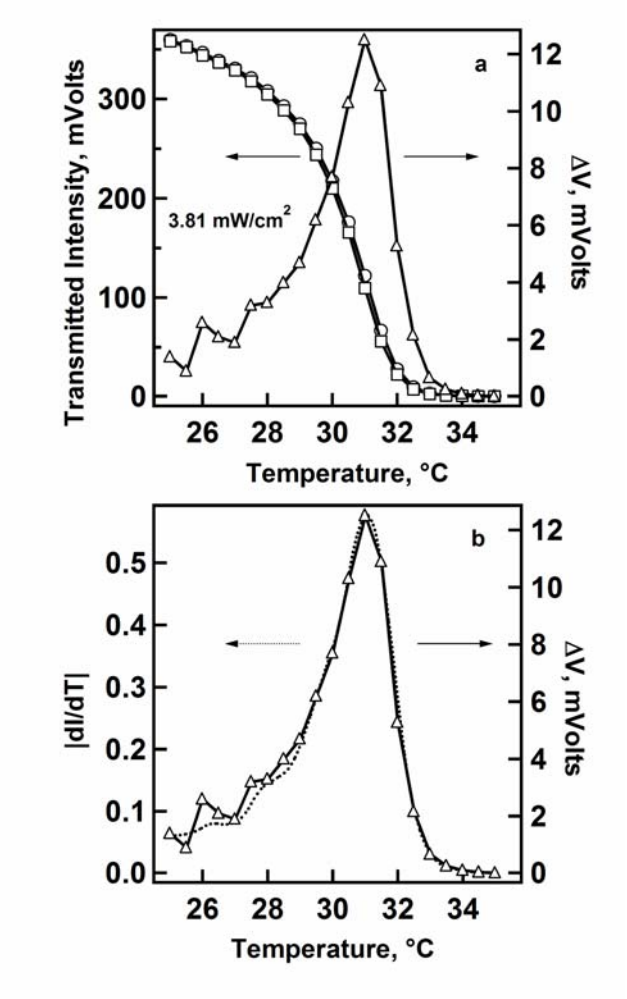

Figure 3-9. a) Transmitted intensity as a function of temperature, (open circles) thermal curve and (open squares) photothermal curve and the difference of the thermal and photothermal curve as a function of temperature (open triangles). b) First derivative of the thermal curve as a function of temperature (dotted line) and difference of the thermal and photothermal curve as a function of temperature (open triangles).

Above 31 °C, the change in turbidity brought about by irradiation decreases. This is expected, as the shape of the thermal turbidity curve is asymmetric, with the instantaneous slope of the curve decreasing at temperatures greater than the VPTT. The impact of the thermal turbidity curve shape on the shape of the photothermal efficiency curve is illustrated in Figure 3-9b, where we compare the photothermal efficiency curve to the first derivative of the thermal curve. The two curves are nearly indistinguishable in shape. Thus, it can be inferred that the shape of the photothermal efficiency curve is a direct result of the asymmetric shape of the thermal curve and that the photothermal efficiency is independent of particle deswelling. Apparently, the increase in polymer density accompanied by particle deswelling does not strongly modulate the rotation of the phenyl rings on the dye.

3.4 Conclusions

We have demonstrated that photoresponsive microgels can be made by conjugating malachite green to pNIPAM microgels. Upon excitation with a HeNe laser the dye molecules undergo a non-radiative decay causing an increase in the temperature of the sample, which in turn causes the microgels to undergo partial or complete deswelling depending on several parameters. The deswelling of the microgels can be manipulated by the amount of dye conjugated to the particles, the bath temperature, and the power of the pump laser. As expected, it is observed that as the bath temperature approaches the VPTT, it becomes easier to deswell the particles photothermally. Interestingly, the increased density of the microgel following deswelling does not directly impact the conformational flexibility of the dye, as evidenced in a deswelling-

independent photothermal yield. This simple particle construct suggests a synthetically trivial route to a wide range photo-modulated colloidal materials based on synthetic polymers.

REFERENCES

(1) Sershen, S. R.; Westcott, S. L.; Halas, N. J.; West, J. L. *J. Biomed. Mater. Res.* **2000**, *51*, 293-298.

(2) Sershen, S. R.; Westcott, S. L.; West, J. L.; Halas, N. J. *Appl. Phys. B* **2001**, *73*, 379-381.

(3) Sershen, S. R.; Westcott, S. L.; Halas, N. J.; West, J. L. *Appl. Phys. Lett.* **2002**, *80*, 4609-4611.

(4) Hoffmann, J.; Plotner, M.; Kuckling, D.; Fischer, W. J. *Sensor. Actuat. A-Phys.* **1999**, *77*, 139-144.

(5) Marshall, A. J.; Blyth, J.; Davidson, C. A. B.; Lowe, C. R. *Anal. Chem.* **2003**, *75*, 4423-4431.

(6) Ikeda, T.; Nakano, M.; Yu, Y. L.; Tsutsumi, O.; Kanazawa, A. *Adv. Mater.* **2003**, *15*, 201-205.

(7) Kungwatchakun, D.; Irie, M. *Makromol. Chem-Rapid* **1988**, *9*, 243-246.

(8) Kamenjicki, M.; Lednev, I. K.; Mikhonin, A.; Kesavamoorthy, R.; Asher, S. A. *Adv. Funct. Mater.* **2003**, *13*, 774-780.

(9) Irie, M.; Kungwatchakun, D. *Makromol. Chem-Rapid.* **1984**, *5*, 829-832.

(10) Irie, M.; Kunwatchakun, D. *Macromolecules* **1986**, *19*, 2476-2480.

(11) Suzuki, A.; Tanaka, T. *Nature* **1990**, *346*, 345-347.

(12) Suzuki, A.; Ishii, T.; Maruyama, Y. *J. Appl. Phys.* **1996**, *80*, 131-136.

(13) Wen, X.; Tolbert, W. A.; Dlott, D. D. *J. Chem. Phys.* **1993**, *99*, 4140-4151.

(14) Jones, C. D.; Lyon, L. A. *J. Am. Chem. Soc.* **2003**, *125*, 460-465.

(15) Jones, C. D.; Lyon, L. A. *Macromolecules* **2000**, *33*, 8301-8306.

(16) Jones, C. D.; Lyon, L. A. *Macromolecules* **2003**, *36*, 1988-1993.

(17) Gan, D.; Lyon, L. A. *J. Am. Chem. Soc.* **2001**, *123*, 7511-7517.

(18) Gan, D.; Lyon, L. A. *J. Am. Chem. Soc.* **2001**, *123*, 8203-8209.

(19) Pelton, R. *Adv. Colloid. Interface Sci.* **2000**, *85*, 1-33.

(20) Jeong, B.; Bae, Y. H.; Lee, D. S.; Kim, S. W. *Nature* **1997**, *388*, 860-862.

(21) Hoffman, A. In *Controlled Drug Delivery: Challenges and Strategies*; Park, K., Ed.; American Chemical Society: Washington, D.C., 1997; pp 485-498.

(22) Kurisawa, M.; Terano, M.; Yui, N. *Macromol. Rapid Commun.* **1995**, *16*, 663-666.

(23) Brondsted, H.; Kopecek, J. *Pharm. Res.* **1992**, *9*, 1540-1545.

(24) Miyata, T.; Jikihara, A.; Nakamae, K.; Uragami, T.; Hoffman, A. S.; Kinomura, K.; Okumura, M. *Adv. Biomater. Biomed. Eng. Drug Delivery Syst., [Iketani Conf. Biomed. Polym.], 5th* **1996**, 237-238.

(25) Miyata, T.; Asami, N.; Uragami, T. *Macromolecules* **1999**, *32*, 2082-2084.

(26) Holtz, J. H.; Asher, S. A. *Nature* **1997**, *389*, 829-832.

(27) Umeno, D.; Kawasaki, M.; Maeda, M. *Bioconj. Chem.* **1998**, *9*, 719-724.

(28) Kawaguchi, H.; Fujimoto, K. *Bioseparation* **1998**, *7*, 253-258.

(29) Bergbreiter, D. E.; Case, B. L.; Liu, Y.-S.; Caraway, J. W. *Macromolecules* **1998**, *31*, 6053-6062.

(30) Bergbreiter, D. E.; Liu, Y.-S.; Osburn, P. L. *J. Am. Chem. Soc.* **1998**, *120*, 4250-4251.

(31) Nagayama, H.; Maeda, Y.; Shimasaki, C.; Kitano, H. *Macromol. Chem. Phys.* **1995**, *196*, 611-620.

(32) Jones, C. D.; Serpe, M. J.; Schroeder, L.; Lyon, L. A. *J. Am. Chem. Soc.* **2003**, *125*, 5292-5293.

(33) Debord, J. D.; Lyon, L. A. *J. Phys. Chem. B* **2000**, *104*, 6327-6331.

(34) Debord, J. D.; Eustis, S.; Debord, S. B.; Lofye, M. T.; Lyon, L. A. *Adv. Mater.* **2002**, *14*, 658-661.

(35) Ishikawa, M.; Ye, J. Y.; Maruyama, Y.; Nakatsuka, H. *J. Phys. Chem. A* **1999**, *103*, 4319-4331.

(36) Duxbury, D. F. *Chem. Rev.* **1993**, *93*, 381-433.

(37) Sundstrom, V.; Gillbro, T. *J. Chem. Phys.* **1984**, *81*, 3463-3474.

(38) Miyata, R.; Terazima, M. *Anal. Sci.* **2001**, *17*, S231-S233.

(39) Lian, T. Q.; Locke, B.; Kholodenko, Y.; Hochstrasser, R. M. *J. Phys. Chem.* **1994**, *98*, 11648-11656.

(40) Indig, G. L.; Jay, D. G.; Grabowski, J. J. *Biophys. J.* **1992**, *61*, 631-638.

(41) Jay, D. G. *Proc. Natl. Acad. Sci. U. S. A.* **1988**, *85*, 5454-5458.

(42) Robl, T.; Seilmeier, A. *Chem. Phys. Lett.* **1988**, *147*, 544-550.

(43) Baptista, M. S.; Indig, G. L. *J. Phys. Chem. B* **1998**, *102*, 4678-4688.

(44) Abedin, K. M.; Ye, J. Y.; Inouye, H.; Hattori, T.; Sumi, H.; Nakatsuka, H. *J. Chem. Phys.* **1995**, *103*, 6414-6425.

CHAPTER 4

HOLLOW THERMORESPONSIVE MICROGELS

Thermoresponsive poly(*N*-isopropylacrylamide) (pNIPAm) microgels possessing a hollow structure have been synthesized from core/shell nanoparticles *via* oxidation of the particle core, followed by removal of the produced polymer segments by centrifugation. *N, N'*-(1, 2-dihydroxyethylene)bisacrylamide (DHEA) is used as a cross-linker for preparing the degradable core, whereas *N, N'*-methylenebisacrylamide (BIS) is used as a cross-linker to add a non-degradable pNIPAm shell. Addition of $NaIO_4$ to these particles in a water suspension leads to controlled degradation of the particle core by cleavage of the 1,2-glycol bond in DHEA. Fluorescence spectroscopy, UV-VIS spectroscopy and photon correlation spectroscopy are used to characterize the thus produced hollow particles.

4.1 Introduction

Environmentally sensitive materials that respond to subtle enviromental stimuli are of immense importance in various fields like drug delivery,[1-3] biosensing,[4] chemical separations,[5] biomaterials,[6] and catalysis.[7,8] These materials can be made responsive to various stimuli such as temperature,[9] pH,[10] light,[11] ionic strength,[12] and magnetic fields.[13] When fabricated at a sub-micron level, these materials have the additional advantage of being useful in various areas of nanotechnology.

In this chapter we demonstrate the synthesis and characterization of a core/shell particle with a degradable core. Traditionally, hollow nanoparticles have been prepared by using a sacrificial core particle onto which a nondegradable shell is added. Degradation of the core leaves behind hollow particles.[14] Zha et al[15] have prepared hollow thermoresponsive particles by functionalizing the surface of silica particles with polymerizable units, followed by polymerization of NIPAm on the core particles. Dissolution of silica particles with HF resulted in pNIPAm microcontainers. Huang et al[16] have prepared hollow nanocapsules by using diblock co-polymer poly(isoprene-*b*-acrylic acid). The micelles formed by this polymer have isoprene groups in the center and the acid groups on the outside. The acid groups in the shell were cross-linked by amidation and the core (isoprene units) was dissolved by oxidation, resulting in hollow capsules.

In this study a degradable cross-linker is used to synthesize core particles, whereas a non-degradable cross-linker is used to add a shell onto the core. Figure 4-1 illustrates the concept, where the degradable cross-linker is *N,N'*-(1,2-dihydroxyethylene)bisacrylamide (DHEA) and the non-degradable cross-linker is *N,N'*-methylenebisacrylamide (BIS). The core is degraded by sodium periodate via cleavage of the vicinal diol in DHEA. The degraded part of the particle is then removed by centrifugation, resulting in a particle with essentially a hollow structure. Hollow nanoparticles are of interest in the fields of medicine, pharmaceutics, material science and paint industry.[17] Responsive hollow particles may hold even more significant promise for various applications such as encapsulation and controlled release of drugs and dyes, protection of environmentally-sensitive catalysts, or in coatings and composites.

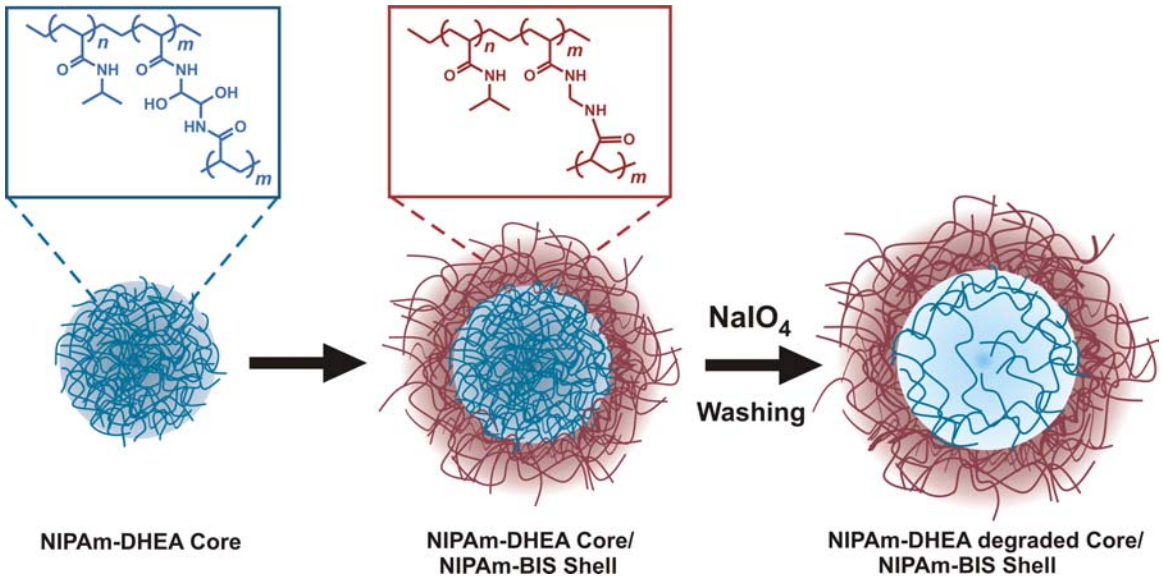

Figure 4-1. Preparation of thermoresponsive hollow particles. Core particles are synthesized with a degradable cross-linker (DHEA). A BIS cross-linked shell is added on the DHEA core followed by degradation of the core particle, which results in a hollow shell.

4.2 Experimental Section

Materials

All chemicals were purchased from Aldrich unless otherwise noted. *N*-Isopropylacrylamide (NIPAm) was recrystallized from hexane (J. T. Baker) before use. *N, N′*-Methylenebis(acrylamide) (BIS), *N, N′*-(1,2-dihydroxyethylene) bisacrylamide (DHEA), ammonium persulfate (APS) and sodium periodate were used as received. (9-Phenanthryl)methyl methacrylate (PheMMA) was synthesized by the reaction of phenanthrylmethanol (reduction product of phenanthracene-9-carboxaldehyde by sodium borohydride) with methacryloyl chloride in presence of tetrahydrofuran (THF) and triethylamine.[18,19] Water used in all experiments was distilled and then purified using a Barnstead E-Pure system operating at a resistance of 18 MΩ. A 0.2 μm filter was incorporated into this system to remove particulate matter.

Synthesis

DHEA Cross-linked Core. PNIPAm microgels were prepared by free-radical precipitation polymerization. A detailed procedure for free radical precipitation polymerization is described elsewhere.[10,20] Briefly, monomer 712 mg of NIPAm, 140 mg of DHEA and 44 mg of surfactant SDS were introduced into 100 mL of deoxygenated water. Nitrogen was bubbled into the reaction mixture at 70 °C for 2 h. 75 μL of 50 mM solution of PheMMA in DMF was added prior to initiation. To initiate 34 mg of APS was added. The polymerization was carried out at 70 °C for 4 h under a stream of nitrogen. It should be noted that the thus-formed polymer is insoluble at the reaction temperature (well above the LCST), whereas the monomer is fully soluble in water. Therefore, the growing oligomers, once reaching a critical length, will precipitate from the solution and

form precursor particles. These nuclei capture newly-formed oligomers and/or aggregate with each other in solution, continuing to grow until polymer conversion is complete. This method of precipitation polymerization produces submicron-sized, spherical network hydrogels (microgels). The polymer solution was filtered through a Whatman filter to remove aggregates, if any. The particles were cleaned several times via centrifugation and resuspension in deionized water to remove unreacted monomer, oligomers and surfactant.

Mixed Cross-linker Synthesis. These particles were synthesized in the same manner as the core particles but with two different cross-linkers BIS (non-degradable) and DHEA (periodate degradable). The total cross-linker density was kept at 10 mol-%. Two samples with different DHEA:BIS (4:1 and 1:4) ratio were synthesized.

Core/Shell Synthesis. Core/shell microgels were constructed *via* two-stage seeded polymerization. We have previously demonstrated that this method affords particles with a core/shell morphology without observable nucleation of new particles.[10,19] Here the DHEA-cross-linked microgels were used as seed particles, upon which a BIS-cross-linked shell was added. A solution of DHEA-cross-linked microgels (5 ml) with 4 mg of SDS and 14 mL of deionized water was heated to 70 °C under a gentle stream of nitrogen. Separately 55.4 mg of NIPAm and 1.5 mg of BIS were dissolved in 5 mL of water. This solution was degassed at room temperature for 1 h and was then added to the heated core solution. Finally 5 mg of APS was added to intiate the reaction. The reaction was allowed to proceed for 4 h at 70 °C. The reaction solution was cooled and cleaned several times by centrifugation and resuspension in deionized water.

Degradation

For both core and core/shell particles degradation was carried out by using sodium periodate. Depending upon the amount of degradation required, an equivalent number of moles of sodium periodate was added to 1 mL of polymer solution and the total volume was made 1.5 mL with deionized water. The reaction was carried out overnight. The amount of DHEA to be degraded was calculated from the amount of DHEA in the pregel solution. The particles after degradation were cleaned by centrifugation and resuspension to remove the degraded material.

UV-Vis Characterization

The turbidity of both the core and the core/shell particles as a function of amount of DHEA degraded was measured by Shimadzu UV 1601 spectrophotometer. The spectra were recorded against deionized water in the reference cell.

Photon Correlation Spectroscopy (PCS)

Particle sizes and size distributions in aqueous solutions were measured by PCS (Protein Solutions, Inc.) with a programmable temperature controller.[21] Prior to taking measurements, the particle solutions were allowed to thermally equilibrate at each temperature for 10 min. Longer equilibration times did not lead to variations in the observed hydrodynamic radii, polydispersities or scattering intensities. All correlogram analyses were performed with manufacturer-supplied software (Dynamics v.5.25.44, Protein Solutions, Inc.). The data presented below are the averaged values of 20 measurements, with a 60 s integration time for each measurement. The deswelling volume ratio (V^0/V) of the particles is the cube of the ratio of PCS measured particle radii

at 25 °C to that at a particular temperature. The deswelling volume ratio is used to define the swollen state of a particle in comparison to its initial state.

Steady State Fluorescence

Fluorescence spectra were recorded on a steady-state fluorescence spectrophotometer (Photon Technology International), equipped with a Model 814 PMT photon-counting detector.[19] The slits were set to achieve a spectral bandwidth of 2 nm, and the spectra were recorded with a step size of 1 nm and an integration time of 1 second. Phenanthrene fluorescence was measured of the cleaned particles at ambient temperature, with an excitation wavelength of 298 nm.

4.3 Results and Discussion

The pNIPAM-based particles were prepared by free-radical precipitation polymerization (see Experimental Section). As widely reported, this method produces nearly monodispersed spherical particles in the sub-micron size range.[9,21] In this synthesis, a cross-linker that has more than one reactive group is typically used to generate polymeric networks, and thus maintain the spherical shape and dimensional stability of the particles after polymerization. The particle/water suspensions for these systems are turbid due to a modest mismatch of the refractive indices between the polymer networks and water. This is in contrast to linear pNIPAm, which exhibits a transparent, colorless solution in water at similar concentrations due to the lower scattering cross-section of the polymer chains. To make degradable cores, DHEA was used as a chemically labile cross-linker. This cross-linker has been used in the past to

prepare bulk gels for electrophoresis.[22] It contains a vicinal diol functionality (Figure 4-1), which can be cleaved by stoichiometric amounts of sodium periodate.[22]

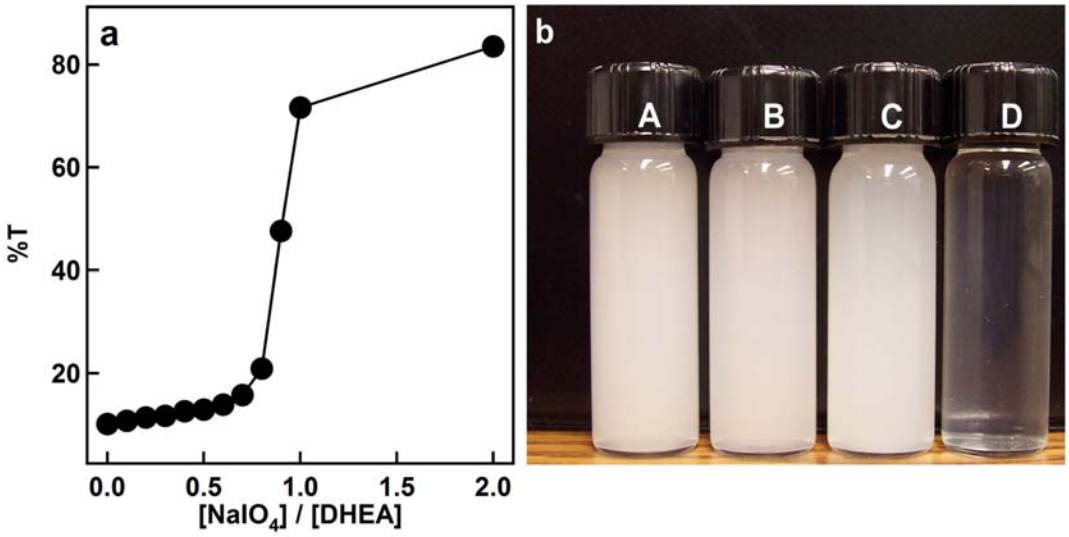

Figure 4-2. a) %T of DHEA cross-linked core particles as a function of periodate/DHEA ratio. b) Pictures of the vials of BIS core particle solutions (vials A and B) and DHEA core particle solutions (vials C and D) before (vials A and C) and after (vials B and D) periodate treatment.

Figure 4-2a shows the change in %T of a solution of DHEA cross-linked core particles as a function of the periodate/DHEA ratio. It is observed that the transmittance increases with an increase in the concentration of sodium periodate, which suggests a decrease in the particle scattering cross-section due to polymer degradation. This result indicates that the 1,2-glycol bond in DHEA is cleaved by $NaIO_4$, which results into formation of small polymer segments that scatter less light than the intact particles. Further visual confirmation is presented in Figure 4-2b, where vial A and B contain an aqueous suspension of BIS cross-linked core particles, and vial C and D contain DHEA cross-linked core particles. For the BIS cross-linked core particles, there is no difference in turbidity between the as-prepared particles (vial A) and those treated with $NaIO_4$ (vial B). On the other hand, the DHEA cross-linked core particle suspension treated with $NaIO_4$ (vial D) is completely clear in comparison to the turbid suspension of untreated particles (vial C).

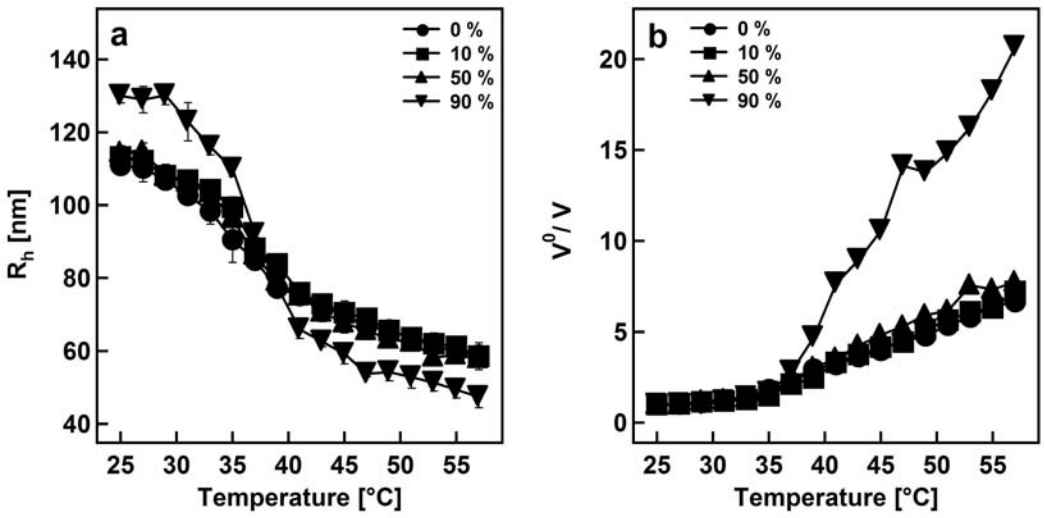

Figure 4-3. a) Variation in R_h of DHEA core particles as a function of temperature for 0%, 10%, 50%, and 90% degraded particles. b) Normalized deswelling volume ratios as a function of temperature for 0%, 10%, 50%, and 90% degraded DHEA core samples.

Since these particles are composed largely of pNIPAM, their thermoresponsivity was studied by variable temperature photon correlation spectroscopy. Figure 4-3a depicts the change in hydrodynamic radius (R_h) as a function of temperature for particles that have been degraded to varying degrees. For the sample that has not been treated with $NaIO_4$, the phase transition curve is relatively broad. While many effects can contribute to phase transition broadening, it is generally the case that highly cross-linked particles such as those used here (10 mol-% cross-linker) have broader transitions than more loosely cross-linked analogues.[21] For samples that have been 10% and 50% degraded, the curves look very similar to the non-degraded one. However, for the 90% degraded sample the R_h of the particles is ~30 nm higher than for the other samples, and the phase transition curve is sharper. This result indicates that the number of cross-links in this sample have decreased substantially, which allows the particle to swell to a greater extent. In Figure 4-2a it is observed that a substantial change in turbidity occurs at concentrations higher than 0.8 moles of $NaIO_4$ / DHEA. This is in agreement with the PCS data, where the curves for the samples with 10% and 50% degradation essentially have the same shape as that for the untreated sample. This suggests that a critical number of cross-links must be disrupted in order to cause a substantial change in the structure of the particle.

Figure 4-3b shows the normalized deswelling volume of the particles as a function of temperature, where deswelling volume is defined as

$$\frac{V^0}{V} = \left(\frac{R_h{}^0}{R_h} \right)^3 \qquad (1)$$

V^0 and R_h^0 are the particle volume and hydrodynamic radius at 25 °C, respectively, and V and R_h are those at a particular temperature. The deswelling volume is a measure of the ability of the particle to swell in a solvent. For the particles which have been 0%, 10% and 50% degraded, the particles deswell by ~6 times their original volume at 25 °C. Also, the deswelling curves for these samples are very similar in shape, which indicates that $NaIO_4$ has not significantly changed the particle density and morphology. For the 90% degraded sample the particles deswell ~20-fold in volume. This indicates that the concentration of $NaIO_4$ used for this sample causes sufficient change in cross-linking density such that the swellability of the particles is altered. The higher swelling capacity also indicates loss of material from the particle, which is brought about by removal of the degraded parts of the particle at high concentrations of periodate. At lower concentrations of periodate, there is presumably cleavage of the cross-links, but not to a point that results in a significant loss of material. Thus, the integrity of the particles is not impacted and no change in the swelling capacity is observed. For 90% degraded samples there is a further increase in number of cleaved cross-links to such an extent that polymer is lost from the particle, thereby increasing the degree of deswelling.

Core particles having two different cross-linkers (DHEA and BIS) were synthesized to study the behavior of partially-degradable particles. We hypothesized that after complete degradation of DHEA the particle would expand due to a reduction in the number of effective cross-links, but would not completely dissolve as is the case with microgels containing only DHEA cross-links. Two sets of particles were prepared, in both the sets the total cross-linker mol-% was kept constant at 10% but the degradable to non-degradable cross-linker ratio was varied. The ratio of DHEA:BIS in the two samples was 4:1 and 1:4. For these particles, DHEA was degraded by several-fold excess of $NaIO_4$. Figure 4-4a shows the variation in R_h of the DHEA:BIS 4:1 sample and Figure 4-4b shows the corresponding deswelling ratio curve for the same sample. Interestingly, after degradation the R_h decreases with a concomitant decrease in the volume phase transition temperature (VPTT). Furthermore, Figure 4-4b does not show any substantial change in deswelling ratio at higher temperature (57 °C) for the degraded sample relative to the non-degraded one. The noticeable increase in the phase transition sharpness following DHEA degradation is evidence of a decrease in the effective cross-link density and/or network heterogeneity. For the sample containing a 1:4 DHEA:BIS ratio (Figure 4-4c and 4-4d) the curves before and after degradation are similar. This indicates that removal of this small number of DHEA cross-links does not have any observable effect on the particle swelling. It should be noted that the VPTT for 1:4 sample occurs at a lower temperature than that of the 4:1 sample, suggesting there is a difference in hydrophobic-hydrophilic ratio between the two samples.

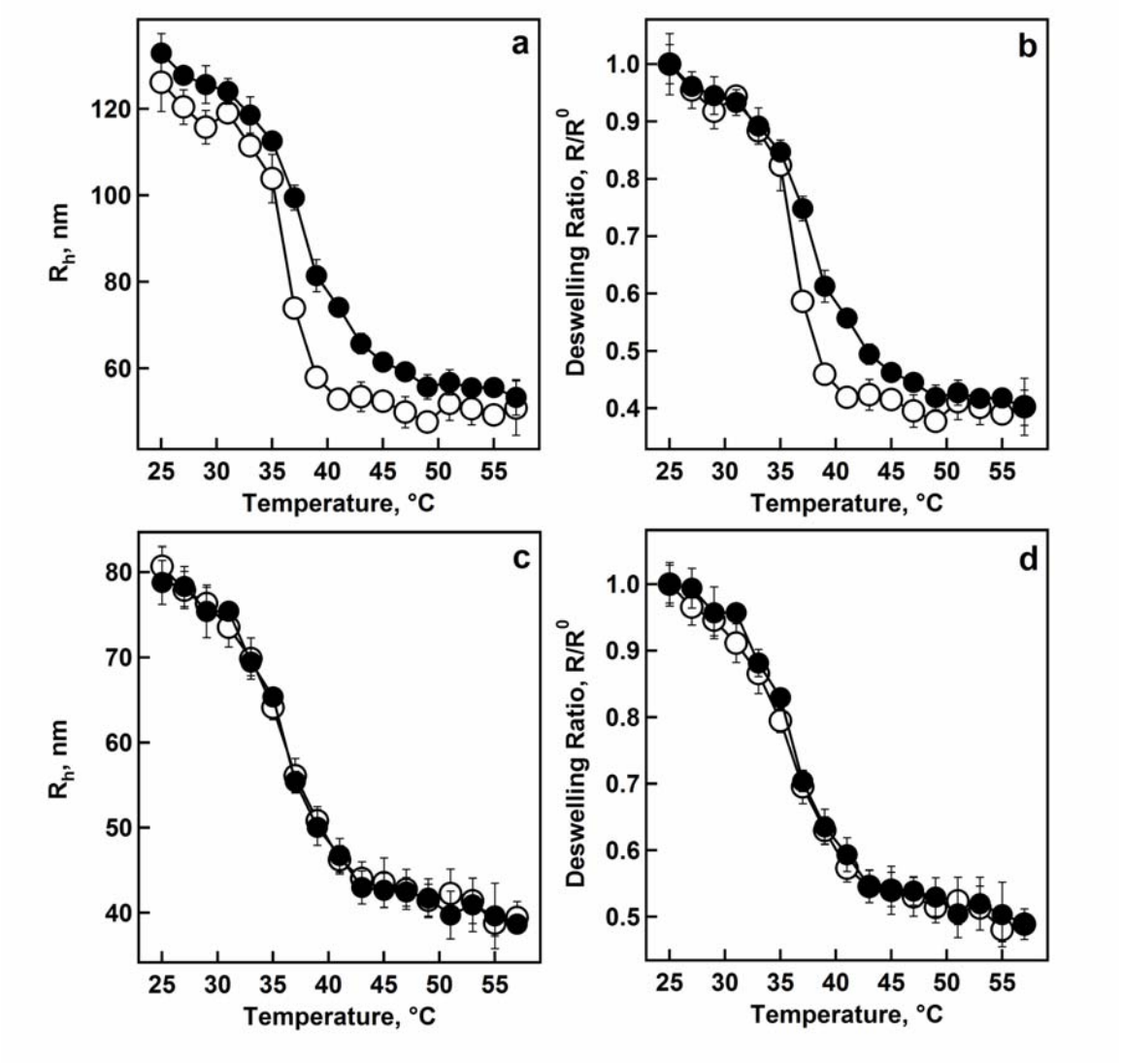

Figure 4-4. a) Variation in R_h of 4:1 DHEA:BIS core particle as a function of temperature before (solid circles) and after (open circles) periodate treatment. b) Deswelling ratio as a function of temperature for 4:1 DHEA:BIS sample before (solid circles) and after (open circles) periodate treatment. c) Variation in R_h of 1:4 DHEA:BIS core particle as a function of temperature before (solid circles) and after (open circles) periodate treatment. d) Deswelling ratio as a function of temperature for 1:4 DHEA:BIS sample before (solid circles) and after (open circles) periodate treatment.

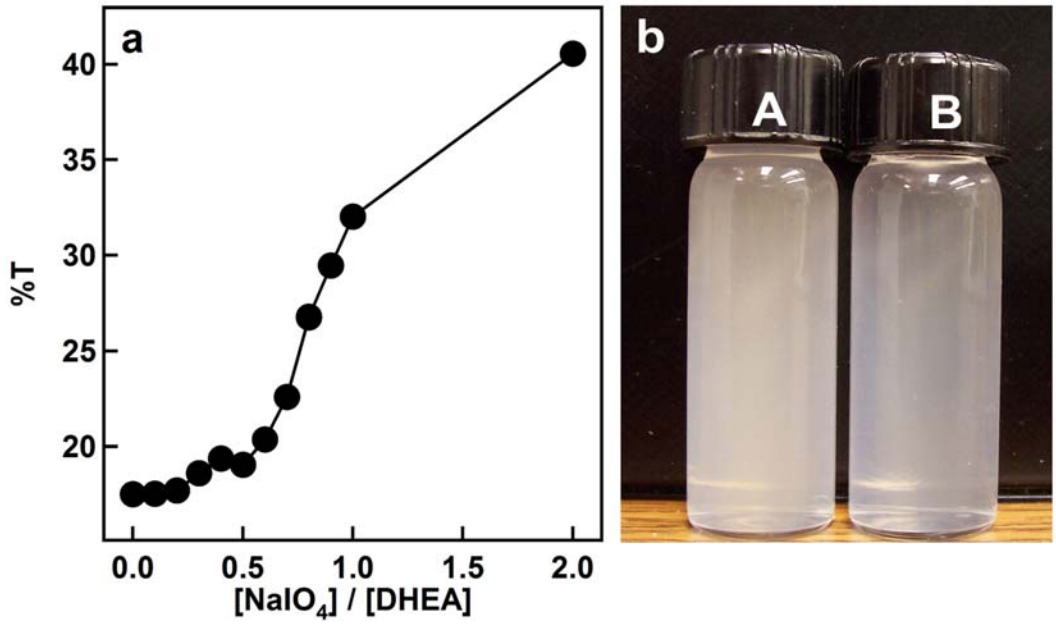

Figure 4-5. a) %T of core/shell particles as a function of periodate/DHEA ratio. b) Picture of the vials of core/shell particle solutions before (vial A) and after (vial B) periodate treatment.

Our group has experience in constructing core/shell particles by a two stage "seed and feed" polymerization method.[10,20,21] In this method, a dilute solution of core particles is heated to a temperature much higher than the LCST of the polymer, followed by addition of the "shell" monomer solution. After initiation of free radical polymerization in the aqueous phase, growing oligomers reach a critical chain length for phase separation, at which point they tend to aggregate on the deswollen seed particles. Continued polymerization, cross-linking, and aggregation of "shell" oligomers onto the core particles eventually leads to a dimensionally-stable core/shell microgel. By this method we are able to introduce different chemical functionalities to radially well-defined positions in the particle.

Core/shell particles were fabricated by using a DHEA cross-linked core (10 mol-%) followed by addition of a BIS cross-linked shell (2 mol-%). Figure 4-5a illustrates the change in %T of the core/shell particle suspension as a function of periodate/DHEA ratio. It is observed that %T increases with increase in concentration of $NaIO_4$, but to a lesser magnitude than was observed for the simple DHEA core particles. This is due to the presence of periodate-insensitive BIS cross-linked shell, which adds to the scattering cross-section of the particle. For complete degradation of the core (maximum solution transmittance), ~2 mole of $NaIO_4$ per mole of DHEA is required as opposed to the ~1 mole of $NaIO_4$ per mole of DHEA that was required for the DHEA core particles (see Figure 4-2). This difference in stoichiometry may arise due to differences in mass transport in the core and the core/shell particles, since the periodate ions have to pass through the shell to reach the core. Figure 4-5b shows the change in turbidity of the core/shell particles before (vial A) and after (vial B) degradation. Unlike what was

observed for the DHEA core particles, the core/shell solution does not become completely clear after degradation of the core. Again, this is due to the intact BIS cross-linked shell structure that remains following degradation.

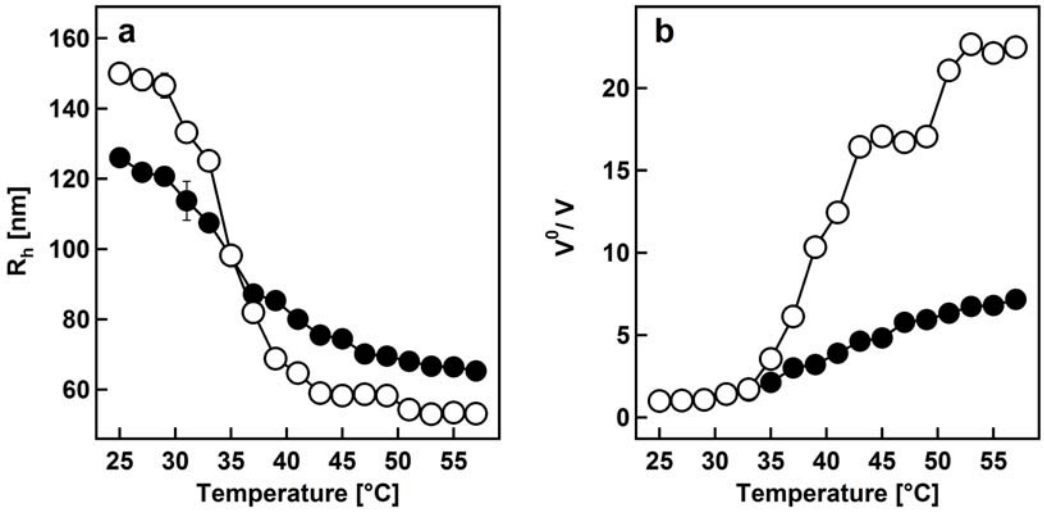

Figure 4-6. a) Variation in R_h of core/shell particles as a function of temperature before (solid circles) and after (open circles) periodate treatment. b) Normalized deswelling volume ratios as a function of temperature for core/shell particles before (solid circles) and after (open circles) periodate treatment.

Figure 4-6a shows the change in R_h of the core/shell particles as a function of temperature. The R_h of the non-degraded core/shell sample at 25 °C is ~125 nm and that of the parent core particle is ~110 nm (Figure 4-3a, 0% degraded), which indicates that a shell of ~15 nm has been added. After complete degradation, the R_h is larger (~150 nm) than before degradation. A similar effect was observed for the DHEA cross-linked core particles alone (Figure 4-3a, 90% degraded) and was rationalized as a substantial decrease in number of cross-links and loss of material, which increases the swellability of the particles. However, in the core/shell particle case, the increase in particle size must be due to swelling of the intact shell component, since the core component is degraded by a large excess of periodate, followed by removal of the degraded network. Since an interpenetrating network is formed at the interface between the core and the shell when these particles are synthesized,[10,20,21,23] the physical nature of the core has some impact on the swellability of the shell. Upon degrading the core, these interpenetrating polymer networks between the core and the shell are disrupted, which releases the shell from the constraints of the more highly cross-linked core. More precisely, since the shell is lightly cross-linked (2% cross-linking density) it has higher intrinsic swelling capacity than the 10% cross-linked core. Thus, the interpenetrated core/shell interface restricts the shell from swelling completely, resulting in core/shell particles that have a higher R_h after core degradation (Figure 4-6a). The deswelling curve for the core/shell microgels (Figure 4-6b) shows a smaller equilibrium swelling volume at high temperatures, a sharper phase transition, and a lower VPTT than the native microgel. All these observations indicate that the core has been degraded and there is loss of material from the particles.

To track the loss of material from the core/shell particles after degradation and cleaning by centrifugation, the DHEA cross-linked core was tagged with a phenantharene dye (see the Experimental Section). The phenanthrene-labeled core/shell particles show a characteristic vibronically-structured phenanthrene emission, with the largest emission peak centered at 373 nm when excited at 298 nm (Figure 5). The peak at 337 nm is due to Raman scattering from water, to which all the spectra were intensity normalized for comparison. After core degradation and centrifugation, the particles show a significantly attenuated fluorescence, indicating that the majority of the degraded material has been removed from the particles. Therefore, it is reasonable to assume that hollow pNIPAm particles have been obtained. Note that the dye integrity is not affected by periodate.

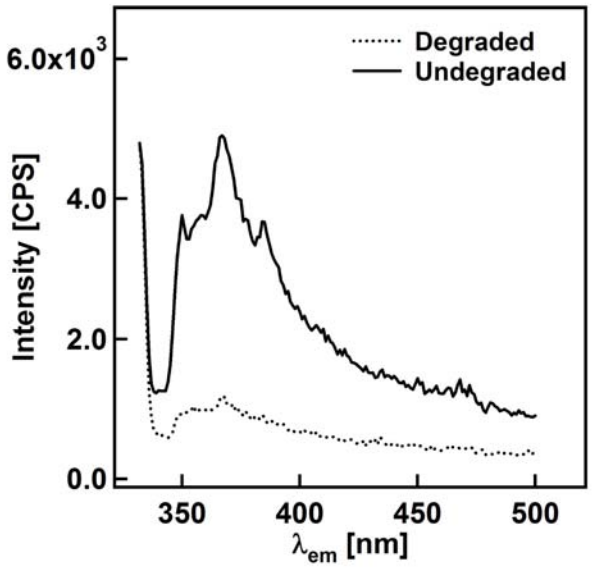

Figure 4-7. Fluorescence spectra (λ_{ex}= 298 nm) of the core/shell particles before (solid line) and after (broken line) degradation with periodate and cleaning by centrifugation.

4.4 Conclusions

The vicinal diol bond in DHEA incorporated into core/shell microgels can be efficiently cleaved using $NaIO_4$ as an oxidant. As a result, DHEA cross-linked pNIPAm microgels can be dissolved into small polymer segments using this $NaIO_4$ treatment. An identical treatment does not cause any degradation of BIS cross-linked microgels. Core/shell particles consisting of a DHEA cross-linked core and a BIS cross-linked shell can be prepared *via* two-stage free-radical precipitation polymerization. Degradation of particle core is then obtained *via* addition of $NaIO_4$ to the core/shell particle suspension. The polymer segments thus produced inside the particles can be efficiently removed from the microgel by centrifugation and resuspension. This treatment leaves behind a "hollow" thermoresponsive particle, as evidenced by fluorescence and light scattering measurements. In comparison to the non-degraded core/shell particles, hollow particles exhibit higher equlibrium swelling volumes below the LCST, and greater deswelling ratios at temperatures above the LCST, suggesting that there is a decrease in number of cross-links in the core and loss of material from the core.

REFERENCES

(1) Hoffman, A. S. *Adv. Drug Deliv. Rev.* **2002**, *54*, 3-12.

(2) Kim, S. W.; Bae, Y. H.; Okano, T. *Pharm. Res.* **1992**, *9*, 283-290.

(3) Nayak, S.; Lee, H.; Chmielewski, J.; Lyon, L. A. *J. Am. Chem. Soc.* **2004**, *126*, 10258-10259.

(4) Hu, Z.; Chen, Y.; Wang, C.; Zheng, Y.; Li, Y. *Nature (London)* **1998**, *393*, 149-152.

(5) Kawaguchi, H.; Fujimoto, K. *Bioseparation* **1998**, *7*, 253-258.

(6) Chen, L.; Kopecek, J.; Stewart, R. J. *Bioconjugate Chem.* **2000**, *11*, 734-740.

(7) Bergbreiter, D. E.; Case, B. L.; Liu, Y.-S.; Caraway, J. W. *Macromolecules* **1998**, *31*, 6053-6062.

(8) Bergbreiter, D. E.; Liu, Y.-S.; Osburn, P. L. *J. Am. Chem. Soc.* **1998**, *120*, 4250-4251.

(9) Pelton, R. *Adv. Colloid. Interface Sci.* **2000**, *85*, 1-33.

(10) Jones, C. D.; Lyon, L. A. *Macromolecules* **2000**, *33*, 8301-8306.

(11) Nayak, S.; Lyon, L. A. *Chem. Mater.* **2004**, *16*, 2623-2627.

(12) McPhee, W.; Tam, K. C.; Pelton, R. *J. Colloid Interface Sci.* **1993**, *156*, 24-30.

(13) Zrinyi, M. *Colloid Polym. Sci.* **2000**, *278*, 98-103.

(14) Meier, W. *Chem. Soc. Rev.* **2000**, *29*, 295-303.

(15) Zha, L.; Zhang, Y.; Yang, W.; Fu, S. *Adv. Mater.* **2002**, *14*, 1090-1092.

(16) Huang, H.; Remsen, E. E.; Kowalewski, T.; Wooley, K. L. *J. Am. Chem. Soc.* **1999**, *121*, 3805-3806.

(17) Peyratout, C. S.; Daehne, L. *Angew. Chem. Int. Ed.* **2004**, *43*, 3762-3783.

(18) Ng, D.; Guillet, J. E. *Macromolecules* **1982**, *15*, 728-732.

(19) Gan, D.; Lyon, L. A. *J. Am. Chem. Soc.* **2001**, *123*, 8203-8209.

(20) Gan, D.; Lyon, L. A. *J. Am. Chem. Soc.* **2001**, *123*, 7511-7517.

(21) Jones, C. D.; Lyon, L. A. *Macromolecules* **2003**, *36*, 1988-1993.

(22) O'Connell, P. B. H.; Brady, C. J. *Anal. Biochem.* **1976,** *76*, 63-73.

(23) Gan, D.; Lyon, L. A. *Analytica Chimica Acta* **2003**, *496*, 53-63.

CHAPTER 5

SYNTHESIS AND CHARACTERIZATION OF ZWITTERIONIC MICROGELS

In this chapter we discuss the synthesis and characterization of thermoresponsive microgels possessing both positive and negative charge. The major component of the microgels is the thermoresponsive polymer, poly(*N*-isopropylacrylamide). Negative charge is imparted by the comonomer acrylic acid (AAc), while the positive charge is introduced by incorporation of *N*-(3-aminopropyl)methacrylamide hydrochloride (APMA). These microgels exhibit pH dependent behavior that is characteristic of their zwitterionic nature. The variation in size of the microgels as a function of temperature and pH is monitored by photon correlation spectroscopy. Measurements of the particle zeta potential as a function of pH roughly correlate with the predicted charge. AAc has a pK_a of 4.25 and the amine of APMA has a pK_b of ~9, hence at pH below the pK_a of AAc the microgels are positively charged, while from pH 5-7 they are zwitterionic. The transition from a polyelectrolytic state to a zwitterionic state is accompanied by a decrease in hydrodynamic radius (R_h) of the microgels, which is brought about by the electrostatic attractive interaction between the oppositely charged regions of the microgel. The largest magnitude of the zwitterionic effect is observed for samples that have a total AAc concentration less than 1.5 mol-% relative to a constant APMA concentration of 0.75 mol-%. The effect disappears above that AAc concentration due to dominant anionic repulsive effects. At zwitterionic pH values, some samples showed

positive phase transition cooperativity, as evidenced by marked sharpening of the phase transition.

5.1 Introduction

Zwitterionic gels have both positively and negatively charged groups. These gels can be made by either having oppositely charged groups on the polymer backbone, commonly termed as polyampholytes or on the same monomer unit known as polybetaines, due to ubiquitous use of betaine monomers.[1-3] Figure 5-1 shows common monomers that have been used in making zwitterionic gels. Polyzwitterionic macromolecules, due to their similarity to biomolecules like proteins, have attracted a great deal of attention. Unlike polyelectrolytes that have just one charge, polyzwitterionic polymers have long range attractive forces that can provide a simplified synthetic model to protein folding.[4,5] Certain zwitterionic polymers have also been known to exhibit both upper critical solution temperature (UCST) and lower critical solution temperature behavior (LCST).[6] Polyampholytic gels have also been used to induce memory effect in the gels for binding certain target analytes.[7]

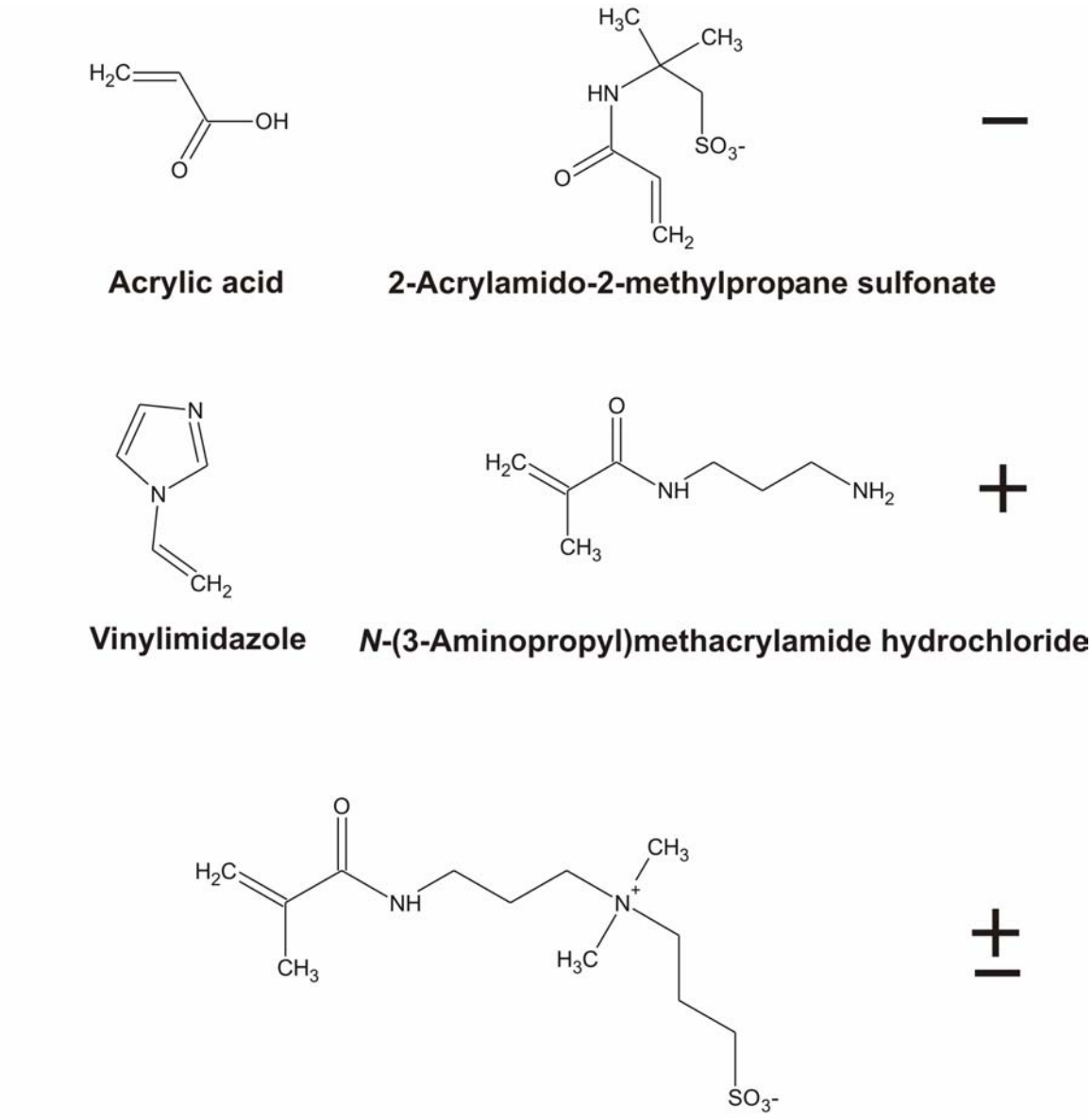

Figure 5-1. Common monomers used in preparation of zwitterionic gels.

Polyelectrolytic gels are swollen at very low ionic strength due to repulsion among the charged groups. By increasing the ionic strength the repulsive forces can be screened, which causes the gel to shrink.[2] In contrast, polyzwitterionic gels have electrostatic attractive forces at low ionic strength, while an increase in ionic strength screens the attractive forces and causes the gel to swell; this behavior is called the anti-polyelectrolyte effect.[8] This antipolyelectrolyte effect is useful for the applications that require the gels to be swollen at high salt concentrations. The behavior of these gels is dependent on the balance of positive and negative charges in the gel. If there is a significant charge imbalance, the gels behave like conventional polyelectrolytes. However, if the relative concentrations of the opposing charges are close, the anti-polyelectrolyte effect is observed.[8] Gels having betaine monomer units most often show the anti-polyelectrolyte effect because the two charged species are present on the same monomeric unit.[3,9,10]

Efforts in the synthesis of zwitterionic microgels have been limited due to their colloidal instability during synthesis, which causes them to aggregate and precipitate out of solution. Two of the most recent examples are by Neyret et al.[11] and Ogawa et al.[12] Neyret et al. synthesized polyampholytic microgels by microemulsion polymerization using sodium 2-acrylamido-2-methylpropanesulfonate (NaAMPS) as anionic monomer, {2-(methacryloyloxy)ethyl}trimethylammonium chloride (MADQUAT) as cationic monomer and N,N'-methylenebisacrylamide (BIS) as a crosslinker. Ogawa et al. synthesized polyampholytic microgels by precipitation polymerization using NIPAm as major monomer, vinylimidazole as the cationic comonomer, acrylic acid (AAc) as the anionic comonomer and BIS as a crosslinker.[12] In this chapter we present the

synthesis and pH dependence of thermoresponsive, zwitterionic microgels. The main component of the microgels is pNIPAm and the two charges are imparted by *N*-(3-aminopropyl)methacrylamide hydrochloride (APMA), which gives positive charge and AAc, which provides the negative charge. It is observed that the microgels show comonomer concentration dependent and pH dependent zwitterionic behavior, which is detected by change in hydrodynamic radius of the microgels. Also, these microgels exhibit positive cooperativity in undergoing temperature dependent deswelling, as observed through a sharpening of the phase transition curve.

5.2 Experimental Section

Materials

N-isopropylacrylamide (NIPAm, Aldrich) was purified by recrystallization from hexane (J. T. Baker) prior to use. Acrylic acid (AAc), *N, N'*-methylenebis(acrylamide) (BIS), ammonium persulfate (APS), sodium dodecyl sulfate (SDS) and sodium chloride were purchased from Aldrich and used as received. *N*-(3-Aminopropyl)methacrylamide hydrochloride (APMA) was purchased from Polysciences. Water was purified with Barnstead E-Pure system to a resistance of 18 MΩ and then filtered through a 0.2 μm filter to remove particulate matter.

Preparation of Zwitterionic Microgels

A detailed procedure for preparation of microgels by free radical precipitation polymerization is described elsewhere.[13,14] The total monomer concentration in the pregel solution was kept constant at 40 mM, out of which 2 mol-% was BIS and 0.75 mol-%

was APMA. The relative concentration of AAc was varied from 0.5% to 3% and the mol-% of NIPAm was adjusted to keep the total monomer concentration constant, as shown in Table 5-1. All the monomers and 7 mg of SDS were dissolved in 25 ml of water and the resulting solution was filtered through 0.2 μm membrane filter (Pall Gelman Metricel) to remove particulate matter. The reaction mixture was heated in a 3-necked round bottom flask equipped with a condenser and inlet for nitrogen. The mixture was heated to 65 °C under a gentle stream of nitrogen for 1 hour. 6 mg of APS was added to initiate the reaction. The reaction mixture was kept at 65 °C for 4 hours to complete the reaction. After synthesis, the microgel solution was filtered using fine porosity filter paper (Fisher Scientific) to remove aggregated material, if any. The particles were then purified by dialysis (Spectra/Por 7 dialysis membrane, MWCO 10,000) against daily changes of water for at least 14 days.

Table 5-1. Chemical Composition of Zwitterionic Microgels

Sample Code	[NIPAm][a]	[BIS]	[APMA]	[AAc]
Z050	96.75	2.00	0.75	0.50
Z075	96.50	2.00	0.75	0.75
Z100	96.25	2.00	0.75	1.00
Z150	95.75	2.00	0.75	1.50
Z200	95.25	2.00	0.75	2.00
Z300	94.25	2.00	0.75	3.00

[a]All concentrations are in mol-%.

Particle Characterization

Particle sizes were determined via photon correlation spectroscopy (PCS, Protein Solutions Inc.) equipped with an integrated Peltier temperature control device (± 0.1 °C), as previously reported.[13,15] All solutions used for PCS measurements were adjusted to the desired pH with HCl and/or NaOH while monitoring with a Corning 430 pH meter. Sodium chloride was then used to adjust each solution to 0.001M total ion concentration. 0.5 ml of 10μg/ml of the particle solution was placed in a three-sided quartz cuvette for determination of the hydrodynamic radii of the particles. The hydrodynamic radii of the particles were calculated from the diffusion coefficient using the Stoke-Einstein equation.

The sample was allowed to equilibrate at the proper temperature for 5 minutes before data collection. Longer equilibration times did not lead to any variation in the measured particle size, scattering intensity or polydispersity. Scattered light from the fiber-coupled diode laser (798 nm) was collected at 90° with a fiber-coupled avalanche photodiode detector connected to a 248-channel autocorrelator board. The data was analyzed with Protein Solutions' Dynamics Software Version 5.25.44. Each data point presented here is an average of five separate size determination. Each size determination consists of 20 total measurements with a 5 second integration time for each acquisition. All particles presented here displayed a size polydispersity between 4 and 15%, suggesting a monomodal particle distribution. It should be noted that *absolute* size and size distribution determinations for particles in the size ranges reported below are possible via single-angle photon correlation spectroscopy only for isotropic, monodisperse particles. The particle sizes presented below may therefore not be exact. Nonetheless, small errors in the absolute sizes do not alter the main conclusions of this work, which are based on the *relative* particle size changes with temperature and pH.

Zeta Potential Measurements

Zeta potential (ζ) for microgels was measured by ZetaPlus instrument (Brookhaven Instruments Co., NY). Samples for the zeta potential were prepared by adding microgel into 1 mM KCl solution and then adjusting the pH with HCl / NaOH. Each measurement was conducted with 6 analyses at 25 °C and zeta potentials are mean values of triplicate measurements at a particular pH. Zeta potential was calculated by the software provided by the manufacturer. It should be noted that it is not clear how buried charges in the hydrogel particle contribute to the observed zeta potential. Thus, these

measurements are meant to roughly illustrate the change in effective surface charge with pH and most likely do not represent the total charge on the particle at any given pH.

5.3 Results and Discussion

Gels that are polyanionic or polycationic exhibit a phenomenon known as the polyelectrolytic effect, where there is a decrease in the water content of the gel with an increase in the ionic strength of the solution. This is due to screening of the repulsive charges by ions. Polyzwitterionic gels (having both the charges) have been known to show an antipolyelectrolyte effect, which is characterized by increase in water content in the gel in response to increase in ionic strength.[2,8] This increase is attributed to screening of the attractive forces among the oppositely charged regions of the gel. Since we want to explore these Coulombic attractive forces in the microgels we chose to use solutions of very low ionic strength (1 mM) where charge screening will be minimized.

Microgels having ionizable groups show pH dependent swelling. We and others[13,16] have previously shown that microgels having AAc groups swell at pH greater than the pK_a of AAc (4.25) due to Coulombic repulsion among the acid groups in the microgels and osmotic swelling due to counterion ingress. Figure 5-2 shows pH dependence of Samples Z300 and Z075 at 31 °C. The monomer feed compositions for these microgels are shown in Table 5-1. Sample Z300, which has high mol-% of AAc (3.00%) in comparison to APMA (0.75%), predominantly acts as an anionic microgel beyond the AAc pK_a. As seen from the Figure, the hydrodynamic radius (R_h) of the microgel remains constant until pH 5 and increases beyond that pH. This increase in size is attributed to the ionization of the acid groups in the microgel and subsequent

Coulombic repulsion and osmotic swelling. In Sample Z075, the mol-% of both AAc and APMA is 0.75%. Hence the microgels are zwitterionic beyond the pK_a of AAc and below the pK_b of the amine co-monomer. The plot for Z075 shows three regions; the first region, pH < 3, is where the microgel is expected to be positively charged due to protonated amines, the second region, 3 < pH < 6.5, it is presumably zwitterionic due to existence of both the charges and in the third region, pH > 7, the microgels possess an overall negative charge due to the deprotonated acid groups of AAc and partial protonation of the amine comonomer. Figure 5-3, where the measurements are carried out at 25 °C, shows the same effect as the Figure 5-2.

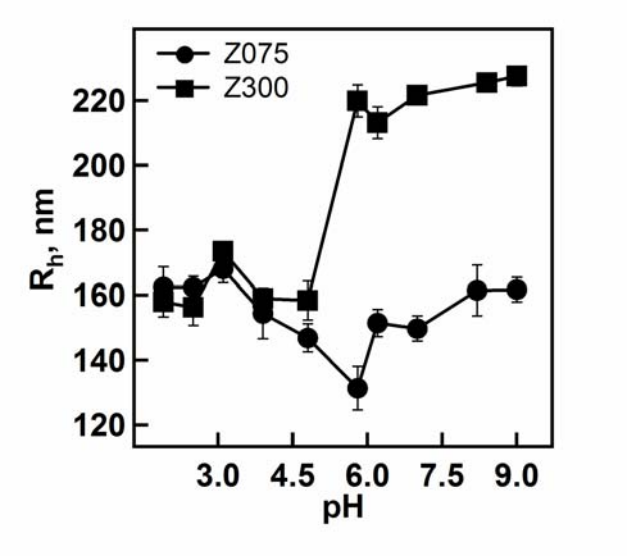

Figure 5-2. Variation in R_h of microgels at 31 °C for samples Z075 (●) and Z300 (■). Error bars represent one standard deviation from the average of five measurements.

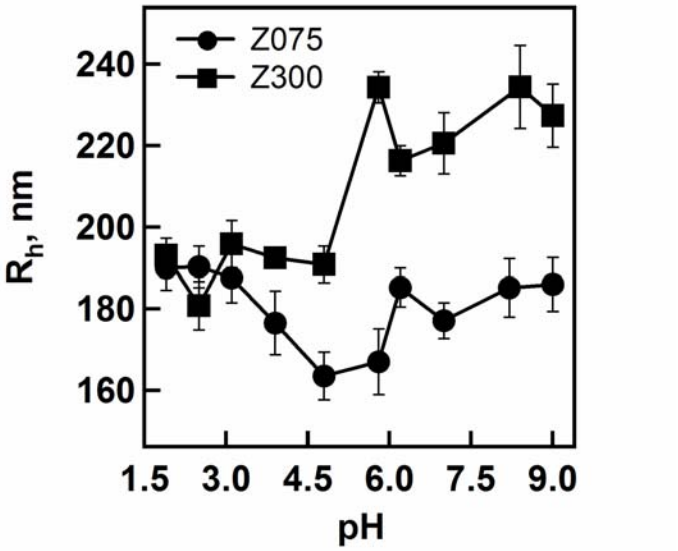

Figure 5-3. R_h as a function of pH for samples Z075 (●) and Z300 (■) at 25 °C. Error bars represent one standard deviation about the average of five measurements.

To confirm these assignments, the zeta potential of sample Z075 was measured as a function of pH (Figure 5-4). It is observed that the microgels are positively charged at pH < 3, almost zero and slightly negatively charged between pH 3 and 5.8 and highly negatively charged at pH > 7, the zeta potential becomes significantly more negative beyond pH 5, which agrees well with the observed increase in the R_h beyond pH 5 in Figure 5-2. In the first region, polycationic repulsion leads to a swollen microgel. In the second region, where the acids are deprotonated, the size depends on the balance of Coulombic attractive and repulsive forces. The attractive forces consist of acid-amide hydrogen bonds and the formation of stable ion-pairs between the COO^- and NH_3^+ groups in the gel. The repulsive forces are due to uncompensated charges (charges that do not take part in ion-pairing) and osmotic swelling. It is observed from Figure 5-2 that the R_h of Z075 decreases beyond pH 5, this decrease is due to excessive attractive forces than repulsive forces. In contrast, sample Z300 displays an increase in R_h beyond pH 5 due to repulsion among excess deprotonated acid groups. Z075 shows a minimum R_h at pH 5.8, which indicates that at this pH maximum number of ion-pairs that are allowed by polymer chain flexibility are formed between the amines and the acids in the microgel. Beyond this pH, in the third region, the size begins to increase, presumably due to further deprotonation of the acid groups and/or a decrease in the number of protonated amines, which disrupts the ion-pairs and causes the microgel to swell. As shown in Figure 5-4, the microgel is largely anionic in this region. It should be noted that even Z300 is zwitterionic beyond pH 5, but has four times more AAc content than Z075. Hence at pH values above the pK_a of AAc this microgel behaves mostly as a polyanionic particle. For Z300 in the region beyond the pK_a of AAc the attractive forces are overpowered by the

repulsive forces due to the presence of excess of anionic moieties in the microgel and hence an increase in R_h beyond the pK_a of AAc is observed. Figure 5-5 illustrates the zeta potential of Z075 at 31 °C, which is very similar to Figure 5-4, thereby confirming that there is not a subsequent change in the charge of the microgels with temperature.

Poly (*N*-isopropylacrylamide) has a lower critical solution temperature (LCST) ~31 °C. Below the LCST the polymer is hydrated due to the hydrogen bonding between water and amide side chains of the polymer. Above the LCST, polymer-polymer interactions become stronger than water-polymer interactions and the polymer undergoes coil-to-globule transition. This thermoresponsive polymer, when conformed into microgels by a crosslinking agent such as BIS, shows a volume phase transition temperature (VPTT). Addition of comonomers, variation in the cross-linking density or any changes in the surrounding medium can affect the VPTT of the microgel. At temperatures lower than the VPTT the microgel is in a swollen state as water molecules fill the individual microgels. Above the VPTT the hydrogen bonding between the water and the polymer side chains is disrupted and the hydrophobic interactions among the neighboring polymer chains increase with a subsequent release of water from the microgels, which is entropically favored. This release of water results in a large magnitude change in the volume of the microgels at the VPTT. Addition of hydrophilic comonomers into hydrogel system increases the VPTT; on the other hand addition of hydrophobic comonomers decreases the VPTT. Based on the results from Figure 5-2 to 5-5, the microgels have a positive charge at pH 3.00 and are zwitterionic at pH 5.00. This is illustrated in Figure 5-6.

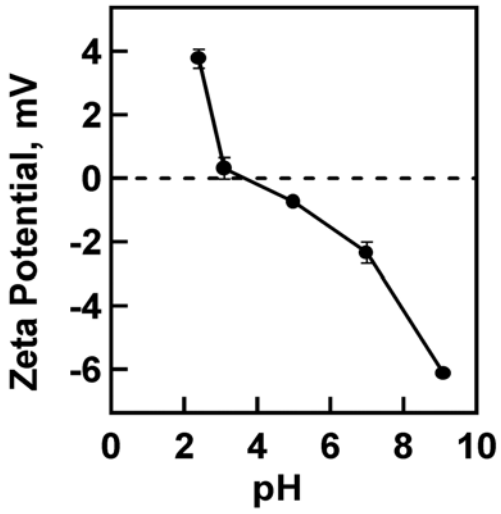

Figure 5-4. Zeta potential values for sample Z075 at 25 °C as a function of pH. Error bars represent one standard deviation from the average of three measurements.

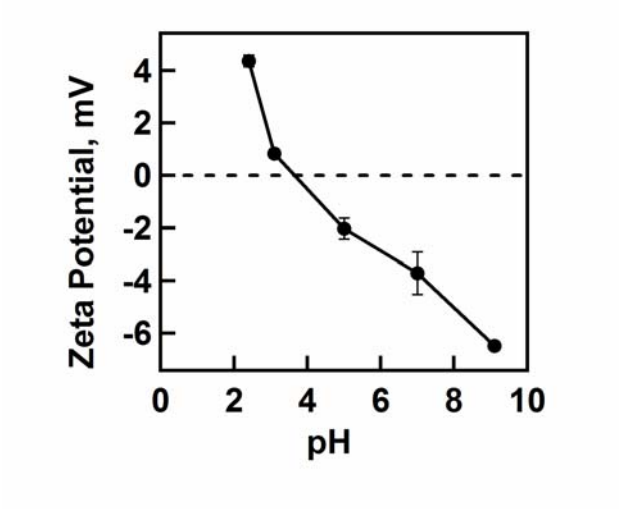

Figure 5-5. Zeta potential values for sample Z075 as a function of pH at 31 °C. Error bars represent one standard deviation from the average of three measurements.

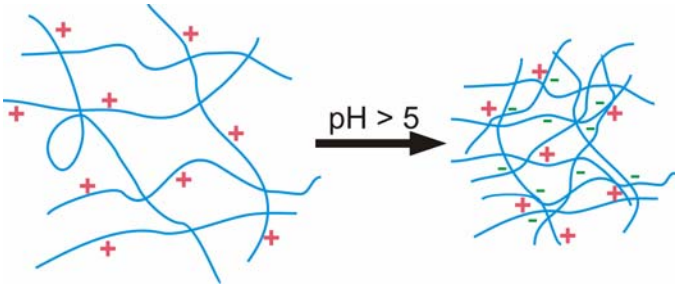

Figure 5-6. At pH < pKa of AAc the microgels are positively charged due to the protonated amines. At pH > pKa of AAc the microgels become zwitterionic due to deprotonation of the acid groups. The oppositely charged regions in the microgels form salt bridges thereby reducing the R_h of the microgels at higher pH.

It is observed from Figure 5-2 that there is a decrease in the R_h of the Sample Z075 upon going from pH 3 to 5, and as mentioned above, the microgels are cationic at pH 3 and zwitterionic at pH 5. To elucidate the thermal deswelling behavior in these two states, volume phase transition curves were obtained by PCS. Figure 5-7 shows the phase transition curves for samples Z050 and Z075 at pH 3 and 5, where R_h is plotted as a function of temperature. The R_h at the outset for both samples is smaller at pH 5 than at pH 3. This is attributed to the Coulombic attraction between the zwitterionic moieties in the microgels at pH 5, which as mentioned above, results in formation of ion-pairs between the oppositely charged species. It is observed that the difference in the R_h for Z050 at 25 °C for the two pHs is ~ 40 nm, while that for Z075 is ~20 nm. It is also evident from Figure 5-7 that the VPTT for both the samples is lower at pH 5 than at pH 3. Finally, the phase transition region is slightly sharper at the higher pH in both cases. The observed differences in R_h, VPTT, and curve sharpness at the two pHs is dictated by the

relative contributions of uncompensated and compensated charges in the microgel. For example, simple microgels containing AAc have pH-dependent VPTTs, where the VPTT increases at pH > pK_a with a concomitant increase in the breadth of the transition region.[13] This is due to electrostatic repulsion between the negatively charged groups and osmotic swelling by counter ion ingress. Hence in the case of Z050 and Z075, where the VPTT is lower at pH 5 than at pH 3, the water content of the microgels must be decreasing on going from lower pH to higher pH. This decrease in water content is brought about by formation of ion-pairs between the deprotonated acid groups and the protonated amine groups.

To find out the difference in VPTT at the two pHs the VPT curve for Z075 is fit to a cubic spline and first derivative is taken as a function of temperature. In Figure 5-8 the first derivative curves for the two pHs are plotted as a function of temperature. The VPTT at pH 5.00 is ~ 2 °C lesser than at pH 3.00. The width of the peaks are different too, at pH 5.00 the peak is sharper, which indicates some sort of positive cooperativity with temperature in deswelling the microgels. At low temperature where the gel is swollen, the oppositely charged regions are not close enough to form strong ion-pairs. Upon heating, the microgels begin to deswell via the thermal (entropically-driven) mechansim, which causes the polymer chains to aggregate. Once a small degree of thermal deswelling has taken place, oppositely charged regions of the microgel may now be in close enough proximity to form ion-pairs. This will result in cooperative deswelling, where each incremental degree of thermal deswelling will increase the probability of ion pairing induced deswelling. In turn, ion pairing will increase the propensity for hydrophobic aggregation of the polymer chains.

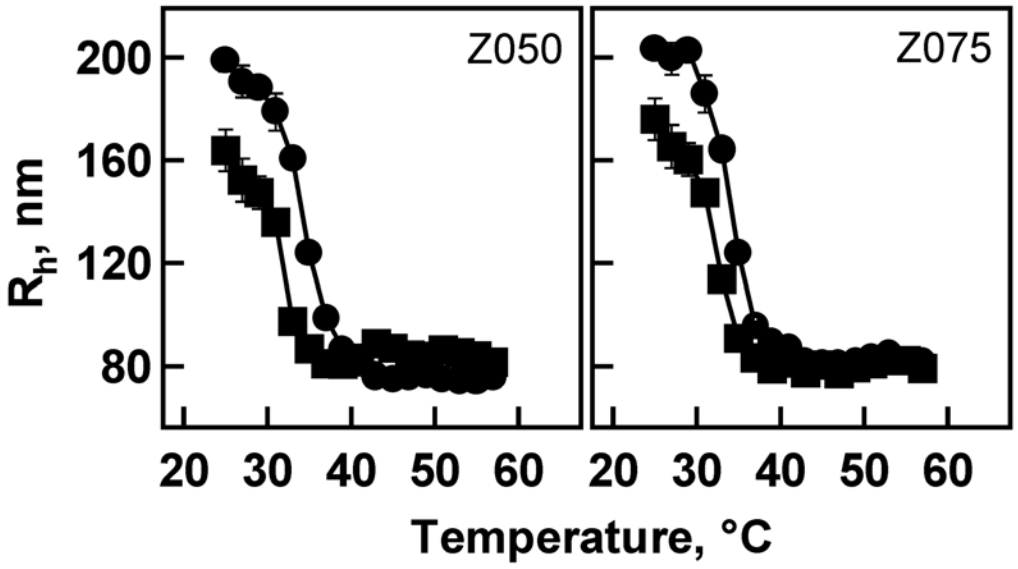

Figure 5-7. Variation in the R_h of samples Z050 and Z075 as a function of temperature at pH 3.00 (●) and pH 5.00 (■). Error bars represent one standard deviation from the average of five measurements.

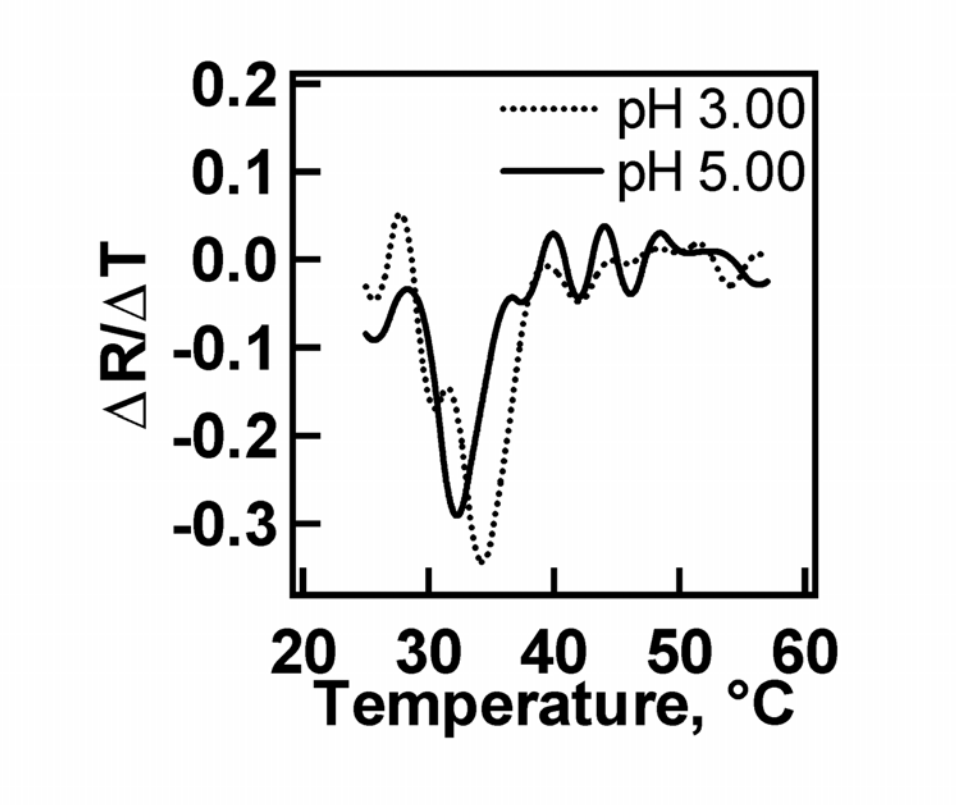

Figure 5-8. First order derivative with respect to temperature of cubic spline fit for sample Z075 at pH 3.00 and pH 5.00.

Figure 5-9 shows the VPT curves for Z150 and Z300 at pH 3 and 5. Unlike the data shown in Figure 5-7, the R_h at 25 °C for both the samples is now larger at pH 5. Since both particles now contain a higher number of acidic sites as compared to basic sites, this effect is most likely due to repulsive forces between negatively charged AAc groups at the higher pH. These Coulombic repulsive forces now dominate the microgel swelling as opposed to any attractive ion pairing forces. It is also observed that the VPTT for these samples is higher at pH 5, while the VPTT was lower at pH 5 vs. 3 for the samples presented in Figure 5-7. Again, this effect is presumably due to increase in Coulombic repulsion between uncompensated anionic charges in the network, as well as an osmotic pressure increase due to counterion ingress. It is also observed that for both of these samples the phase transition region appears somewhat sharper at pH 5 than at pH 3.

To determine the effect of increasing mol-% of AAc on the zwitterionic behavior, the R_h of different microgel samples at 31 °C (Table 5-1) was plotted as a function of mol-% AAc at both pH 3 and 5, see Figure 5-10. It is observed that the R_h for various mol-% AAc samples is invariant with acid content at pH 3 as the amount of amine is constant for all the samples. At pH 5, however, the R_h increases with an increase in the concentration of AAc, which arises from the increase in uncompensated charge on the microgel. For the samples having concentrations of AAc less than 1.5%, the R_h at pH 5 is less than that at pH 3 while for samples with concentrations of AAc higher than 1.5% the R_h at pH 5 is higher than that at pH 3. As explained above, this effect is due to the ability of oppositely charged species to form ion-pairs and affect a decrease in the size of the microgels. On further increasing the concentration of AAc beyond 1.5 mol-%, the

zwitterionic effect on particle size seems to disappear due to an increase in repulsive forces between the negatively charged acid groups.

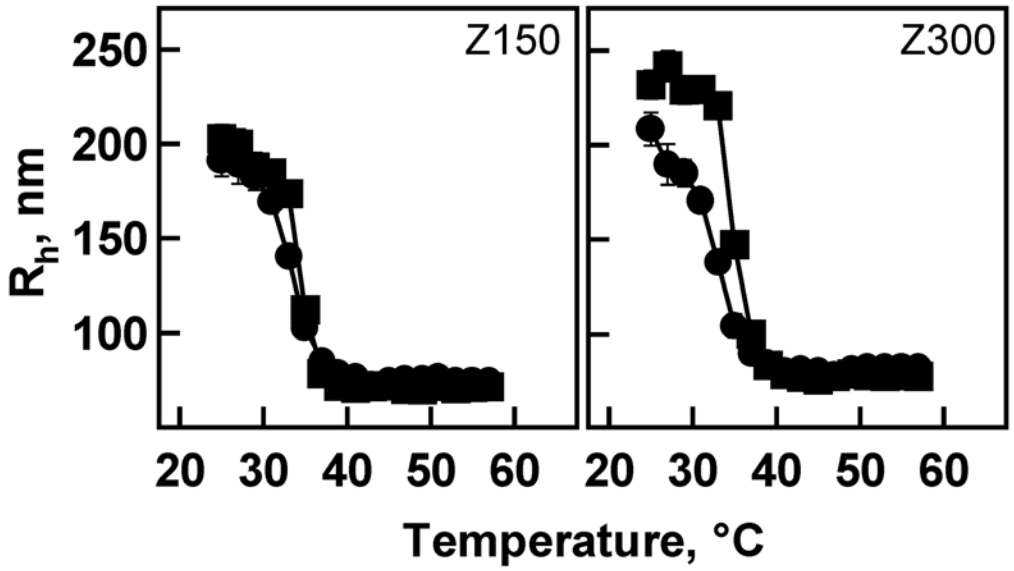

Figure 5-9. Variation in the R_h of samples Z150 and Z300 as a function of temperature at pH 3.00 (●) and pH 5.00 (■). Error bars represent one standard deviation from the average of five measurements.

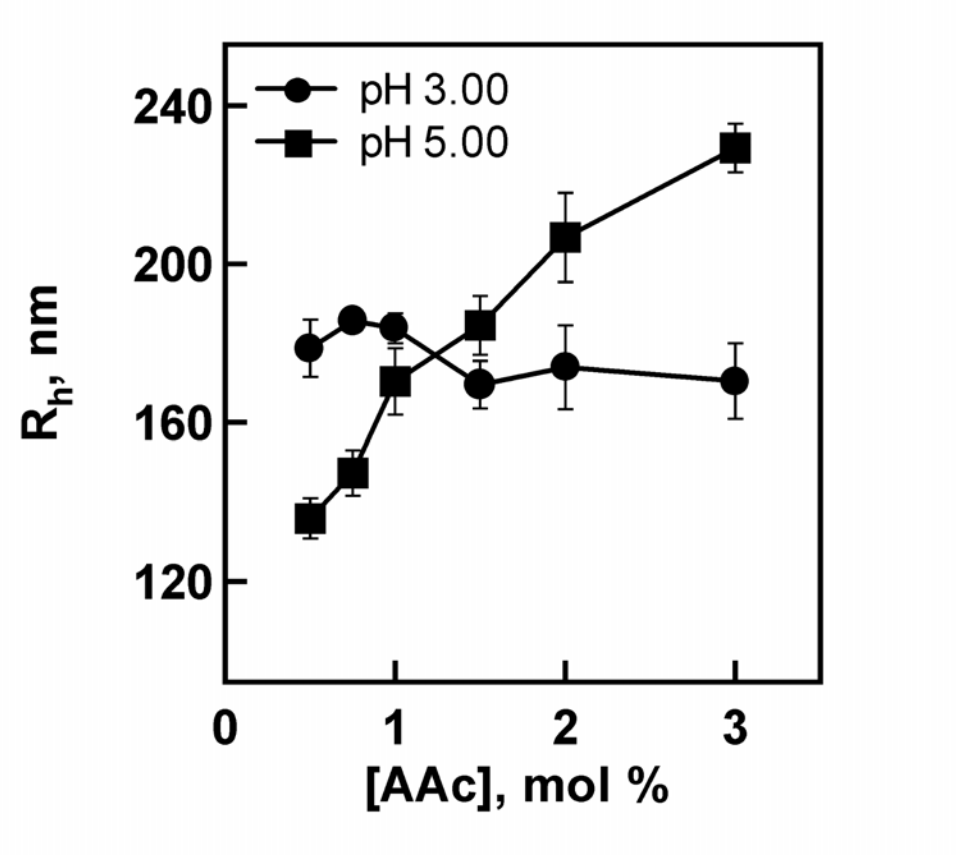

Figure 5-10. Dependence of the microgel R_h at pH 3.00 (●) and pH 5.00 (■) as a function of AAc concentration. Error bars represent one standard deviation from the average of five measurements.

Based on the comments of one of the reviewers for this paper, we found that our method for cleaning the microgels (dialysis) was not optimum. For dialysis we used the tubing with 10,000 dalton cutoff. It is possible that there are some large oligomers, which cannot pass through the dialysis tubing and might affect the behavior of the microgels. To overcome this difficulty we cleaned our Z075 sample by dialysis. The size of the cleaned microgels was determined by DLS as a function of pH. It was observed that the microgels did exhibit the zwitterionic effect but not to the extent that was seen before centrifugation. Hence the zwitterionic effect that was observed all through this chapter was a combination of some free charged polymer and the microgels. Due to this, the behavior of the microgels becomes more difficult to explain.

5.4 Conclusions

We have synthesized zwitterionic microgels, which show pH-dependent swelling. But the method of cleaning the microgels was not optimum and hence the results obtained by all the experiments carried out for this project are ambiguous. We are working on fabricating microgels by a different method, which will be discussed in the future work chapter.

REFERENCES

(1) Lowe, A. B.; McCormick, C. L. *Chem. Rev.* **2002**, *102*, 4177-4189.

(2) Nisato, G.; Munch, J. P.; Candau, S. J. *Langmuir* **1999**, *15*, 4236-4244.

(3) Lee, W. F.; Chen, Y. J. *J. Appl. Polym. Sci.* **2001**, *81*, 2888-2900.

(4) English, A. E.; Tanaka, T.; Edelman, E. R. *Polymer* **1998**, *39*, 5893-5897.

(5) English, A. E.; Tanaka, T.; Edelman, E. R. *Macromolecules* **1998**, *31*, 1989-1995.

(6) Arotcarena, M.; Heise, B.; Ishaya, S.; Laschewsky, A. *J. Am. Chem. Soc.* **2002**, *124*, 3787-3793.

(7) Alvarez-Lorenzo, C.; Hiratani, H.; Tanaka, K.; Stancil, K.; Grosberg, A. Y.; Tanaka, T. *Langmuir* **2001**, *17*, 3616-3622.

(8) Baker, J. P.; Blanch, H. W.; Prausnitz, J. M. *Polymer* **1995**, *36*, 1061-1069.

(9) Xue, W.; Champ, S.; Huglin, M. B. *Eur. Polym. J.* **2001**, *37*, 869-875.

(10) Lee, W. F.; Yeh, P. L. *J. Appl. Polym. Sci.* **1999**, *74*, 2170-2180.

(11) Neyret, S.; Vincent, B. *Polymer* **1997**, *38*, 6129-6134.

(12) Ogawa, K.; Nakayama, A.; Kokufuta, E. *Langmuir* **2003**, *19*, 3178-3184.

(13) Jones, C. D.; Lyon, L. A. *Macromolecules* **2000**, *33*, 8301-8306.

(14) Pelton, R. *Adv. Colloid. Interface Sci.* **2000**, *85*, 1-33.

(15) Jones, C. D.; Lyon, L. A. *Macromolecules* **2003**, *36*, 1988-1993.

(16) Eichenbaum, G. M.; Kiser, P. F.; Simon, S. A.; Needham, D. *Macromolecules* **1998**, *31*, 5084-5093.

CHAPTER 6

FOLATE-MEDIATED CELL TARGETING AND CYTOTOXICITY USING THERMORESPONSIVE MICROGELS

6.1 Introduction

One of the major concerns regarding cancer treatment is the low therapeutic index of the drugs used.[1] This limitation can be partially overcome by using drugs that are specifically targeted to cancer cells. Several classes of targeting species have been used such as sugars, lectins, vitamins and peptides.[2-4] In this chapter we report the use of thermoresponsive hydrogel nanoparticles as a potential drug delivery system. These nanoparticles are decorated with folic acid, which is a ligand for folate receptors (FR). FRs are overexpressed in number of human tumors, most often in epithelial cancers of ovary, mammary gland, lung, nose, throat, brain and colon.[1] Cancer cells require excessive FRs to enable their rapid proliferation. In the past, conjugates of folic acid have been used for targeted delivery of radionuclides,[5] oligonucleotides[6] and drugs[7] to cancer cells, wherein these conjugates enter cells via folate-receptor mediated endocytosis.[8] Here we report selective endocytosis of temperature responsive hydrogel nanoparticles that are conjugated to folic acid. We also show that these nanoparticles reside in the cytosol following uptake and exhibit a pronounced temperature dependent cytotoxicity.

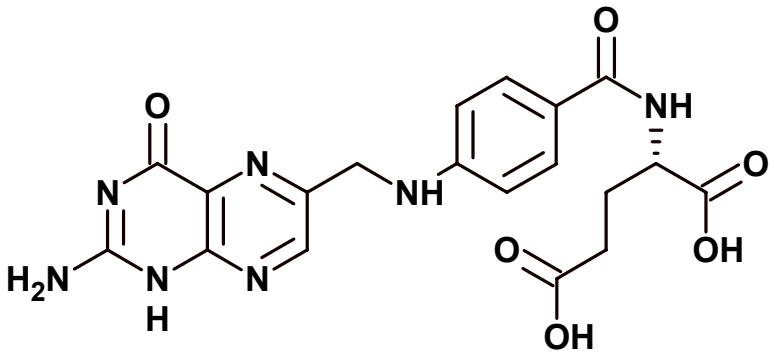

Figure 6-1. Structure of folic acid.

A considerable amount of effort has been invested in using folic acid as a targeting moiety for cancer cells because of its high tumor to non-target tissue ratio.[1] Figure 6-1 shows the structure of folic acid. Many particulate carriers such as dendrimers,[9] polymer particles,[10] liposomes[11] and micelles[12] have been conjugated with folic acid to target cells that overexpress FR. The advantages of using a particulate carrier relate to the environmental protection of the drugs, a relaxation of the need for covalent attachment of the drugs and potential for higher payloads.[13] In this work we use folic acid conjugated hydrogel nanoparticles as a potential drug delivery agent for targeting cancer cells.

6.2 Experimental Section

Microgel Synthesis.

Hydrogel core-shell nanoparticles were synthesized by aqueous free radical precipitation polymerization. A detailed description of this polymerization can be found elsewhere.[14] In brief, a fluorescently labeled core was synthesized by dissolving 700 mg of hexane recrystallized *N*-isopropylacrylamide (NIPAm), 21 mg of *N*,*N'* methylenebisacrylamide (BIS), 2.8 mg of 4-Acrylamidofluorescein (AFA) monomer, which was synthesized as described previously.[15] and 57 mg of sodium dodecyl sulfate (SDS) in 100 mL of deionized water. The solution was heated to 70 °C under gentle stream of nitrogen. After stabilizing the solution for 1 h, 45 mg of ammonium persulfate (APS) dissolved in 1 mL of water was added to initiate the reaction. The reaction was allowed to proceed for 4 h at 70 °C. After polymerization the solution was filtered. The detailed procedure of the shell addition to the core can be found in previous submissions.[16,17] In brief, 20 mL of the core microgel solution was taken in a three-necked round bottom flask, to which 20 mg of SDS and 70 mL of deionized water was added. The solution was heated under nitrogen to 70 °C. Separately, 400 mg of NIPAm, 12 mg of BIS and 7 mg of *N*-(3-aminopropyl)methacrylamide hydrochloride (APMA) were dissolved in 10 mL of deionized water. This solution was degassed at room temperature for 1 h and then was added to the heated core solution. Finally, 32 mg of APS dissolved in 1 mL of water was added to the solution to initiate the reaction. The reaction was allowed to proceed for 4 h at 70 °C and then was cooled and filtered. The polymer solution was then dialyzed for three weeks against daily changes of water.

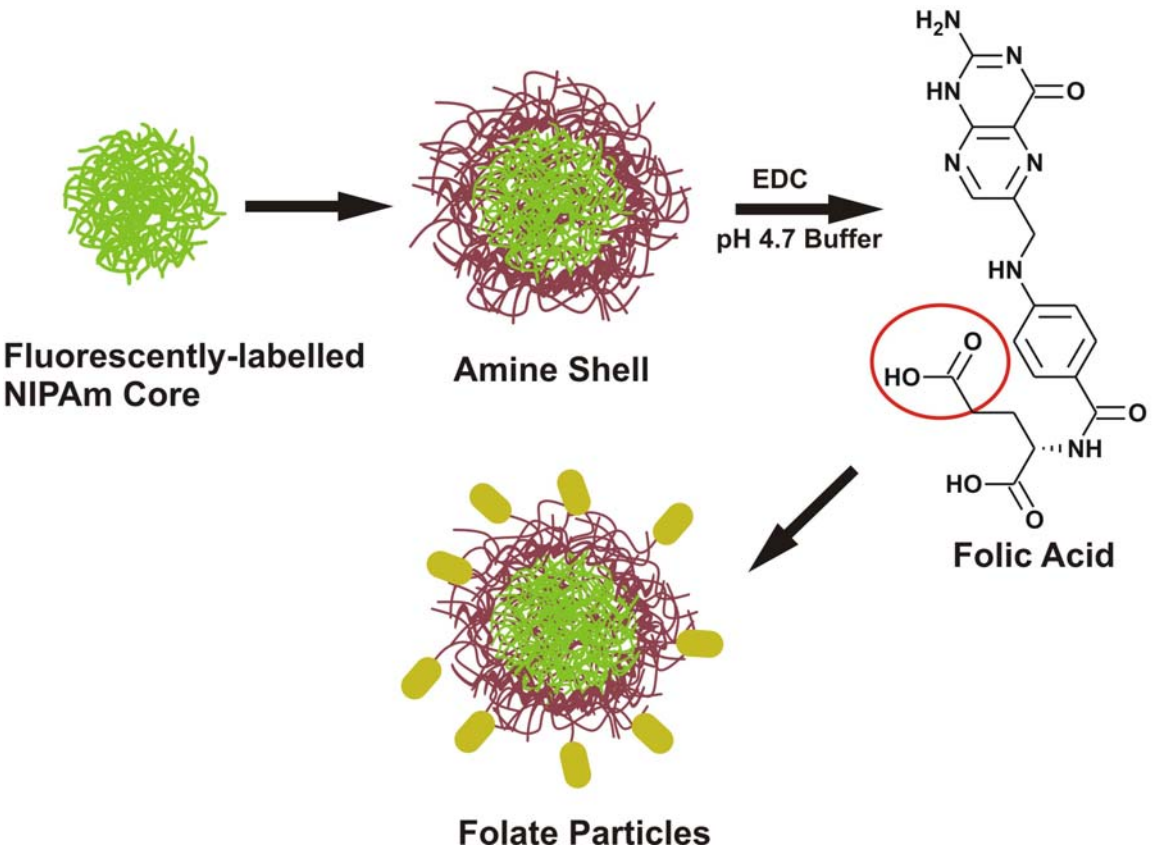

Figure 6-2. Synthesis of folate particles. An amine shell is synthesized on fluorescently-labeled cores. The γ-carboxylic acid of folic acid is conjugated to the amines.

Conjugation of Folic acid.

Figure 6-2 depicts the process of conjugating folic acid to core/shell microgels. Hydrogel core-shell particles were conjugated with folic acid by following the procedure of Dube et al.[18] 50 mL of the dialyzed core-shell solution was lyophilized and then resuspended in 50 mL of 10 mM phosphate buffer pH 4.7. 5.3 mg of folic acid was dissolved in 1 mL DMSO and to it 3.4 mg of 1-ethyl-3-(3-dimethylaminopropyl)carbodiimide (EDC) was added to activate the acid groups on folic acid; the solution was then mixed for 30 min. The activated folic acid solution was added to 25 mL of resuspended polymer solution. The mixture was stirred overnight in dark. The solution was brought to pH 9 by the addition of NaOH and was filtered and then dialyzed against phosphate buffered saline (PBS) for one week with daily changes of PBS, and then against deionized water for two weeks in the dark with daily changes of water. A control sample of the core-shell particles was also made by following the above procedure exactly but without using EDC.

Photon Correlation Spectroscopy.

Particle sizes were determined via photon correlation spectroscopy (PCS, Protein Solutions Inc.) equipped with an integrated Peltier temperature control device (± 0.1 °C), as previously reported.[17,19] The hydrodynamic radii of the particles were calculated from the diffusion coefficient using the Stoke-Einstein equation. The sample was allowed to equilibrate at the proper temperature for 10 minutes before data collection. Scattered light from the fiber-coupled diode laser (784.8 nm) was collected at 90° with a fiber-coupled avalanche photodiode detector connected to a 248-channel autocorrelator board. The data was analyzed with Protein Solutions' Dynamics Software Version 5.25.44.

Cellular Uptake Studies.

KB cells in 2 mL of folate deficient RPMI medium supplemented with 10% of heat-inactivated fetal bovine serum (FCSHI) and 100 units/mL of penicillin/streptomycin (PS) (Sigma) were seeded into 12-well plates and grown in a humidified 5% CO_2 atmosphere at 37 °C for 24 h. The cells were incubated for 4 h at 25 °C in the presence of a 100 μL suspension of AFA-171-2 or AFA-FOL-171-2 at a concentration of 10 mg/mL. Following incubation, the cells were washed with PD (Ca^{+2} and Mg^{+2} deficient buffer) (2x) and pH 3 saline (2x). The cells were gently dislodged from the wells with 1 mL of cell dissociation solution (Sigma). Mean fluorescence values were measured on a BD FACSCalibur Flow Cytometer with excitation of fluorescein at 488 nm.

Confocal Microscopy.

KB cells were seeded into LabTek chamber slide dishes in folate deficient RPMI culture media supplemented with 10% FCSHI and grown in a humidified 5% CO_2 atmosphere at 37 °C for 24 h. The cells were incubated in the presence of a 20 μL suspension of AFA-171-2 or AFA-FOL-171-2 at a concentration of 10 mg/mL. After 4 h incubation at 25 °C, the cells were washed with PBS (2x) and pH 3 saline (2x), and PBS buffer (600 μL) was added. Fluorescence images were recorded on a Biorad MRC 1024 Confocal Laser Scanning microscope. Images were recorded at slow speed using a 60X-oil objective and a 488 nm laser for excitation of FITC.

LysoTracker Experiments.

KB cells were seeded into LabTek chamber slide dishes in folate deficient RPMI culture media supplemented with 10% FCSHI and PS, and grown in a humidified 5% CO_2 atmosphere at 37 °C for 24 h.The cells were incubated in the presence of a 50 μL

suspension of AFA-171-2 or AFA-FOL-171-2 at a concentration of 10 mg/mL. After 4 h incubation at 25 °C, the LysoTracker probe (50 nM) was added and the cells were reincubated for an additional hour at 25 °C or 37 °C. The cells were washed with PBS (2X) and pH 3 saline (2x), and PBS buffer (200 μL) was added. Images were recorded at slow speed using a 60X-oil objective and a 488 nm laser for excitation of FITC and a 568 nm laser line for excitation of LysoTracker.

Cell Toxicity.

KB cells in 2 mL of folate deficient RPMI medium supplemented with 10% of heat-inactivated fetal bovine serum (FCSHI) and 100 units/mL of penicillin/streptomycin (PS) (Sigma) were seeded into 12-well plates and grown in a humidified 5% CO_2 atmosphere at 37 °C for 24 h. The cells were incubated for 4 h at 25 °C in the presence of a 100 μL suspension of AFA-FOL-171-2 at concentrations of 0.05, 0.4, and 2.4 mg/mL. The AFA-FOL-171-2 solution was removed by washing with fresh medium (3x) and pH 3 saline (2x), followed by incubation in 1 mL of fresh medium at either 25 °C or 37 °C for 4 h. A 5 mg/mL solution of methylthiazolyldiphenyl-tetrazolium bromide (MTT) (50 μL) was added into each well and further incubated for one hour. After the one-hour incubation with the MTT reagent, the unreacted MTT reagent and cells were removed by washing the wells with water (3x). The purple, non-water soluble crystals remaining in the bottom of the wells were dissolved with 1 mL of isopropyl alcohol, and 100 μL of the resulting solution was used for UV measurements at 590 nm. Control experiments using only KB cells and KB cells with the addition of AFA-171-2 (2.4 mg/mL) at 37 °C were also performed as above. Percentage of cell viability was calculated using the equation: A_{590nm} with AFA-FOL-171-2 / A_{590nm} no AFA-FOL-171-2 x 100.

6.3 Results and Discussion

The hydrogel nanoparticles described in this work are of a core-shell morphology, where both the core and the shell are composed mainly of pNIPAM. The core is fluorescently labeled to enable particle tracking, while the shell contains an amine comonomer to enable conjugation with folic acid (Figure 6-2). The rationale for using a core-shell morphology is to provide a higher number of amine groups on the surface of the particles and consequently a higher number of folic acid groups, which can then easily interact with the FRs on the cell. For conjugation of folic acid to the particles, we use standard carbodiimide coupling method.[20] The variation of size of the folate-conjugated particles as a function of temperature was obtained by photon correlation spectroscopy (PCS) (Figure 6-3). The particles were found to undergo a phase transition at ~32 °C, and exhibited a hydrodynamic radius of ~135 nm at 25 °C (T < VPTT) and ~50 nm at 37 °C (T > VPTT). At the concentrations used for PCS no aggregation was observed at T > VPTT, even though the particles are more hydrophobic.

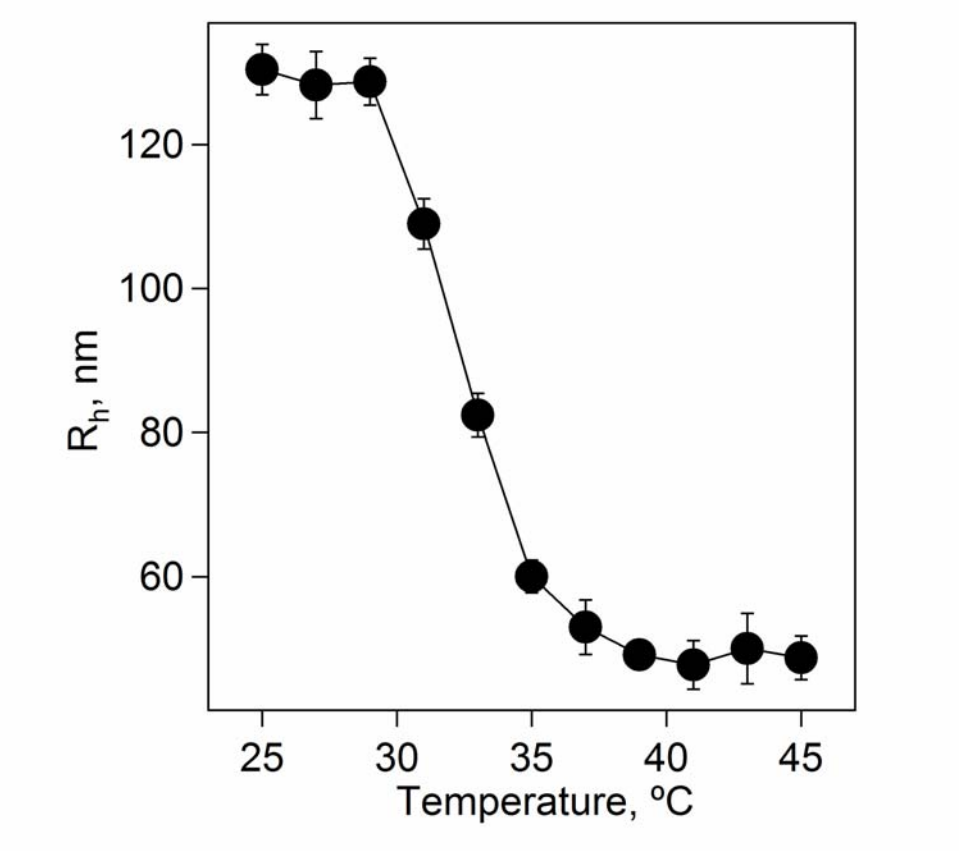

Figure 6-3. Hydrodynamic radius (R_h) of AFA-FOL-171-2 in 10 mM PBS pH 7.5 as a function of temperature.

Folic acid has a high affinity for FR (K_D=100 pM).[1] The binding of folic acid to FR initiates a receptor mediated endocytosis process, and cytosolic endosomal compartments are generated. [3,8] The bound ligand is detached from the receptor during proton influx in the endosome and is released in the cytosol. In this study, KB cells were chosen to investigate the cellular uptake of the folate conjugated microgels. The cells were first cultured in folate depleted medium to induce overexpression of FRs on the cell membrane. Both the folate conjugated microgels (AFA-FOL-171-2) and the control microgels (AFA-171-2) were incubated with KB cells for 4 h at 25 °C, Figure 6-4. From the flow cytometry experiments we find that the fluorescence from AFA-FOL-171-2 incubated cells is ~10 times higher than that measured for AFA-171-2 incubated cells (Figure 6-5). The slight fluorescence observed for AFA-171-2 may be due to non specific uptake or electrostatic binding of the polymer particles to the cells. Note that the AFA-171-2 particles possess a slightly positive surface charge due to the amine co-monomer in the particle shell. The subcellular localization of the fluorescently labeled particles was confirmed by confocal microscopy of KB cells following incubation with each particle type. The fluorescence images of AFA-171-2 (Figure 6-4a) and AFA-FOL-171-2 (Figure 6-4b) suggest that only the folate positive particles are internalized by the cells. Also, the punctate fluorescence observed for AFA-FOL-171-2 (Figure 6-4b) may suggest that these particles are located within the endosomes.

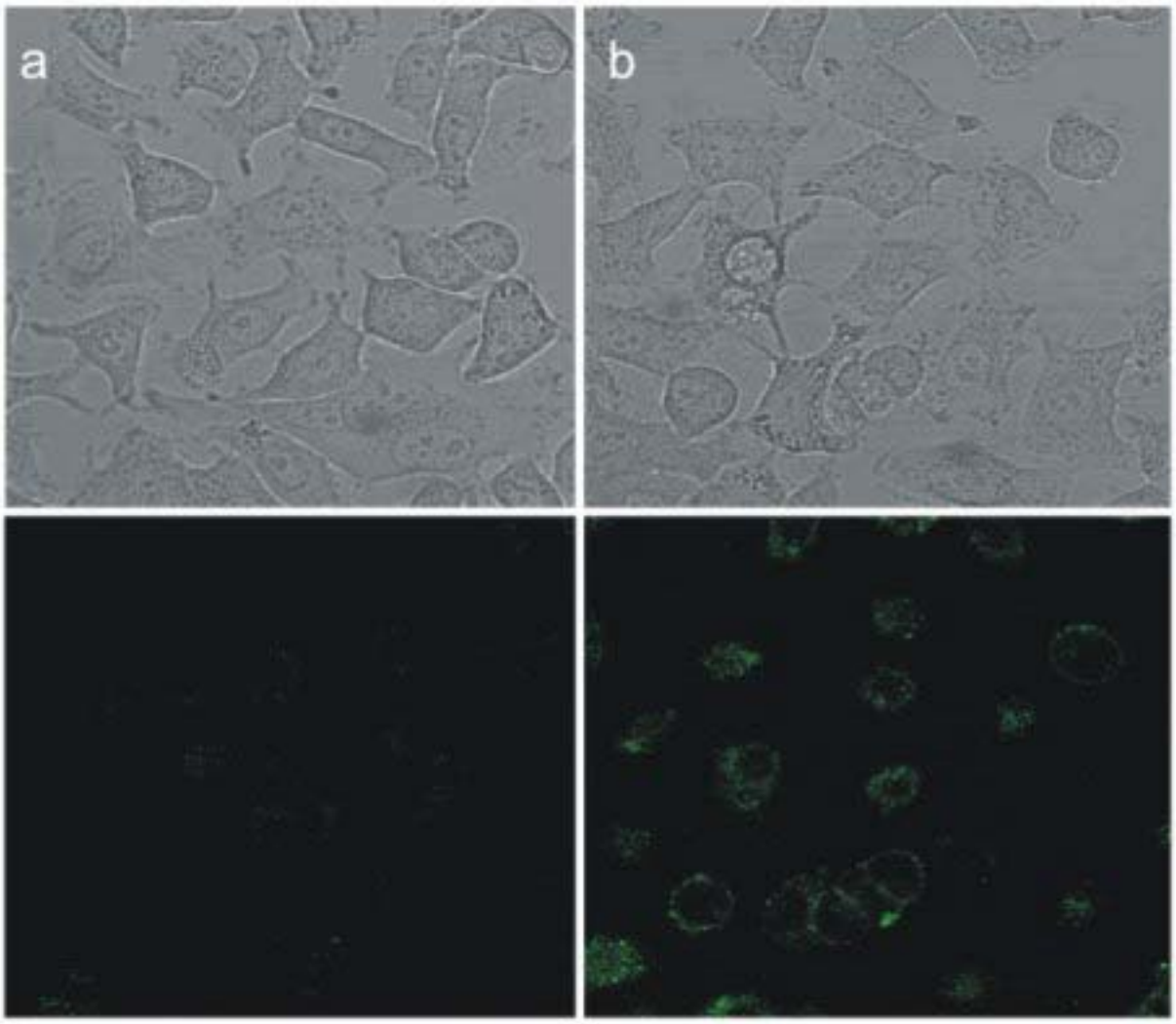

Figure 6-4. Confocal microscopy images of treated KB cells incubated at 25°C - transmittance image (top) and fluorescence image (bottom) for (a) AFA-171-2 and (b) AFA-FOL-171-2.

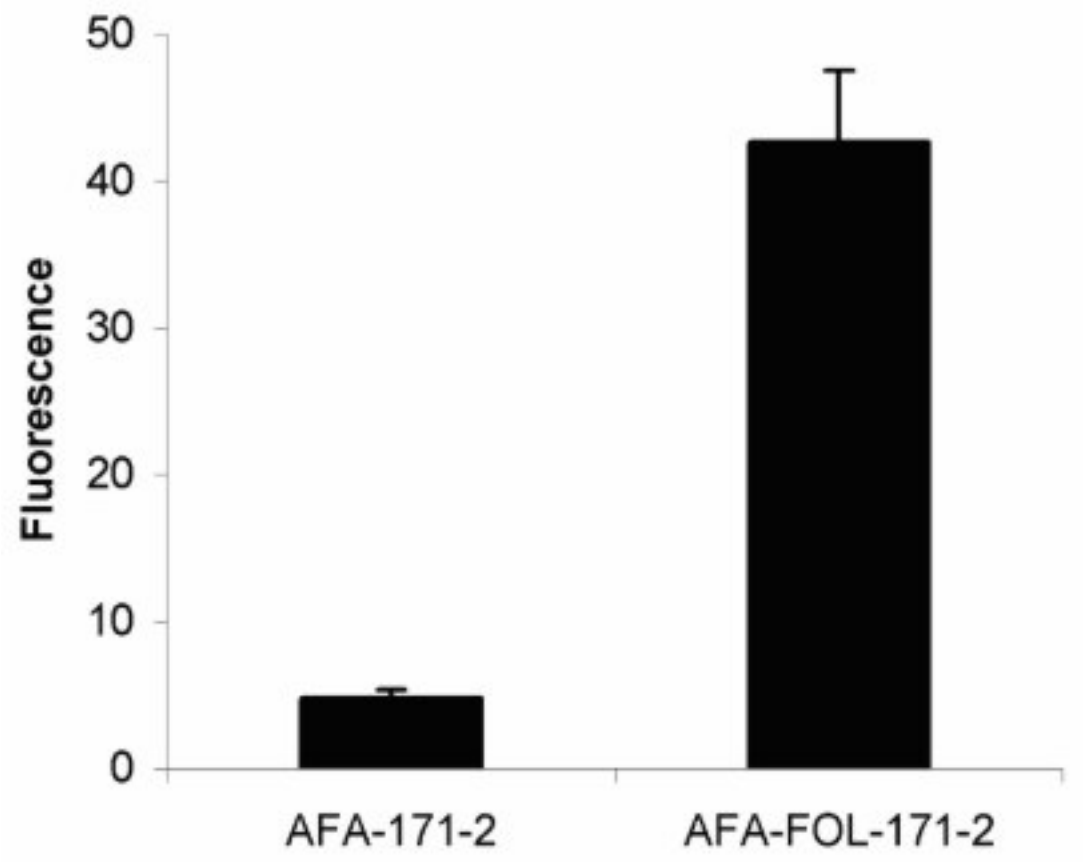

Figure 6-5. Flow cytometry analysis of KB cells incubated at 25°C with AFA-171-2 and AFA-FOL-171-2. Each bar represents the average fluorescence of 10,000 living cells.

To determine if the particles internalized by the cells are indeed in endosomal compartments, a secondary dye staining method was used to track the acidic compartments in the cells. The cells were incubated with AFA-FOL-171-2 and lysotracker red dye at 27 °C (Figure 6-6a) and at 37 °C (Figure 6-6b). The left images in Figure 6-6 show the fluorescein (particle) channel, while the right images show the lysotracker channel; the central image is the overlap of the two channels. It is evident that the majority of the particles lie outside of the endosomes, since the green fluorescence is largely anticorrelated with the red fluorescence channel, which marks the periphery of the endosomes. This suggests that the punctate fluorescence initially observed is not due to localization of the particles in the endosomes, but maybe due to isolated particles or aggregation of the particles within the cells. Also, the observed behavior does not appear to be temperature dependent. There is no marked difference in the fluorescence pattern when the particles were incubated at 27 °C (Figure 6-6a), which is below VPTT of the particles, as compared to incubation at 37 °C (Figure 6-6b), which is above VPTT and where the particles are more hydrophobic. This observed behavior of the particles being endocytosed but not being retained in the endosomes greatly increases the potential applicability of these materials for cytosolic drug delivery. Similar behavior has been observed previously for block copolymer micelles.[21] For cytosolic delivery to be efficient, any drug-folate conjugate must be released into the cytosol following endocytosis.[22] For most particulate carriers, it is generally assumed that in addition to the presence of a targeting ligand, a secondary triggering mechanism must occur in the endosome in order to release the drug in the cytosol.[11,23,24] Most of these mechanisms are based on a drop in endosomal pH. Interestingly, our hydrogel nanoparticles lack any

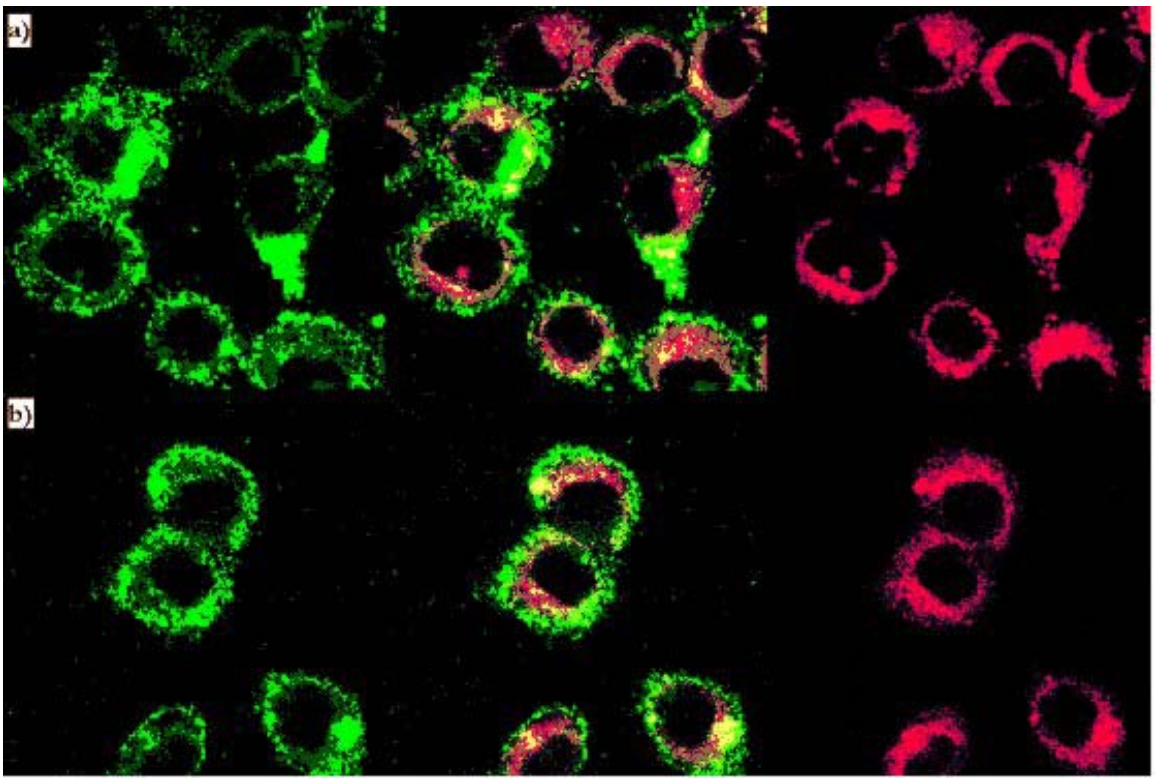

Figure 6-6. Cellular localization of AFA-FOL-171-2 and Lysotracker red dye within KB cells. At (a) 27°C: left - fluorescein channel, right - Lysotracker red channel, center - overlap of the two channels, and (b) 37°C: left - fluorescein channel, right - Lysotracker red channel, center - overlap of the two channels.

purposely designed secondary mechanism, and yet are efficiently delivered into the cytosol after being endocytosed. Hence, these structures have potential to be used as carriers for cytosolic delivery of drugs to cells that overexpress FRs.

Particle induced cytotoxicity was investigated in order to evaluate the impact of uptake on cell viability. Cytotoxicity was determined as a function of concentration of the polymer particles and incubation temperature (Figure 6-7) by a standard MTT cell viability assay. Figure 6-7 shows that cytotoxicity increases with an increase in the concentration of the polymer at 27 °C, but for each concentration there is a marked decrease in viable cells at 37 °C. Thus, a simple temperature switch induces cell death following particle uptake. Since there are no obvious chemical inhibitors of cellular metabolism in the polymer structure, the cytotoxicity may be of some physical origin. For example, pNIPAM hydrogel nanoparticles become relatively hydrophobic at temperatures above their VPTT and can aggregate in aqueous media as a result. The presence of residual anionic charges from the initiator used during the polymerization typically prevents this aggregation.[25] However, in high ionic strength solutions such as cell growth media, these charges can be shielded and the particles can aggregate at high temperature.[26] We therefore tentatively attribute the observed temperature dependent cytotoxicity to particle aggregation in the cytosol. It is further known that pNIPAM at high temperatures causes protein adsorption and denaturation, which is also most likely associated with particle aggregation in the cytosol.[27]

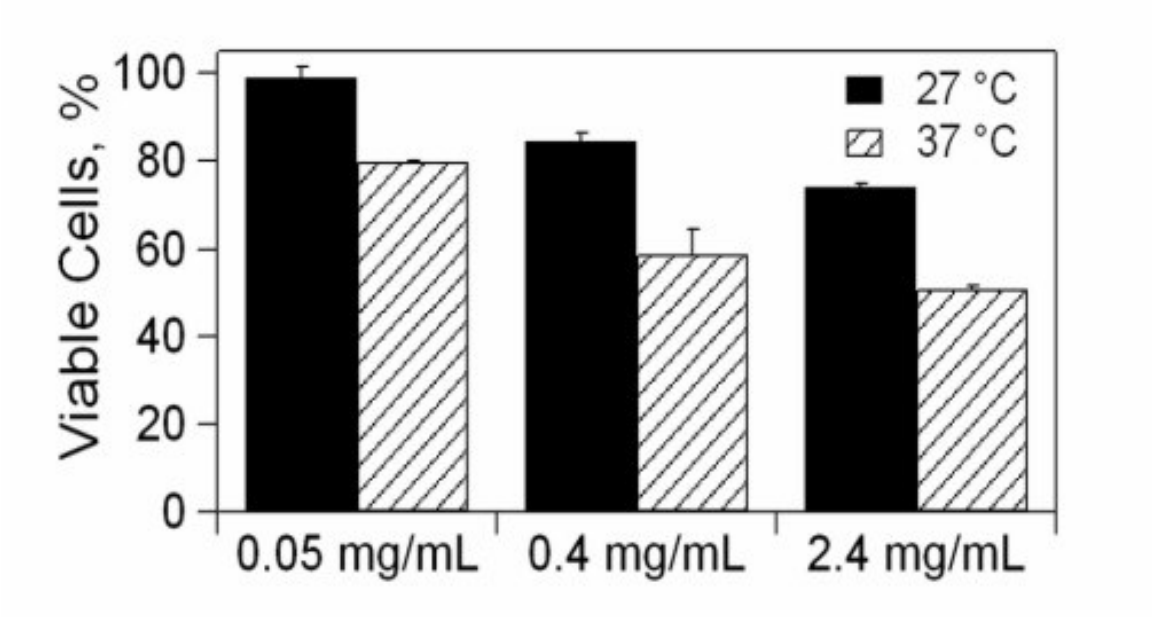

Figure 6-7. KB cell viability at varying concentrations of AFA-FOL-171-2 at 27°C and 37°C after 4 h incubation.

To determine if the endocytosis is cell-specific, we incubated the folate particles with HeLa cells that overexpress folate receptors. Figure 6-8 shows the confocal images of HeLa cells with the control particles AFA-171-2. Figure 6-9 shows the confocal images of the HeLa cells with AFA-FOL-171-2. It can be observed that the folate positive particles show higher cytosolic fluorescence than the control particles. Hence these particles can be used to target any type of cells that overexpress folate receptors.

6.4 Conclusions

Folate conjugated hydrogel nanoparticles provide a novel model system for specific targeting of cancer cells. The ability of the particles to escape from the endosome into the cytosol, in addition to their large swelling capacities makes them potential candidates for cytosolic delivery of drugs. Also, the temperature dependent cytotoxicity suggests a route to cell-specific, externally triggered, non-pharmacological anti-tumor activity. The temperature at which this cytotoxicity is observed (37 °C) is not necessarily physiologically useful and hence further work is required to shift the induced cytotoxicity to slightly higher temperatures.

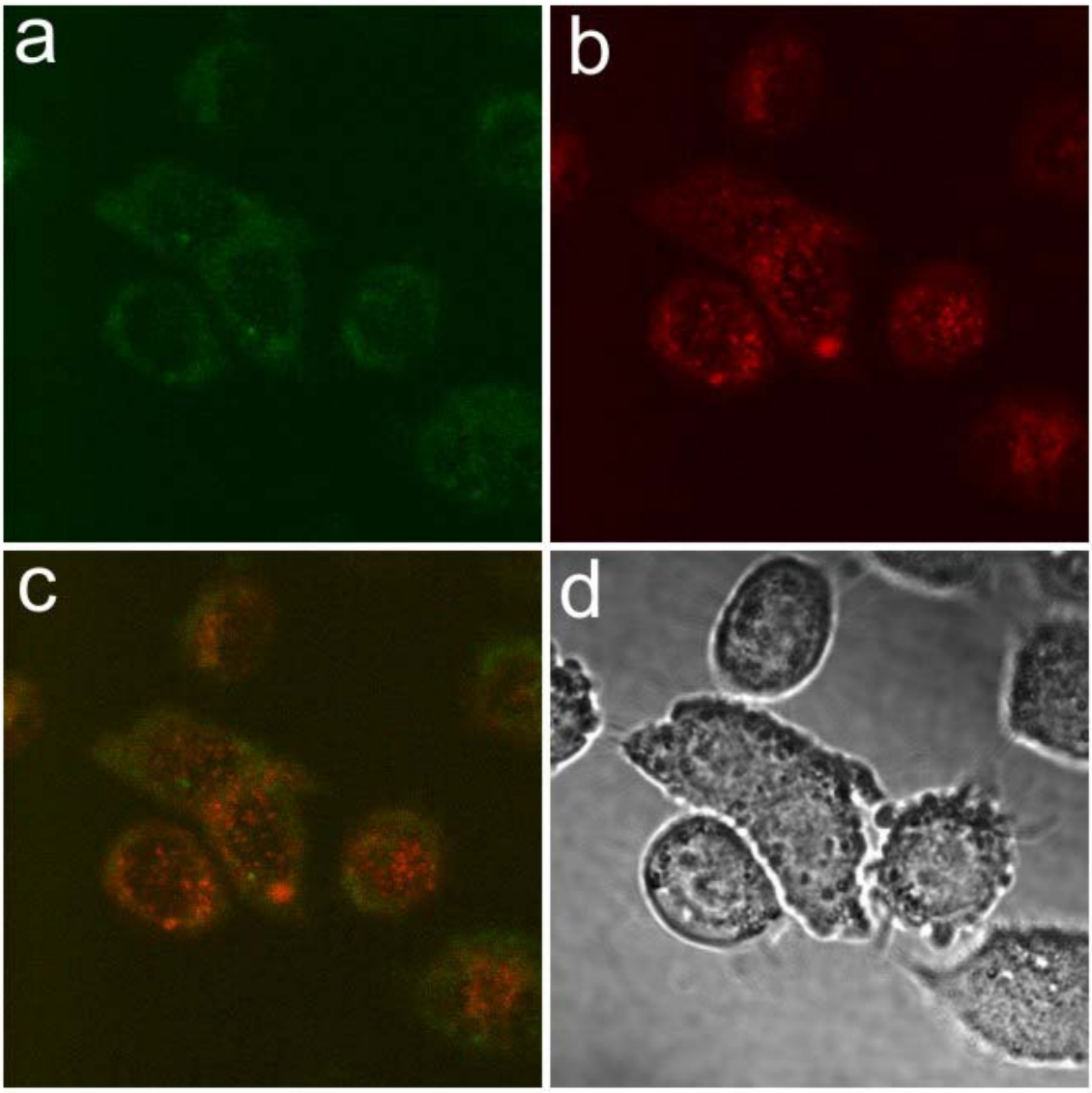

Figure 6-8. Confocal images of HeLa cells incubated with AFA-171-2. a) Green fluorescent particle channel, b) lysotracker red dye channel, c) overlap of both the channels and d) transmittance image of the cells.

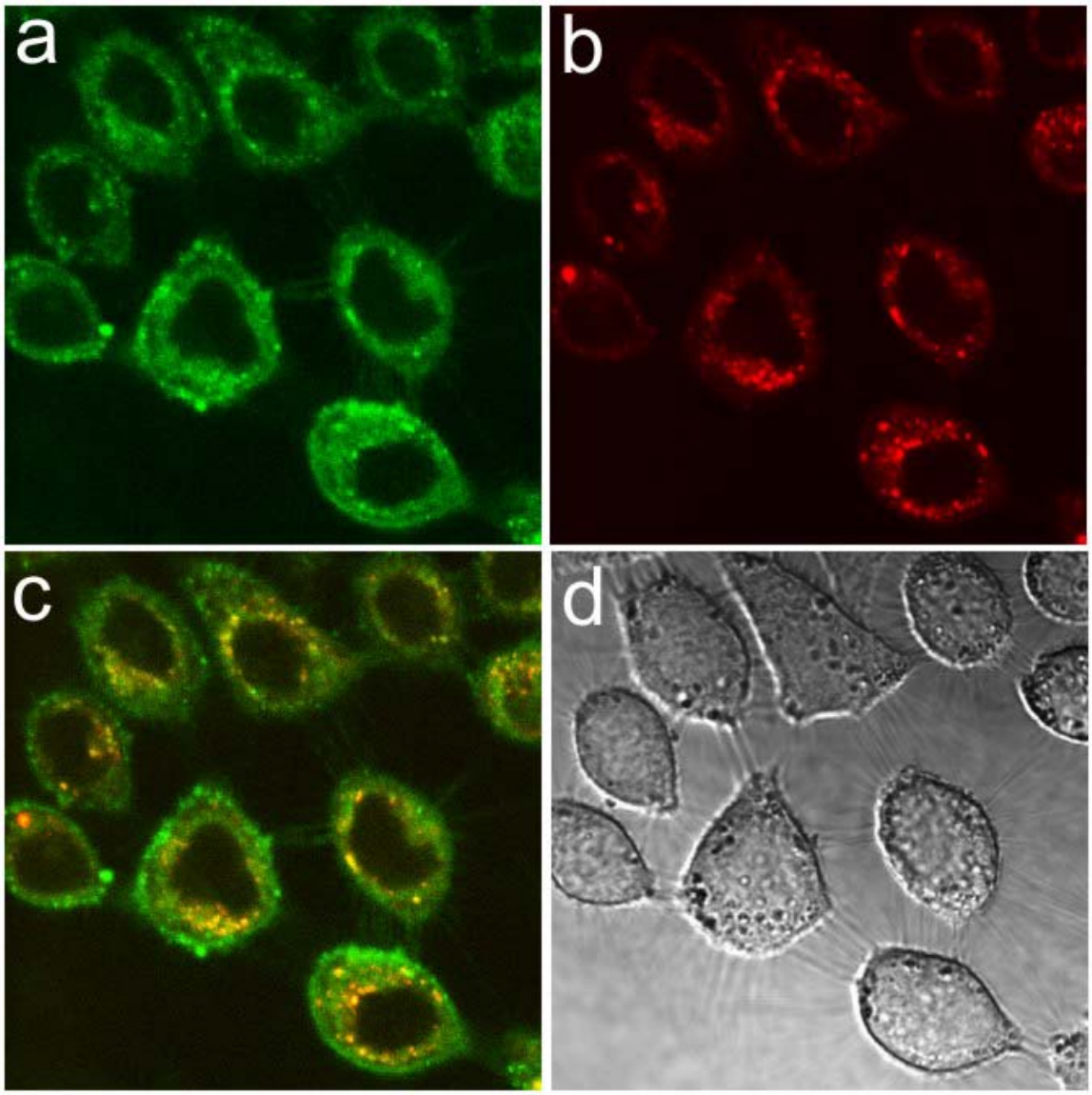

Figure 6-9. Confocal images of HeLa cells incubated with AFA-FOL-171-2. a) Green fluorescent particle channel, b) lysotracker red dye channel, c) overlap of both the channels and d) transmittance image of the cells.

REFERENCES

(1) Leamon, C. P.; Low, P. S. *Drug Discov. Today* **2001**, *6*, 44-51.

(2) Bies, C.; Lehr, C.-M.; Woodley, J. F. *Adv. Drug Deliv. Rev.* **2004**, *56*, 425-435.

(3) Sudimack, J.; Lee, R. J. *Adv. Drug Deliv. Rev.* **2000**, *41*, 147-162.

(4) Tkachenko, A. G.; Xie, H.; Coleman, D.; Glomm, W.; Ryan, J.; Anderson, M. F.; Franzen, S.; Feldheim, D. L. *J. Am. Chem. Soc.* **2003**, *125*, 4700-4701.

(5) Wang, S.; Luo, J.; Lantrip, D. A.; Waters, D. J.; Mathias, C. J.; Green, M. A.; Fuchs, P. L.; Low, P. S. *Bioconj. Chem.* **1997**, *8*, 673-679.

(6) Leamon, C. P.; Cooper, S. R.; Hardee, G. E. *Bioconj. Chem.* **2003**, *14*, 738-747.

(7) Lee, R. J.; Low, P. S. *Biochim. Biophys. Acta-Biomembr.* **1995**, *1233*, 134-144.

(8) Anderson, R. G. W.; Kamen, B. A.; Rothberg, K. G.; Lacey, S. W. *Science* **1992**, *255*, 410-411.

(9) Shukla, S.; Wu, G.; Chatterjee, M.; Yang, W.; Sekido, M.; Diop, L. A.; Mueller, R.; Sudimack, J. J.; Lee, R. J.; Barth, R. F.; Tjarks, W. *Bioconjugate Chem.* **2003**, *14*, 158-167.

(10) Pan, D.; Turner, J. L.; Wooley, K. L. *Chem. Commun.* **2003**, 2400-2401.

(11) Vogel, K.; Wang, S.; Lee, R. J.; Chmielewski, J.; Low, P. S. *J. Am. Chem. Soc.* **1996**, *118*, 1581-1586.

(12) Lee, E. S.; Na, K.; Bae, Y. H. *J. Control. Release* **2003**, *91*, 103-113.

(13) Marcucci, F.; Lefoulon, F. *Drug Discov. Today* **2004**, *9*, 219-228.

(14) Gan, D.; Lyon, L. A. *J. Am. Chem. Soc.* **2001**, *123*, 7511-7517.

(15) Serpe, M. J.; Jones, C. D.; Lyon, L. A. *Langmuir* **2003**, *19*, 8759-8764.

(16) Gan, D.; Lyon, L. A. *J. Am. Chem. Soc.* **2001**, *123*, 8203-8209.

(17) Jones, C. D.; Lyon, L. A. *Macromolecules* **2003**, *36*, 1988-1993.

(18) Dube, D.; Francis, M.; Leroux, J. C.; Winnik, F. M. *Bioconj. Chem.* **2002**, *13*, 685-692.

(19) Jones, C. D.; Lyon, L. A. *Macromolecules* **2000**, *33*, 8301-8306.

(20) Leamon, C. P.; Low, P. S. *Proc. Natl. Acad. Sci. U. S. A.* **1991**, *88*, 5572-5576.

(21) Savic, R.; Luo, L.; Eisenberg, A.; Maysinger, D. *Science* **2003**, *300*, 615-618.

(22) Leamon, C. P.; Low, P. S. *J. Biol. Chem.* **1992**, *267*, 24966-24971.

(23) Rui, Y. J.; Wang, S.; Low, P. S.; Thompson, D. H. *J. Am. Chem. Soc.* **1998**, *120*, 11213-11218.

(24) Lackey, C. A.; Press, O. W.; Hoffman, A. S.; Stayton, P. S. *Bioconj. Chem.* **2002**, *13*, 996-1001.

(25) Pelton, R. *Adv. Colloid. Interface Sci.* **2000**, *85*, 1-33.

(26) Duracher, D.; Sauzedde, F.; Elaissari, A.; Pichot, C.; Nabzar, L. *Colloid Polym. Sci.* **1998**, *276*, 920-929.

(27) Kawaguchi, H.; Fujimoto, K.; Mizuhara, Y. *Colloid Polym. Sci.* **1992**, *270*, 53-57.

CHAPTER 7

LIGAND-FUNCTIONALIZED CORE/SHELL MICROGELS WITH PERMSELECTIVE SHELLS

7.1 Introduction

Recently the field of nanotechnology has received immense attention, in part due to its potential impact on biotechnology. Nanometric materials find application in many fields such as chemical sensing[1] and biosensing,[2] catalysis,[3] optics,[4] separations[5] and drug delivery.[6] Nanomaterials offer new advantages in such arenas due to the potential for new or enhanced optical, chemical, mechanical, or electrical properties. Of particular interest is the creation of multifunctional nanoparticles, which contain multiple chemistries such that they interact with their environment in a more complex fashion. Here we report the synthesis of a well-defined, yet chemically and topologically complex colloidal particle. This structure comprises a porous, thermosensitive, hydrogel "core" particle that is modified with a ligand (biotin). This particle is contained within a porous, thermoresponsive, hydrogel "shell" that sterically excludes transport and binding of the protein for which biotin is a tight-binding ligand (avidin). However, by using a chemically-cleavable cross-linker in the shell, the ability of avidin to penetrate the particle and bind to the core can be chemically tuned with a high degree of fidelity.

The polymer used in the construction of these particles is mainly composed of poly(*N*-isopropylacrylamide) (pNIPAm), which is a classic stimuli responsive polymer.[7] As mentioned in previous chapters, pNIPAm can be cross-linked into nanoparticles by

emulsion or precipitation polymerization with good size control from tens of nanometers to tens of microns.[8] Our group has developed precipitation polymerization methods to create a class of core/shell hydrogel particles based upon pNIPAm. The specific concept employed for the chemically and topologically complex particles presented herein is shown in Figure 7-1. A biotinylated hydrogel core nanoparticle is coated with a hydrogel shell containing the cleavable cross-linker *N,N'*-(1,2-Dihydroxyethylene)-bisacrylamide (DHEA). At the initial cross-link density, the pore size of the shell is too small to allow passage of avidin through to the core to bind biotin. Upon chemical cleavage of the cross-links, the pore size increases enough to allow avidin to pass through and bind biotin.

7.2 Experimental Section

Materials

N-isopropylacrylamide (NIPAm, Aldrich) was purified by recrystallization from hexane (J. T. Baker) prior to use. *N,N'*-methylenebis(acrylamide) (BIS), ammonium persulfate (APS), sodium dodecyl sulfate (SDS), acrylic acid (AAc), *N,N'*-(1,2-Dihydroxyethylene)- bisacrylamide (DHEA) and sodium periodate were purchased from Aldrich and used as received. 1-ethyl-3-(3-dimethylaminopropyl) carbodiimide (EDC), biotin hydrazide, avidin, avidin-horse radish peroxidase conjugate (avidin-HRP) and 2-(4'-hydroxyazobenzene) benzoic acid (HABA) were purchased from Pierce. Water was purified with Barnstead E-Pure system to a resistance of 18 MΩ and then filtered through a 0.2-μm filter to remove particulate matter.

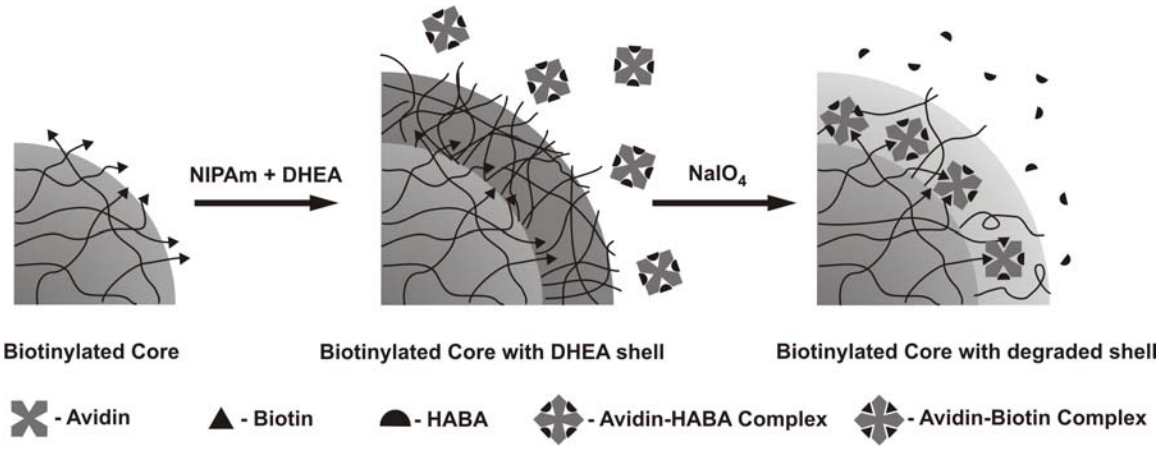

Figure 7-1. A NIPAm/AAc core is biotinylated with biotin hydrazide and EDC, followed by addition of a NIPAm/DHEA shell. The cross-linker density of the shell is such that the pore size is smaller than the avidin-HABA complex, hence preventing the protein from passing through the shell. Upon treatment with periodate, the DHEA cross-linker degrades, which subsequently increases the pore size to allow passage of avidin-HABA complex. The K_d for avidin-HABA (10^{-6}) is higher than the K_d for avidin-biotin (10^{-15}). Therefore, HABA is released from avidin when biotin binds to avidin. This binding is detected by UV-VIS spectrophotometry.

Microgel Synthesis

A detailed procedure for preparation of microgels by free radical precipitation polymerization is described elsewhere.[9] The total monomer concentration in the pregel solution was kept constant at 70 mM, out of which 10 mol-% was BIS and 10 mol-% was AAc, with the remaining 80 mol-% being NIPAm. All the monomers and 11 mg of SDS were dissolved in 25 mL of water and the resulting solution was filtered through a 0.2-μm-membrane filter (Pall Gelman Metricel) to remove particulate matter. The reaction mixture was heated in a 3-neck round bottom flask equipped with a condenser and inlet for nitrogen. The mixture was heated to 70 °C under a gentle stream of nitrogen for 1 hour, after which 8 mg of APS dissolved in 1 mL of water was added to initiate the reaction. The reaction mixture was kept at 70 °C for 4 hours to complete the reaction. After synthesis, the microgel solution was filtered using fine porosity filter paper (Fisher Scientific) to remove aggregated material, if any. The particles were then purified by centrifugation and resuspension in water at room temperature at least seven times to remove any unreacted monomer and oligomer. 1H NMR measurements of pNIPAm particles prepared from 20 mol-% DHEA pregel solutions reveal ~95% cross-linker incorporation efficiency into the particles.

Conjugation of Biotin

Cleaned particles were freeze-dried and resuspended in 25 mL of phosphate buffer of pH 4.7. 84 mg of EDC was added to the resuspended polymer to activate the acid groups in the microgels, the solution was then agitated for 30 min. 46 mg of biotin hydrazide dissolved in 2 mL of DMSO was added to the EDC-treated polymer solution.

The reaction was allowed to proceed overnight at room temperature. These biotinylated particles were cleaned by dialysis with daily changes of water for 4 weeks.

Addition of Shell

The detailed procedure of the shell addition to the core can be found in previous work.[10] In brief, 5 mL of the core (biotinylated or non-biotinylated) microgel solution was taken in a three-necked round bottom flask, to which 8 mg of SDS and 44 mL of deionized water was added. The solution was heated under nitrogen to 70 °C. Separately, 271 mg of NIPAm and 120 mg of DHEA were dissolved in 5 mL of deionized water. This solution was degassed at room temperature for 1 h and then was added to the heated core solution. Finally, 10 mg of APS dissolved in 1 mL of water was added to the solution to initiate the reaction. The reaction was allowed to proceed for 4 h at 70 °C and then was cooled and filtered. The polymer solution was then cleaned by centrifugation and resuspension to remove unreacted monomer and oligomers. The above procedure is for 20 % cross-linked shells. For 15% cross-linker, we used 288 mg of NIPAm and 90 mg of DHEA. For 2% cross-linker, we used 330 mg of NIPAm and 12 mg of DHEA.

Degradation of Shell

Since the shell has diol cross-linker we use sodium periodate to degrade it. For each degradation 1 mL of core-shell solution was used for quantitative degradation of the shell. Depending upon the amount of degradation required, an equivalent number of moles of sodium periodate solution was added to the polymer solution and the total volume was made up to 1.5 mL. The amount of DHEA to be degraded was calculated from the amount of DHEA used in pregel solution.

Biotin Assay

To determine the amount of avidin binding to the biotin in the core, we use the avidin-HABA assay.[11] The avidin-HABA solution was prepared by dissolving 100 mg of avidin in 10 mL of 0.1 M PBS followed by addition of 6 mL of 10 mM HABA solution. Finally, the total volume was made up to 200 mL by further addition of PBS. For the avidin-HRP-HABA complex, 5 mg of avidin-HRP was dissolved in 5mL of PBS and to it 130 μL of 10 mM HABA solution was added. Final volume was made up to 10 mL with PBS

For the assay 250 μL of appropriately degraded polymer solution is used. To it 750 μL of the avidin-HABA or avidin-HRP-HABA solution is added. The mixture is allowed to equilibrate for 4 h before characterization.

UV-VIS characterization

The absorbances of the polymer-avidin-HABA mixture were obtained using a Shimadzu UV 1601 spectrophotometer. For each measurement, the reference cell had the same volume of polymer solution as used in the sample cell but instead of avidin-HABA mixture it had same volume of PBS.

Photon Correlation Spectroscopy

Particle sizes were determined via photon correlation spectroscopy (PCS, Protein Solutions Inc.) equipped with an integrated Peltier temperature control device (± 0.1 °C), as previously reported.[12] The hydrodynamic radii of the particles were calculated from the diffusion coefficient using the Stokes-Einstein equation. The sample was allowed to equilibrate at the proper temperature for 10 minutes before data collection. Scattered light from the fiber-coupled diode laser (784.8 nm) was collected at 90° with a fiber-coupled

avalanche photodiode detector connected to a 248-channel autocorrelator board. The data was analyzed with Protein Solutions' Dynamics Software Version 5.25.44.

7.3 Results and Discussion

Our group has synthesized core/shell hydrogel nanoparticles by a multi-stage "seed and feed" method, where pre-formed thermoresponsive hydrogel nanoparticles are used as seeds for addition of either chemically similar or distinct hydrogel shells.[10] In the present study, the core is predominantly composed of pNIPAm with acrylic acid as a minor component (10 mol-%). The acid groups are used for attaching biotin to the nanoparticles by carbodiimide coupling. These biotinylated cores are then used as seed particles, to which a shell is added. The shell also consists of pNIPAm but is cross-linked with the cleavable diol cross-linker DHEA (same as that used in Chapter 4). Traditionally, bulk gels cross-linked with DHEA have been used for electrophoretic protein separation.[13] Since the vicinal diols in the cross-linker can be cleaved by stoichiometric amounts of sodium periodate, the pore size of the gel can be varied quantitatively by degradation of the cross-linker (Figure 7-2). Figure 1 shows the hydrodynamic radius (R_h) measured at 25 °C of the core/shell particle as a function of cleavage of the cross-links in the shell (filled circles). The filled squares represent the R_h of the core. From this we see that the initial R_h of the core is ~115 nm, while that of the core/shell particle prior to periodate addition is ~150 nm. Upon addition of periodate to the solution, the shell swells, as suggested by the increase in the R_h of the core/shell particle as a function of periodate concentration. This is expected, as decreasing the cross-link concentration in the network should result in a larger equilibrium swelling

volume. Ultimately, the R_h of the core/shell particle increases by ~20 nm following complete cleavage of the periodate cross-links.

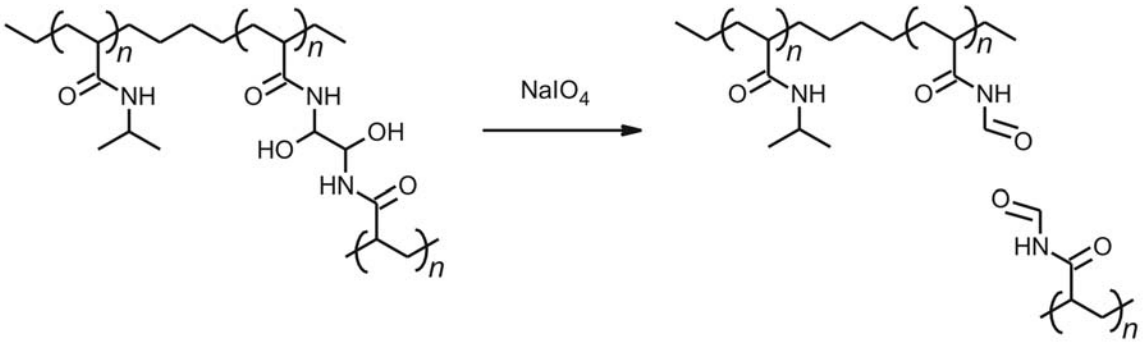

Figure 7-2. Chemical structure of the cleavable polymer. Sodium periodate cleaves the 1,2-glycol bond of DHEA by oxidizing the vicinal diols to aldehydes.

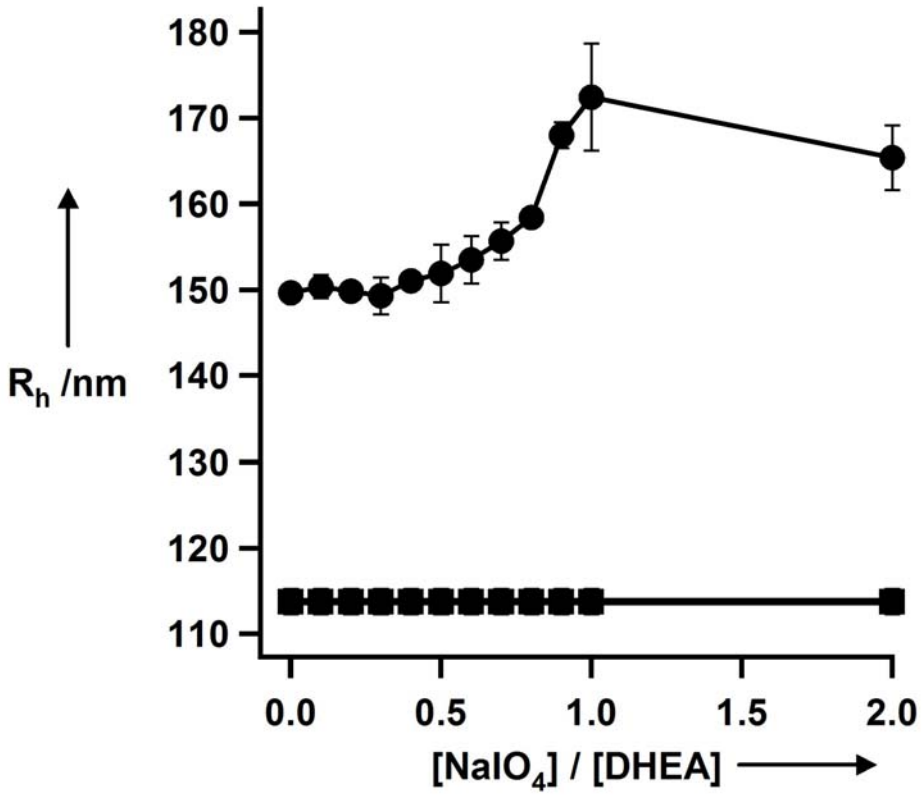

Figure 7-3. Hydrodynamic radius (R_h) of the core/shell particles (filled circles) as a function of the periodate/DHEA ratio. The R_h of the core is represented by filled squares. The error bars represent one standard deviation about the average of five separate measurements.

To detect the sieving of avidin through the shell we used the colorimetric 2-(4'-hydroxyazobenzene) benzoic acid (HABA) assay.[11] Four equivalents of HABA bind (K_d = 10^{-6} M)[14] weakly to avidin at the biotin binding site; this complex has an absorption band at 500 nm. In presence of biotin, HABA is displaced from avidin (K_d for avidin-biotin system is 10^{-15} M)[15] and the absorbance at 500 nm decreases. Figure 7-4 shows the structures of HABA and biotin. Figure 7-5 shows the absorption spectra of the avidin-HABA complex in the presence and absence of biotinylated core particles. The amount of biotin conjugated to the core particle was determined by titrating the acid groups before and after conjugation. Subtracting the moles of acid in the biotinylated sample from that in the non-biotinylated one reveals that ~160 mg of biotin is conjugated to one gram of core particles. From the avidin-HABA assay it was determined that only ~25 mg of biotin is available for binding to avidin in one gram of core particles. This means that out of the total amount of biotin conjugated to the polymer, only ~16% is avidin accessible.

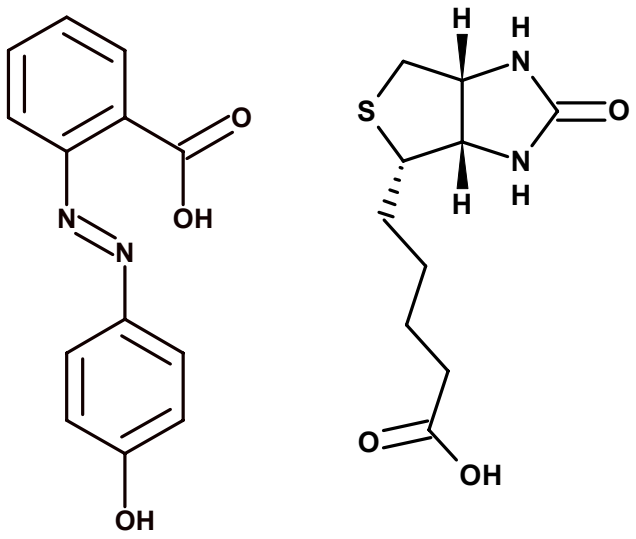

HABA **Biotin**

Figure 7-4. Chemical structures of HABA and Biotin

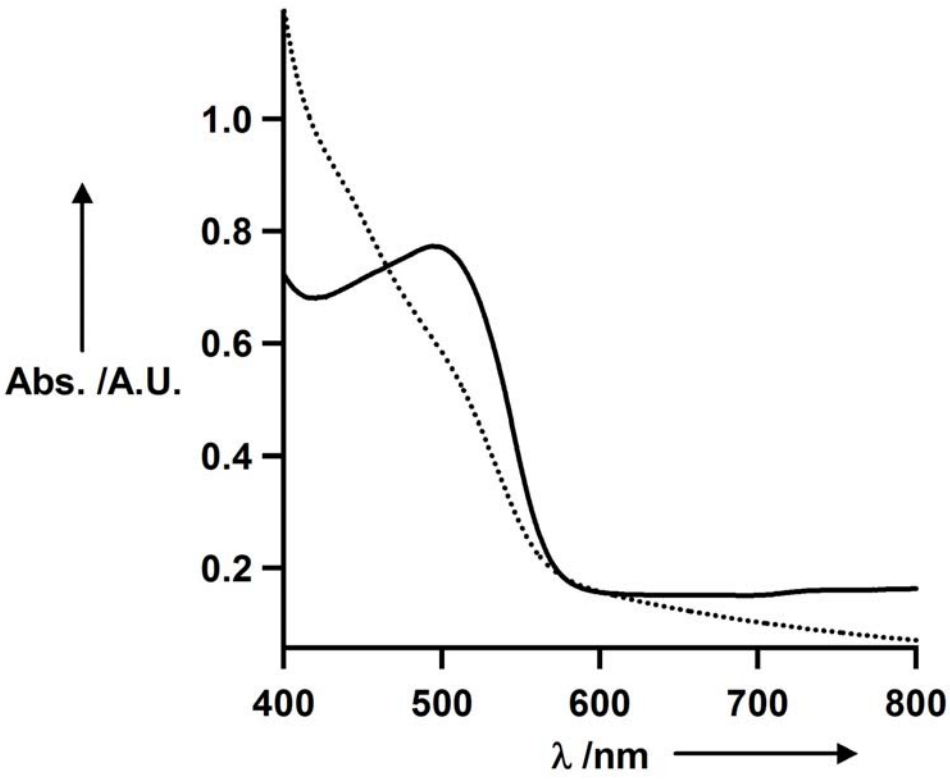

Figure 7-5. Absorption spectra of avidin-HABA complex in presence (dotted line) and in absence (solid line) of biotinylated core particles.

Figure 7-6 shows the change in absorbance of the avidin-HABA complex at 500 nm as a function of the periodate/DHEA ratio for particles with 20%, 15% and 2% cross-linked shells. For the 20% cross-linked shell, the absorbance at 500 nm is essentially invariant with periodate concentration until approximately 70% of the diols are cleaved. The absorbance decreases precipitously beyond that concentration, which is an indication of HABA being displaced from avidin by the core-bound biotin. This clearly implies that until ~70% degradation, the pore size of the shell is not big enough to allow passage of avidin-HABA. At >70% degradation, the pore size becomes big enough to allow avidin-HABA to pass through the shell and bind biotin. Figure 7-6 also shows the variation in absorbance for control particles, where in these particles the core is not biotinylated. No substantial change in absorbance is observed for the control samples, further confirming that the change in absorbance observed in biotinylated samples is indeed due to binding of biotin to avidin. The 15% cross-linked shell shows the same trend as the 20% cross-linked sample, but the decrease in absorbance starts slightly earlier. This is presumably due to the larger initial pore size in the 15% cross-linked shell relative to the 20% cross-linked shell. For 2% cross-linked shells the absorbance for 0% degradation is already smaller than that for the 20% and 15% cross-linked samples that have been treated with a 2-fold excess of periodate. This result indicates that the pore size for this cross-linking density is so large that it makes the shell "leaky", thereby allowing avidin to bind biotin in the core without any degradation of the shell. The increased degree of binding also suggests that more biotin molecules are avidin accessible, as the more open network structure of the 2% cross-linked shell imposes less steric hindrance to the transport of the protein. Also further degradation does not bring any substantial change in the absorbance,

which indicates that almost all of the biotin molecules are already accessible to avidin prior to any degradation.

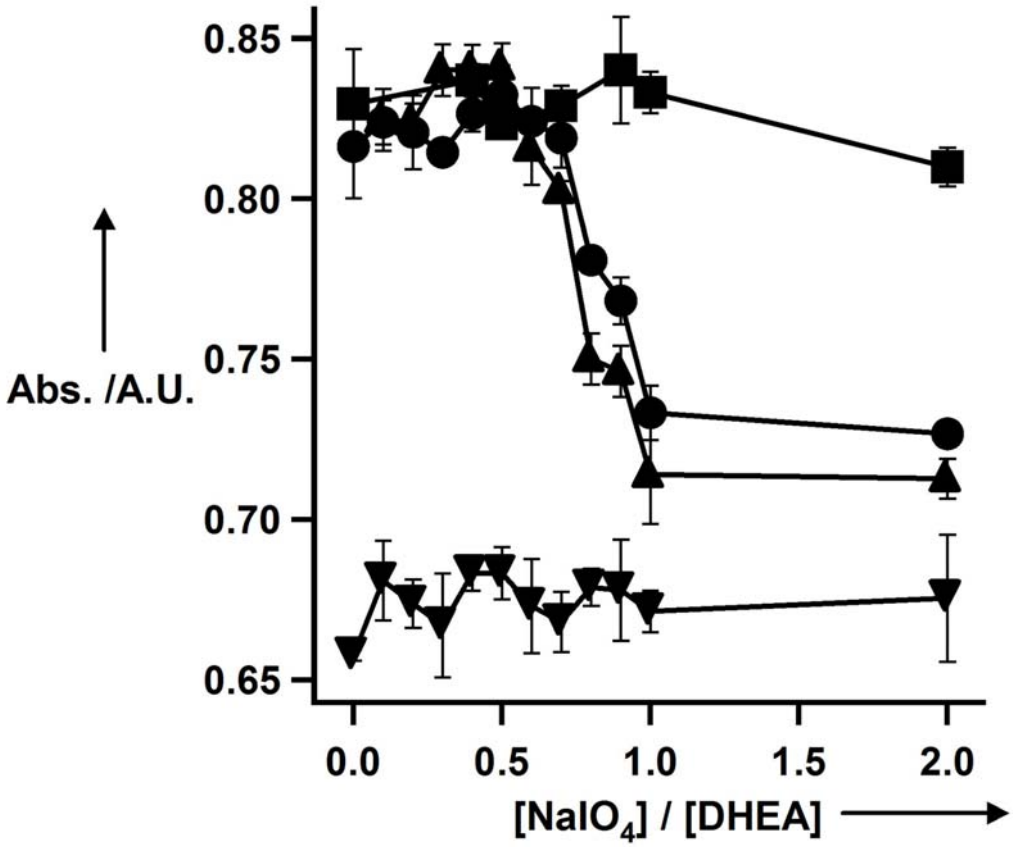

Figure 7-6. Absorbance of the avidin-HABA complex at 500 nm as a function of the periodate/DHEA ratio for 20% cross-linked shell particles (filled circles), 15% cross-linked shell particles (filled triangles), 2% cross-linked shell particles (filled inverted triangles) and biotin-free control particles (filled squares). The error bars represent one standard deviation about the average of three different samples.

To evaluate how a change in protein radius impacts transport through the particle shell, we chose an avidin-horseradish peroxidase conjugate (avidin-HRP). Two moles of HRP are conjugated to one mole of avidin. The molecular weight of this conjugate is ~154 kDa, as compared to that of regular avidin, which is ~66 kDa. Avidin-HRP binds both biotin and HABA with the same affinity as free avidin. Figure 7-7 shows the change in absorbance of the avidin-HRP-HABA complex at 500 nm as a function of the periodate/DHEA ratio for the 20% cross-linked shell particles. No significant decrease in absorbance is observed until approximately 2-fold excess periodate is added to the sample. Again, normal avidin begins to sieve through the shell at ~70% degradation. This indicates that the avidin-HRP complex is too big to sieve through the shell until all of the cross-links are cleaved. Presumably, the excess periodate is needed to drive the reaction in more highly cross-linked (less accessible) regions of the particle shell; the reaction proceeds under stoichiometrically equivalent conditions in free solution.

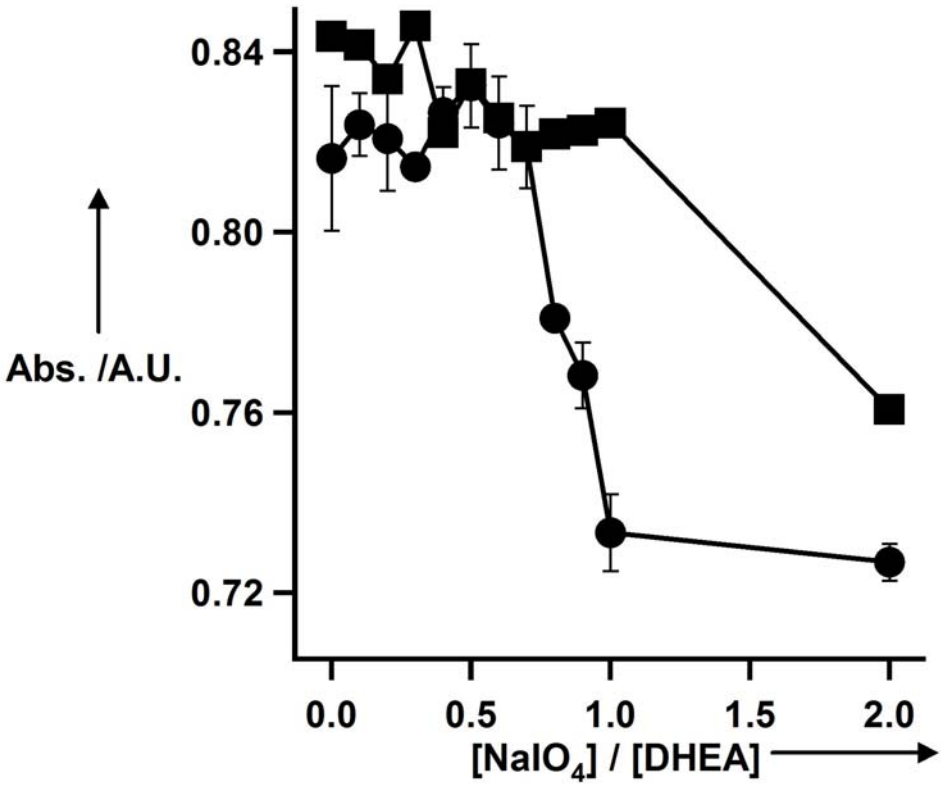

Figure 7-7. Absorbance of the avidin-HABA complex (filled circles) and avidin-HRP-HABA complex (filled squares) as a function of percent degradation of 20% cross-linked shell particles. The error bars represent one standard deviation about the average of three different samples.

7.4 Conclusions

We have demonstrated the synthesis of complex hydrogel nanoparticles that bind to a protein based on both native protein-ligand interactions, as well as due to steric sieving. These core/shell nanoparticles are formed by a simple "seed and feed" polymerization method where the shell has cleavable cross-links. The sieving of proteins to the core is then simply controlled by manipulating the pore size of the shell through cleavage of those cross-links. At a particular cross-linker density, only avidin is allowed to sieve through the shell, with larger protein structures being excluded from binding. Particles such as these could find applications in protein separations, where the shell could essentially behave as a molecular weight cutoff membrane, thus eliminating binding of macromolecules and assemblies that are larger than the protein of interest. Affinity-based sensors and assays that are required to work in complex biological fluids could also benefit from size-selecting structures. Finally, the specific ligand:protein system used here (biotin:avidin) has become important for a wide range of surface modification and bioconjugation methods. Thus, one could imagine using the system presented here for preparation of a wide range of microgel bioconjugates in which access to the biomacromolecule can be reversibly tuned.

REFERENCES

(1) Lin, S.-Y.; Liu, S.-W.; Lin, C.-M.; Chen, C.-h. *Anal. Chem.* **2002**, *74*, 330-335.

(2) Bailey, R. C.; Nam, J.-M.; Mirkin, C. A.; Hupp, J. T. *J. Am. Chem. Soc.* **2003**, *125*, 13541-13547.

(3) Shen, S.; Hidajat, K.; Yu, L. E.; Kawi, S. *Adv. Mater.* **2004**, *16*, 541-545.

(4) Jones, C. D.; Lyon, L. A. *J. Am. Chem. Soc.* **2003**, *125*, 460-465.

(5) Guihen, E.; Glennon, J. D. *Anal. Lett.* **2003**, *36*, 3309-3336.

(6) Brigger, I.; Dubernet, C.; Couvreur, P. *Adv. Drug Deliv. Rev.* **2002**, *54*, 631-651.

(7) Wu, C.; Wang, X. *Phys. Rev. Lett.* **1998**, *80*, 4092-4094.

(8) Pelton, R. *Adv. Colloid. Interface Sci.* **2000**, *85*, 1-33.

(9) Gan, D.; Lyon, L. A. *J. Am. Chem. Soc.* **2001**, *123*, 7511-7517.

(10) Jones, C. D.; Lyon, L. A. *Macromolecules* **2000**, *33*, 8301-8306.

(11) Green, N. M. *Biochem. J.* **1965**, *94*, 23c-24c.

(12) Jones, C. D.; Lyon, L. A. *Macromolecules* **2003**, *36*, 1988-1993.

(13) O'Connell, P. B. H.; Brady, C. J. *Anal. Biochem.* **1976**, *76*, 63-73.

(14) Hofstetter, H.; Morpurgo, M.; Hofstetter, O.; Bayer, E. A.; Wilchek, M. *Anal. Biochem.* **2000**, *284*, 354-366.

(15) Livnah, O.; Bayer, E. A.; Wilchek, M.; Sussman, J. L. *Proc. Natl. Acad. Sci. U. S. A.* **1993**, *90*, 5076-5080.

CHAPTER 8

FUTURE OUTLOOK

Some of the projects mentioned in the previous chapters can benefited by carrying out more experiments. Some of those experiments are mentioned in this chapter.

- In Chapter 4 a vicinal diol crosslinker was used to prepare microgels that can be degraded by periodate. If these microgels are to be degraded in vivo periodate-degradation is not an appropriate route. One can imagine preparing microgels with disulfide or acid cleavable cross-linker, which can be cleaved in the cells and hence will be more useful.
- In Chapter 5 we discussed the synthesis of zwitterionic microgels but it was found that the microgels may have short oligomers which contributes to the zwitterionic effect. This problem can be solved in two ways: one synthesizing microgels with different concentrations of the charged monomers, which exhibit zwitterionic effect after cleaning the particles via centrifugation and second using a completely different synthetic route. For the second case one can imagine synthesizing microgels with just acrylic acid and cleaning them via centrifugation. The acid groups then can be conjugated with small molecule like ethylene diamine, which has two amine groups out of which one amine group can be used in conjugating to the acid groups and the second amine group will impart positive charge to the particle. These particles can be studied by various scattering techniques as a function of pH.

- In Chapter 6, synthesis and characterization of folate particle was discussed. These particles were used to target cancer cells which overexpress folate receptors. For this project, number of experiments can be conducted to make these particles a better targeting drug delivery agent. Cell lines other than HeLa and KB should be tested for internalization of the folate particles. The particles that were used for previous studies were ~ 270 nm, which are very big for targeting tumor cells, hence particles should be smaller, ideally smaller than 100 nm. Also drug loading studies on the particles can be carried out to understand the drug release profile of these particles. Instead of just drugs these particles can also be loaded with siRNA and DNA for potential applications in gene therapy. Currently the VPTT of the particles is ~32 °C, which is lesser than the body temperature. If one wants to use thermal switch to deliver drugs or other payloads the transition temperature should be slightly higher than the body temperature. This can be done by using comonomers with higher LCST.
- In Chapter 7 we observed pore-size dependent permeation of proteins in the microgels. This construct is very useful if one needs to separate proteins of different sizes. Also since the polymer is thermoresponsive, one can study the temperature dependent permeation of proteins.